

A Levelized Comparison of Pulsed and Steady-State Tokamaks

by

Daniel Joseph Segal

B.S. Engineering Physics, University of Wisconsin (2014)

Submitted to the Department of Nuclear Science and Engineering
in partial fulfillment of the requirements for the degree of

Master of Science in Nuclear Science and Engineering

at the

MASSACHUSETTS INSTITUTE OF TECHNOLOGY

February 2018

© Massachusetts Institute of Technology 2018. All rights reserved.

Author

Department of Nuclear Science and Engineering

November 11, 2018

Certified by

Jeffrey P. Freidberg

KEPCO Professor Emeritus

Thesis Supervisor

Certified by

Anne E. White

Cecil and Ida Green Associate Professor

Thesis Reader

Accepted by

Ju Li

Battelle Energy Alliance Professor

Chair, Department Committee on Graduate Students

A Levelized Comparison of Pulsed and Steady-State Tokamaks

by

Daniel Joseph Segal

Submitted to the Department of Nuclear Science and Engineering
on November 11, 2018, in partial fulfillment of the
requirements for the degree of
Master of Science in Nuclear Science and Engineering

Abstract

~~The goal of fusion energy research is to build a profitable reactor. This thesis develops a cost estimate model for fusion reactors from a physicist's perspective. It then applies it to the two main modes of operation for a tokamak reactor: pulsed and steady-state. In the end, an apples-to-apples comparison is developed, which is used to explain: the relative advantages of pulsed and steady-state operation, as well as, the design parameters that provide the most leverage in lowering machine costs. The most notable of these is the magnetic field strength—which should be doubled by ongoing research efforts at MIT using high-temperature superconducting (HTS) tape.~~

The goal of fusion energy research is to build an economically competitive reactor. This is difficult due to the complicated system composing a reactor and the nonlinearities it entails. Practically, to even get to the neighborhood of an economic reactor requires hundreds of simulations – which in turn necessitate quick running fusion systems codes. Moving towards these economic reactors then involves finding what design parameters provide the most leverage in lowering reactor costs.

As highlighted by the difference between European and American designs, however, the most important decision for tokamaks is whether to run them as *pulsed* or *steady-state*. This paper aims to fairly compare the two modes of operation using a single, comprehensive model. Benchmarked against other codes, this model actually shows that no fusion reactor is achievable without some technological advancements. This can be seen through every referenced design using nonstandard values of H and N_G .

The interesting result this paper shows is that developing high-temperature superconducting (HTS) tape could actually make both steady-state and pulsed tokamaks economically competitive against solar and coal. Further, this HTS tape actually has different best uses for the two modes of operation, appearing in the magnet structures of: TF coils for steady state and the central solenoid for pulsed. Developments in this technology should produce economic reactors within the coming decade.

Thesis Supervisor: Jeffrey P. Freidberg

Title: Professor of Nuclear Science and Engineering (Emeritus)

Contents

37	1	Introducing Fusion Reactor Design	15
38	1.1	Distinguishing Pulsed from Steady-State	17
39	1.2	Pricing a Fusion Reactor	19
40	1.3	Modeling Fusion Systems	22
41	1.4	Discussing HTS Magnet Technology	23
42	2	Designing a Steady-State Tokamak	27
43	2.1	Defining Plasma Parameters	28
44	2.1.1	Understanding Tokamak Geometry	28
45	2.1.2	Prescribing Plasma Profiles	30
46	2.2	Solving the Steady Current	33
47	2.2.1	Enforcing the Greenwald Density Limit	33
48	2.2.2	Declaring the Bootstrap Current	36
49	2.2.3	Deriving the Fusion Power	38
50	2.2.4	Using Current Drive	41
51	2.2.5	Completing the Steady Current	42
52	2.3	Handling Current Drive Self-Consistently	43
53	3	Formalizing the Systems Model	45
54	3.1	Explaining StaticFixed Variables	46
55	3.2	Connecting DynamicFloating Variables	46
56	3.3	Enforcing Power Balance	50
57	3.3.1	Collecting Power Sources	51
58	3.3.2	Approximating Radiation Losses	52

59	3.3.3	Estimating Heat Conduction Losses	53
60	3.3.4	Writing the Lawson Parameter Criterion	55
61	3.3.5	Finalizing the Primary Constraint	58
62	3.4	Collecting Limiting Secondary Constraints	61
63	3.4.1	Introducing the Beta Limit	62
64	3.4.2	Giving the Kink Safety Factor	63
65	3.4.3	Working under the Wall Loading Limit	64
66	3.4.4	Setting a Maximum Power Cap	65
67	3.4.5	Listing the Heat Loading Limit	66
68	3.5	Summarizing the Fusion Systems Model	67
69	4	Designing a Pulsed Tokamak	71
70	4.1	Modeling Plasmas as Circuits	72
71	4.1.1	Drawing the Circuit Diagram	72
72	4.1.2	Plotting Pulse Profiles	74
73	4.1.3	Specifying Circuit Variables	78
74	4.1.4	Constructing Reasoning the Pulse Length	82
75	4.2	Producing Salvaging Flux Balance	83
76	4.2.1	Rearranging the Circuit Equation	83
77	4.2.2	Adding Importing Poloidal Field Coils	85
78	4.3	Improving Tokamak Geometry	86
79	4.3.1	Defining Central Solenoid Dimensions	87
80	4.3.2	Calculating Measuring Component Thicknesses	88
81	4.3.3	Revisiting Central Solenoid Dimensions	90
82	4.4	Piecing Together the Generalized Current	92
83	4.5	Simplifying the Generalized Current	93
84	4.5.1	Recovering the Steady Current	94
85	4.5.2	Extracting the Pulsed Current	94
86	4.5.3	Rationalizing the Generalized Current	96
87	5	Completing the Systems Model	97

88	5.1	Describing a Simple Algebra	97
89	5.2	Generalizing Previous Equations	99
90	5.2.1	Including Limiting Constraints Rehashing the Limits	99
91	5.2.2	Minimizing Intermediate Derived Quantities	101
92	5.2.3	Pinning Dynamic Floating Variables	102
93	5.2.4	Detailing the Equation Solver	104
94	5.3	Wrapping up the Logic	105
95	6	Presenting the Code Results	107
96	6.1	Testing the Validating Code against with other Models	108
97	6.1.1	Comparing with the PSFC Arc Reactor	109
98	6.1.2	Contrasting with the Aries Act Studies	110
99	6.1.3	Benchmarking with the Process DEMO Designs	112
100	6.2	Developing Prototype Reactors	120
101	6.2.1	Navigating around Charybdis	125
102	6.2.2	Pinning down Proteus	125
103	6.2.3	Highlighting Operation Differences	125
104	6.3	Learning from the Data	126
105	6.3.1	Picking a Design Point	126
106	6.3.2	Utilizing High Field Magnets	131
107	6.3.3	Looking at Design Alternatives	134
108	7	Planning Future Work for the Model	141
109	7.1	Incorporating Stellarator Technology – Ladon	141
110	7.2	Making a Composite Hybrid Reactor – Janus	143
111	7.3	Bridging Confinement Scalings – Daedalus	144
112	7.4	Addressing Model Shortcomings	145
113	7.4.1	Integrating Pedestal Temperature Profiles	145
114	7.4.2	Expanding the Radiation Loss Term	145
115	7.4.3	Taking Flux Sources Seriously	146

116	8 Concluding Reactor Discussion	147
117	A Cataloging StaticFixed Variables	149
118	B Simulating with Fussy.jl	151
119	B.1 Getting the Code to Work	151
120	B.2 Sorting out the Codebase	152
121	B.2.1 Typing out Structures	153
122	B.2.2 Referencing Input Decks and Solutions	155
123	B.2.3 Acknowledging Utility Functions	155
124	B.2.4 Mentioning Base Level Files	155
125	B.3 Delving into Reactor Methods	156
126	B.4 Demonstrating Code Usage	157
127	B.4.1 Initializing the Workspace	158
128	B.4.2 Running a Study	158
129	B.4.3 Extracting Results	159
130	B.4.4 Plotting Curves	160
131	C Discussing Fusion Power	165
132	C.1 Fusion Power – P_F	165
133	C.2 Reactivity – (σv)	167
134	D Selecting Plasma Profiles	171
135	D.1 Density – n	171
136	D.2 Temperature – T	173
137	D.3 Pressure – p	175
138	D.4 Bootstrap Current – f_{BS}	175
139	D.5 Volume Averaged Powers	177
140	E Determining Plasma Flux Surfaces	179
141	E.1 Flux Surface Coordinates	179
142	E.2 Cross-sectional Area and Volume	181

143	E.3 Surface and Volume Integrals	182
144	F Expanding on the Bootstrap Current	185
145	F.1 Summarized Results	185
146	F.2 Detailed Analysis	186

147 List of Figures

148	1-1	Cut-Away of Tokamak Reactor	16
149	1-2	Comparison of Pulsed and Steady-State Current	18
150	1-3	Steady State Magnet Components	25
151	1-4	Pulsed Magnet Components	25
152	2-1	Geometry of a Tokamak	29
153	2-2	Geometric Parameters	30
154	2-3	Radial Plasma Profiles	31
155	2-4	Greenwald Density Limit	35
156	3-1	Current Balance in a Tokamak	49
157	3-2	Power Balance in a Reactor	56
158	3-3	H-Mode Confinement Time Scaling	58
159	4-1	A Simple Plasma Transformer Description	73
160	4-2	Time Evolution of Circuit Profiles	75
161	4-3	Dimensions of Tokamak Cross-Section	87
162	5-1	Equation Selection for Fusion System	98
163	5-2	Minimize Cost Step II/III – Optimize Reactor	103
164	6-1	Act Studies Cost Dependence on the H Factor	111
165	6-2	Arc Model Comparison	115
166	6-3	Aries Act I Model Comparison	116
167	6-4	Aries Act II Model Comparison	117
168	6-5	Demo Steady Model Comparison	118
169	6-6	Demo Pulsed Model Comparison	119

170	6-7	Designing Reactor Prototypes How to Build a Fusion Reactor	122
171	6-8	Steady State Prototype Comparison	123
172	6-9	Pulsed Prototype Comparison	124
173	6-10	Limiting Constraint Regimes Limit Regimes as function of B_0	127
174	6-11	Steady State Cost Curves	129
175	6-12	Pulsed Cost Curves	130
176	6-13	Pulsed B_{CS} Sensitivity	132
177	6-14	Pulsed Monte Carlo Sampling	133
178	6-15	Bootstrap Current Monte Carlo Sampling	135
179	6-16	Internal Inductance Sensitivities	136
180	6-17	Pulsed H Sensitivities	138
181	6-18	Steady State Current Drive Efficiency	139
182	6-19	Current Drive Efficiency vs Launch Angle	140
183	7-1	Cut-Away of Stellarator Reactor	142
184	7-2	Current Balance in a Tokamak	143
185	B-1	A Blank Plot	161
186	B-2	An Empty Plot	162
187	B-3	An Unscaled Plot	163
188	B-4	A Scaled Plot	163
189	C-1	Comparing Nuclear Fusion and Fission	166
190	C-2	The D-T Fusion Reaction	167
191	D-1	Radial Plasma Profiles	171
192	E-1	Cut-Away of Tokamak Reactor	179
193	E-2	Dimensions of Tokamak Cross-Section	181

194 List of Tables

195	3.1	Dynamic Variables	46
196	4.1	Piecewise Linear Scheme for Pulsed Operation	75
197	4.2	Example TF Coils and Central Solenoid Critical Values	90
198	5.1	Main Equation Bank	100
199	6.1	Arc Variables	115
200	6.2	Act I Variables	116
201	6.3	Act II Variables	117
202	6.4	Demo Steady Variables	118
203	6.5	Demo Pulsed Variables	119
204	6.6	Charybdis Variables	123
205	6.7	Proteus Variables	124
206	6.8	Proteus and Charybdis Comparison	126
207	A.1	List of Static Fixed Variables	149

208 List of Equations

209	1.1	Magnetic Energy – W_M	19
210	1.3	Cost per Watt – C_W	21
211	2.1	Minor Radius – a	29
212	2.2	Density Profile – n	31
213	2.4	Temperature Profile – T	32
214	2.5	Current Profile – J	32
215	2.6	Internal Inductance – l_i	33
216	2.7	Normalized Poloidal Magnetic Field – b_p	33
217	2.8	Current Balance – I	33
218	2.11	Greenwald Density – \bar{n}	36
219	2.15	Bootstrap Current – I_{BS}	38
220	2.20	Dilution Factor – f_D	39
221	2.21	Volume Integral – Q_V	40
222	2.23	Fusion Power – P_F	40
223	2.28	Current Drive – I_{CD}	42
224	2.30	Steady Current – I_P	43
225	2.31	Current Drive Efficiency – η_{CD}	44
226	3.1	Scanned Temperature – \bar{T}	47
227	4.75	Generalized Current – I_P	93
228	C.1	Fusion Energy – E_F	165
229	C.3	Alpha Power – P_α	167
230	C.4	Neutron Power – P_n	167

Chapter 1

Introducing Fusion Reactor Design

The central goal of fusion energy research is to build an economically competitive nuclear reactor. It has long been joked, though, that fusion power will always be twenty years away. This is mainly due to the nonlinearities inherent to a reactor system and the high upfront cost of building a new machine. The model developed for this paper uses standard theory and empirical fits to find cost trends from this nonlinear system. An important conclusion is that building an economic reactor using existing technology would be impossible. One solution may be improving magnet technology – as MIT is exploring with high-temperature superconducting (HTS) tape.

As can be seen by comparing the European and American/Asian fusion reactor design efforts, though, one of the most important decisions is whether to run the reactor as pulsed (EU¹) or steady-state (US² and Korea³). The distinction between the two mainly manifests itself in the choice of auxiliary current drive: inductive for pulsed and lower hybrid for steady-state.⁴ With the model built for this thesis, it is possible to perform a direct comparison of these two modes of operations.

Due to the speed and simplicity of the model, hundreds of reactors can be simulated in minutes. Further, the model has been benchmarked against other ones from the literature,^{2,5–7} allowing it to answer several critical questions regarding the comparison of the two modes of operation. A major finding of this is that HTS tape should

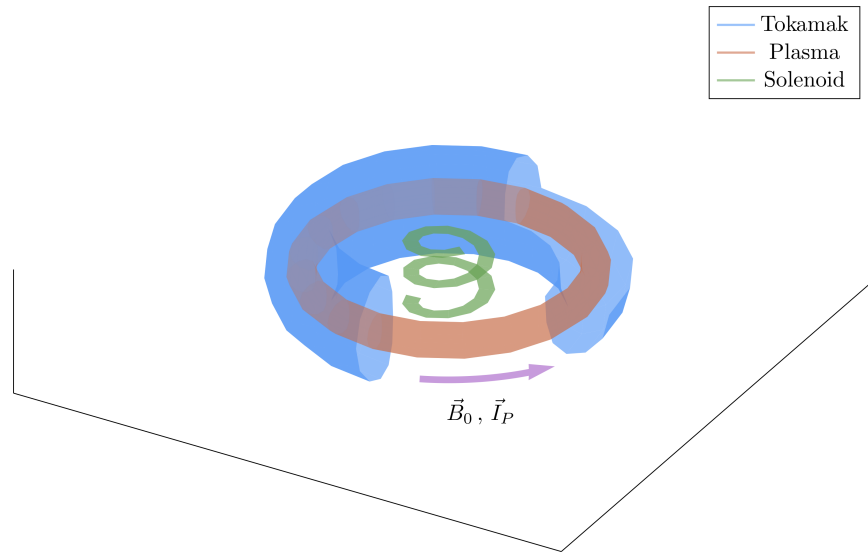


Figure 1-1: Cut-Away of Tokamak Reactor

The three main components of a magnetic fusion reactor are: the tokamak structure, the plasma fuel, and the spring-like solenoid at the center. Here, the directions of the magnetic field (B_0) and plasma current (I_P) variables are shown to be in the toroidal direction.

appear in different places for the two modes of operation: within the central solenoid for pulsed machines and inside the TF coil magnets for steady-state ones.

The central goal of fusion energy research is to build a profitable nuclear reactor. It has long been joked though that fusion power will always be 20-50 years away. This paper lays a framework for exploring reactor space for functional, efficient designs —based on world experiments during the last half-century. Due to the speed and simplicity of the model, hundreds of reactors can be explored in minutes (outpacing the domestic program slightly).

With this proposed model, interesting reactors can be pinpointed long before engineers hit the blueprints. This should help shorten the time until a profitable reactor, as well as illuminate ways to improve modern plasma theory. Further, it verifies the reasoning of MIT's PSFC to invest in high field, high-temperature superconducting (HTS) tape—as this technology would lead to much smaller devices.

1.1 Distinguishing Pulsed from Steady-State

The leading candidate for the first economic, power-producing fusion reactor is a tokamak. As shown in Fig. 1-1, tokamaks are doughnut-shaped metal structures that use magnets to confine their fusion-grade plasmas. The challenge in building such a device comes from the various physics and engineering constraints it must satisfy – i.e. not surpassing acceptable levels of neutron damage, plasma pressure, etc.

One of the most contentious points of reactor design, however, is whether to run it as: pulsed (the European effort¹) or steady-state (the American/Asian approach^{2,3}). Here, pulsed operation refers to how a reactor is ramped up and down several times a day. Whereas steady-state implies a machine is functionally kept ramped up the entirety of its fifty-year campaign. These behaviors are shown in Fig. 1-2. The difficulties involved with the two modes of operation are then: cyclical stresses for pulsed and expensive current drive for steady state.⁴

~~When people talk about fusion, they usually talk about plasma physics, and when people talk about plasma physics, they often talk about things like: the sun, lightning, and the aurora borealis. Of these three, the sun is the only nuclear reactor. However, the sun can stay on all day because the massive gravity of its fuel source helps keep it self-contained in space. On Earth, this is not possible — the plasma fuel needs to be contained by other means (i.e. with magnets).~~

~~A tokamak is one of the leading candidates for a profitable fusion reactor. It shares the shape of a doughnut, using magnets to keep a hula hoop of plasma swirling inside it. The difficulty of keeping this plasma swirling though, is that it does not enjoy being spun too fast or squeezed too hard. Conversely, the tokamak housing the plasma does not like taking too much of a beating or being scaled to T-Rex sized proportions. This sets the stage for tokamak reactor design — building on the various plasma physics and nuclear engineering constraints of the day.~~

~~One of the most contentious points of building a tokamak, however, is whether it will be run as: pulsed (the European approach¹) or steady-state (the United States effort~~

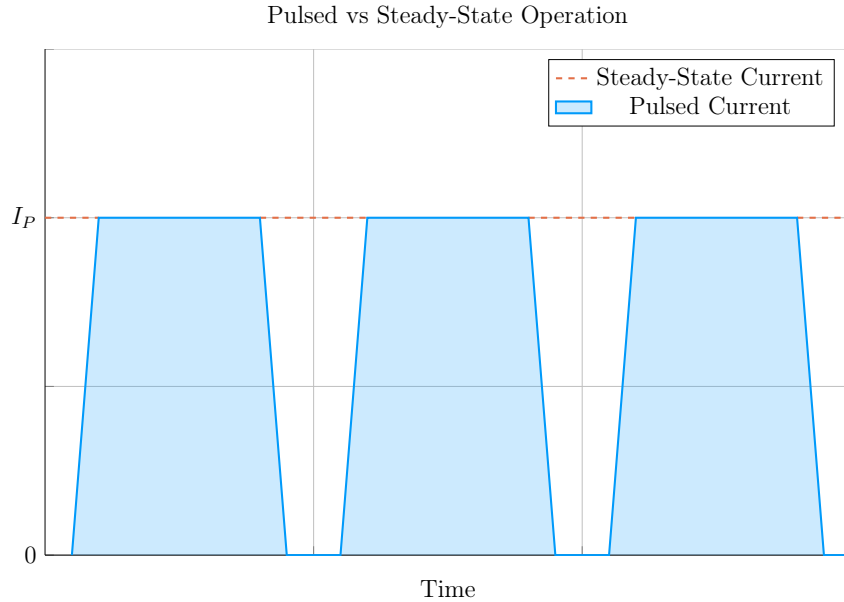


Figure 1-2: Comparison of Pulsed and Steady-State Current

Inside a pulsed reactor, current is ramped up and down several times a day – with downtime in-between. Steady state reactors are meant to remain on for weeks or months.

292 ²⁾. Here, pulsed operation refers to how a reactor is turned on and off periodically
 293 —around ten times a day. Whereas, steady state machines are meant to be left on
 294 nearly the entirety of their 50-year campaigns. These behaviors are shown in Fig. 1-2.
 295 The main way theseThese two modes of operation, *pulsed* and *steady-state*, greatly
 296 influence reactor design, though, is the design through the current balance equation
 297 (derived later). What this means practically is a tokamak plasma requires some cur-
 298 rent to stay in equilibriumtokamaks need current to spin their plasma hoops at some
 299 required speed and this current has to be partially generated by auxiliary systems:
 300 inductively for pulsed and non-inductively for steady-state.come from somewhere.
 301 Luckily, the plasma naturally enjoys spinning and provides some assistance through
 302 the bootstrap current. The remaining current must then be produced by external
 303 means. To fairly compare the two modes of operation thus requires a generalized
 304 handling of current balance that can incorporate both auxiliary systems.
 305 The source of external current drive is what distinguishes pulsed from steady-state
 306 devices. Steady-state devices provide the required current assistance either through

307 ~~lasers or particle beams — this paper’s model focusing on a type of laser assistance~~
308 ~~called lower-hybrid current drive (LHCD).⁴ Pulsed machines, on the other hand, rely~~
309 ~~on inductive sources — which by definition require cycles of charging and discharging~~
310 ~~several times a day.~~

311 ~~The goal of this document is to show that pulsed and steady-state operation are~~
312 ~~actually two sides of the same coin. This yields the simple conclusion that a single~~
313 ~~comprehensive model can run both modes at the flip of a switch. It even opens the~~
314 ~~opportunity of a hybrid reactor that exists somewhere in between the two.~~

315 1.2 Pricing a Fusion Reactor

316 To ~~truly~~ compare tokamaks used as fusion ~~reactors, though,reactors~~ the obvious met-
317 rics are costs. ITER – the ~~second~~ most expensive experiment ~~in the world^{8,9}today~~
318 ~~(only behind the LHC)~~ – has a history ~~full of rich in~~ countries backing out for high
319 ~~construction costsprice tags~~ and rejoining only ~~afterwhen~~ they finally get lowered.⁴
320 The problem is \$20B is a lot of money and 20 years is a long time. Moreover, ap-
321 proximating true costs ~~is difficult due to thebecomes even trickier when designers~~
322 need to project (or neglect) economies-of-scale for expensive components, such as the
323 ~~superconducting~~ magnets and irradiated materials.

324 ~~Therefore,As such,~~ this paper adopts stand-ins for the conventional capital cost and
325 cost-per-watt metrics. This is done for simplicity, ~~both in:for both:~~ formulating the
326 ~~relations andmodeling reasons as well as~~ conveying the two metrics to physicists.
327 ~~The approximation for theTo begin, the relevant approximation for~~ capital cost –
328 how much a tokamak costs to build – is the magnetic energy.¹⁰

$$W_M \propto R^3 B^2 \tag{1.1}$$

329

330 In this magnetic energy proportion relation, the tokamak’s major radius – R – is

involved in a volumetric term (R^3) and B is the strength (in Teslas) of the toroidal magnetic field. ~~hooped shape magnetic field that lays nested within the plasma's shell (near its core).~~ This quantity simply states that the two surefire ways to make a machine more expensive ~~are to build it bigger and to use stronger magnets. to build are: making it larger and using stronger magnets.~~ As these terms also improve confinement, this cost introduces a trade-off between size and magnet technology. This is why the proposed ARC reactor – designed with HTS tape – could be half the size of ITER, which uses conventional LTS technology.

The next metric, the cost-per-watt, is defined by dividing the capital cost (i.e. the magnetic energy) by the main source of power output. For a tokamak, this source of power is fusion – discussed in more detail in Appendix C. The cost-per-watt thus measures how economically competitive a reactor will be once it is build. This is how to compare the rate of return for different base-load power sources (e.g. fission, coal, and solar). ~~This quantity measures how profitable a reactor will be once it is built. In a tokamak, the main power output is assumed to be fusion power, which relies on light elements (i.e. two Hydrogens) fusing into a heavier one (i.e. one Helium) – hopefully releasing enough energy to offset the expense of causing it to happen in the first place. Although fusion power will not be defined till later, it does highlight the fact that this measure of cost-per-watt actually has units of time!~~

$$\tilde{C}_W = \frac{W_M}{P_F} \quad (1.2)$$

~~The final piece of the costing puzzle is a duty factor that levelizes the comparison of pulsed and steady-state tokamaks. As pulsed machines may be off 20% of the time, their fusion power output should be reduced by that percentage. This is accounted for in the duty factor, which is simply the ratio of the flattop – the time when pulsed machines are approximately held at steady-state – to the entire length of the pulse. In pulsed machines, the entire pulse includes charging the inductive sources as well as flushing out the tokamak between runs. These non-flat-top portions of time can last around thirty minutes (where the reactor makes no money). As steady-state machines~~

lack these non-flattop portions, their duty factors are rightfully one. Analysis in Fig. 4.1.4 and discussion with several researchers, however, show that the same will probably hold true for a pulsed reactor, too. Summarizing, the cost-per-watt coupled with the duty factor provides an ad hoc pricing metric, C_W , given by:

A final correction can be made on the cost-per-watt to account for reactor downtime, which is fundamental to pulsed operation. This is handled through the duty factor (f_{Duty}) that is defined as the ratio of a reactor's quasi-steady-state flattop duration to the entire pulse length of a tokamak. In the context of the cost-per-watt, it scales down the fusion power:

$$C_W = \frac{W_M}{f_{Duty} \cdot P_F} \quad (1.3)$$

For a steady-state reactor, this duty factor is assumed to be held at one. Pulsed machines, on the other hand, can see around thirty minutes of downtime,⁷ which leads to duty factors around 80%. Analysis in Section 4.1.4, however, shows that pulsed reactors may also have duty factors near unity.

It serves as a cornerstone for comparing the entire landscape of tokamak reactors—whether they run in pulsed or steady-state operation. Although not a true engineering cost metric (i.e. in dollars per watt), it does provide an obvious physics meaning. Coupled with the magnetic energy stand-in for capital cost, these two costs allow researchers to pinpoint profitable and inexpensive tokamaks within reactor space.

Combined, these two cost metrics allow designers to pinpoint economically competitive tokamaks within reactor space. Although not rigorous in an engineering context, these capital cost and cost-per-watt approximations do provide true physics meaning while comparing different machines – whether they run as pulsed or steady-state.

1.3 Modeling Fusion Systems

Before reactors can be ~~priced~~~~costed~~, though, they have to be modeled. Therefore the first half of this thesis is devoted to the theory behind tokamak design. ~~Emphasis~~~~A~~ ~~priority~~ is placed more on a physicist's intuition than an engineer's costing rigor. This is justified by the nonlinearities inherent to ~~the~~ fusion systems and rationalized by this paper's results matching more sophisticated ~~models~~~~frameworks~~ with high fidelity.

Stepping back, a fusion systems model is an approach to designing reactors based on satysfying various physics and engineering constraints. Zero-dimensional (0-D) systems models are then a particular subclass of these that reduce the inherently 3-D problem of design to a collection of scalar, averaged values. This reduction in complexity allows models to be orders of magnitude faster. The natural corollary of this is that hundreds of reactors can be simulated in minutes.

Within the context of reactor design, these 0-D systems models serve an important role due to their speed and simplicity. Although not truly self-consistent,* these models are capable of exploring large areas of reactor space. This is especially important in the early stages of tokamak planning when researchers are selecting a design point. These models also have use in finding general costing trends – as shown in this document.

What makes this paper's ~~systems~~ model different from ~~other ones, though,~~~~others in the field~~ is ~~it~~~~the~~ generalized handling of both modes of tokamak operation: pulsed and steady-state. This was necessitated by a desire to ~~fairly~~ compare the ~~two~~~~two modes on a level playing field~~. The most fundamental result of this analysis is that both modes are actually capable of leading to economically competitive reactors~~What this shows is that both pulsed and steady-state tokamaks could make for profitable fusion reactors~~ – assuming some technological advancements.

*For speed concerns, 0-D fusion systems models often ignore self consistency in quantities like pressure profiles and use empirical fits to estimate values such as the confinement time.

1.4 Discussing HTS Magnet Technology

As mentioned, no economically competitive fusion reactor can be built using existing technology – regardless of whether it runs as pulsed or steady-state. This is why MIT has been exploring HTS magnet technology for their Arc reactor in an effort to nearly double the maximum achievable field strength. What this paper shows is that this logic is indeed correct and HTS may be the final magnet advancement needed for the conventional fusion paradigm (i.e. D-T fuel, H-Mode, etc.)

~~One technological advancement that could lead to major wins is improving magnet components. This is why MIT has championed high-field designs for the better part of the last century. In their latest effort, the PSFC team has explored new high-temperature superconducting (HTS) tape capable of doubling the maximum achievable field strength. What this paper shows is that this logic is indeed correct and that HTS tape is all that is needed to build optimum reactors.~~

More concretely, this paper shows that new HTS ~~tape~~ technology is capable of lowering reactor costs – both for pulsed and steady-state operation.~~both pulsed and steady-state tokamak costs.~~ Further, this HTS tape has different uses within the two modes of operation – as set by cost concerns (see Figs. 1-3 and 1-4). This analysis shows that HTS should be employed in the TF coils for steady-state reactors *and* in the central solenoid for pulsed ones. This is because pulsed machines require lower toroidal field strengths, which are achievable with less expensive LTS magnets.~~Further, the benefits of doubling the magnet strength bring the situation to a realm of significantly diminished rates of return. HTS is thus the end goal for the conventional D-T fusion paradigm.~~

~~Moreover, this model shows that HTS is best utilized in different components for pulsed and steady-state operation. Steady-state tokamaks favor HTS use in the D-shaped magnets that circle the machine (i.e. the TF coils). Whereas pulsed devices would benefit from employing HTS in the central solenoid – that produces most of a reactor’s inductive current. A corollary of this is the more conventional low-temperature~~

434 ~~superconducting (LTS) magnets (i.e. less expensive ones) can be used for pulsed TF~~
435 ~~coils, as their improved confinement levels off at much lower field strengths.~~

436 Now that the problem has been thoroughly introduced, we will go over the theory
437 behind steady-state and, then, pulsed tokamaks. A couple ~~detourssegues~~ will be taken
438 along the way to show how the model can be incorporated into a fusion systems code.
439 This code – Fussy.jl – is the topic of Appendix B and is freely available at:

440 git.io/tokamak

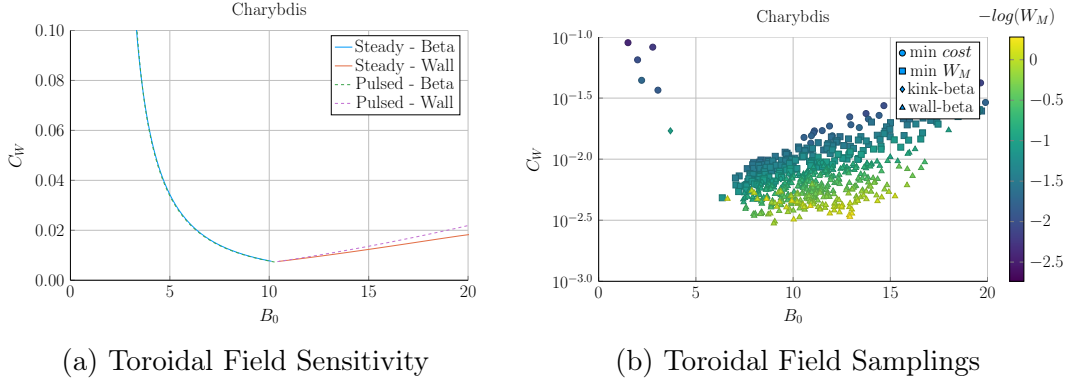


Figure 1-3: Steady State Magnet Components

Steady-state reactors benefit from increased toroidal field strength until neutron wall loading starts to dominate design (at around 10-15 T for Charybdis). This is well within the range accessible to HTS magnets.

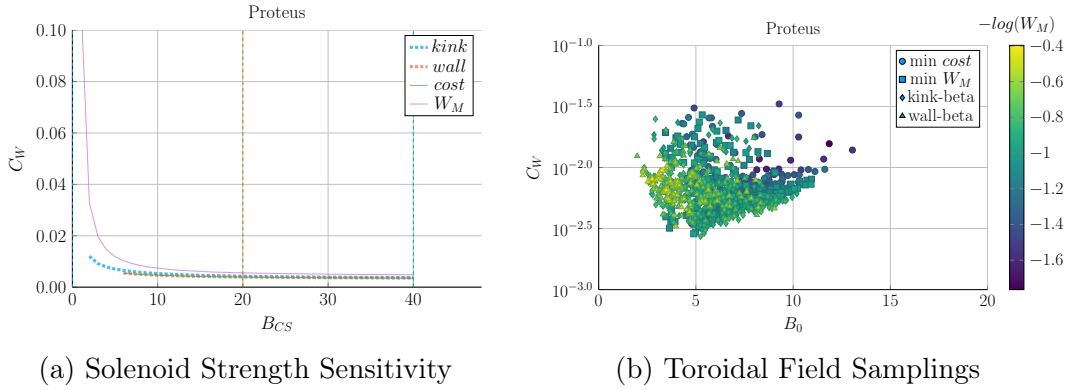


Figure 1-4: Pulsed Magnet Components

Pulsed reactors are shown to receive strong decreases in reactor cost as the central solenoid field strength is increased, until around 20 T. However, the TF coils do not receive the same cost reduction with field strength – as shown by the minimum cost appearing at 5 T.

Chapter 2

Designing a Steady-State Tokamak

This chapter explores a simple model for designing steady-state tokamaks. In the next couple chapters, the model is first formalized for use in a systems code and then generalized to handle pulsed operation. These derivations highlight that the only difference between the two modes of operation is how they generate their auxiliary plasma current: LHCD for steady-state operation and inductive sources for when a reactor is purely pulsed.

Along the way, equations will be derived that get rather complicated. To remedy the situation, a distinction between `dynamicfloating` and `staticfixed` values is now given, which will allow splitting most equations into `staticfixed` and `dynamicfloating` parts. `DynamicFixed` values – i.e. the tokamak’s major radius (R_0) and magnet strength (B_0), as well as the plasma’s current (I_P), temperature (\bar{T}), and density (\bar{n}) – are first-class variables in the model (see Table 3.1). Everything is derived to relate them. `StaticFixed` values, on the other hand, can be treated as code inputs, which remain constant throughout a reactor solve. These most obviously include the various geometric and profile parameters introduced next section.

The overall structure of this chapter, then, is built around developing an equation for plasma current in a steady-state tokamak. It is shown that this value arises from balancing current in a reactor using both a plasma’s own bootstrap current (I_{BS}),

as well the tokamak's auxiliary driven current (I_{CD}). These relations necessitate geometric parameters and plasma profiles, which will be given shortly. Along the way, definitions will also be needed for the Greenwald density (N_G) and the fusion power (P_F). What is shown is that the current does not actually depend directly on the major radius (R_0) or magnet strength (B_0) of a tokamak – allowing these variables to be put off until next chapter.

2.1 Defining Plasma Parameters

As mentioned previously, the zero-dimensional model derived here can closely approximate solutions from higher-dimensional codes that might take many hoursweeks to run. The essence of boiling down three-dimensional behaviors to one dimensional profiles – and zero-dimensional averaged values – begins with defining the most important plasma parameters. These are the: current density (J), temperature (T), and density (n) of a plasma.

Solving this problem most generally usually involves decoupling the geometry of the plasma from the shaping of its nearly parabolic radial-profiles – both of which will be explained shortly.

2.1.1 Understanding Tokamak Geometry

The first thing people see when they look at a tokamak is its geometry – see Fig. 2-1. How big is it? Is it stretched out like a bicycle tire or compressed to the point of being nearly spherical? Would a slice across the major radius result in two cross-sections that were: circular, elliptic, or triangular?~~Is it stretched out like a tire or smooshed together like a bagel? If it were torn in two, would the exposed areas look like: circles, ovals, or triangles?~~

These questions lend themselves to the three important geometric variables – the inverse aspect ratio (ϵ), the elongation (κ), and the triangularity (δ). The inverse

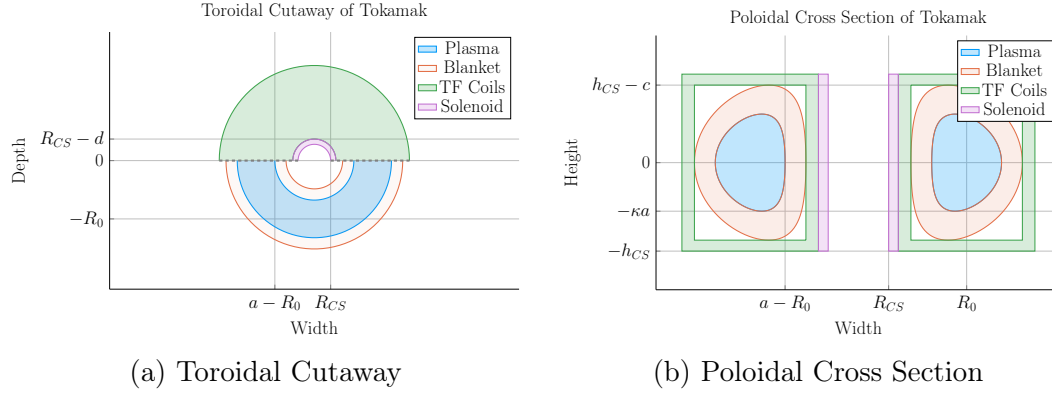


Figure 2-1: Geometry of a Tokamak

This diagram is of a tokamak's toroidal (top) view and the poloidal cross section of a slice across the major axis. Included are the four components of a reactor: the plasma, its metallic blanket, the toroidal field magnets surrounding them, and the central solenoid. These have thicknesses of a , b , c and d , respectively. R_{CS} is where the solenoid starts.

aspect ratio is a measure of how stretched out the device is, or formulaically:

$$a = \epsilon \cdot R_0 \quad (2.1)$$

This says that the minor radius (a), measured in meters, is related to the major radius of the machine (R_0) through ϵ . Or more tangibly, the minor radius is related to the two small ~~cross-section circles~~ that result from a slice across the major radius of the machine. ~~come from tearing a bagel in two. Whereas the major radius is related to the overall circle of the bagel when viewing it from the top.~~

The remaining two geometric parameters – κ and δ – are related to the shape of the torn halves. As the name hints, elongation (κ) is a measure of how stretched out the tokamak is vertically – is the cross-section a circle or an oval? The triangularity (δ) is then how much the cross-sections point outward from the center of the device. All three's effects can be seen in Fig. 2-2. ~~Their exact usage within describing flux surfaces is shown in Appendix E.~~

These geometric factors allow the volumetric and surface integrals governing fusion power and bootstrap current to be condensed to simple radial ones – see Eqs. (E.24)

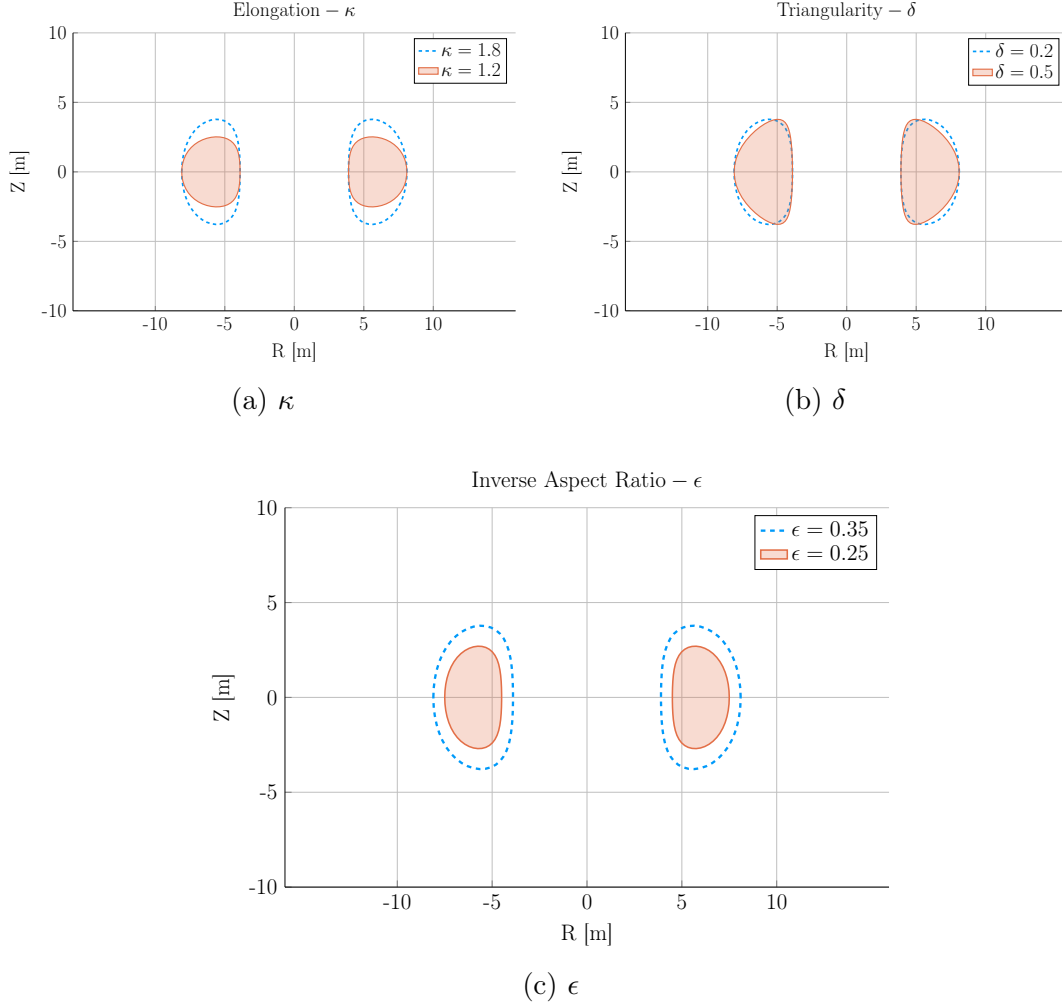


Figure 2-2: Geometric Parameters

These three geometric parameters allow the toroidal cross-sections to scale radially, stretch vertically, and become more triangular – thus improving upon simple circular slices.

500 and (E.25). The only remaining step is to define the radial profiles for: the density,
 501 temperature, and current of a plasma.

502 2.1.2 Prescribing Plasma Profiles

503 The first step in defining radial profiles is realizing that all three quantities are **essen-**
 504 **tially parabolas**~~basically parabolas~~ – i.e. the temperature, density and current **density**,
 505 shown in Section 2.1.2, are peaked at some radius (usually the center) and then decay
 506 to zero somewhere before the walls of the tokamak enclosure.

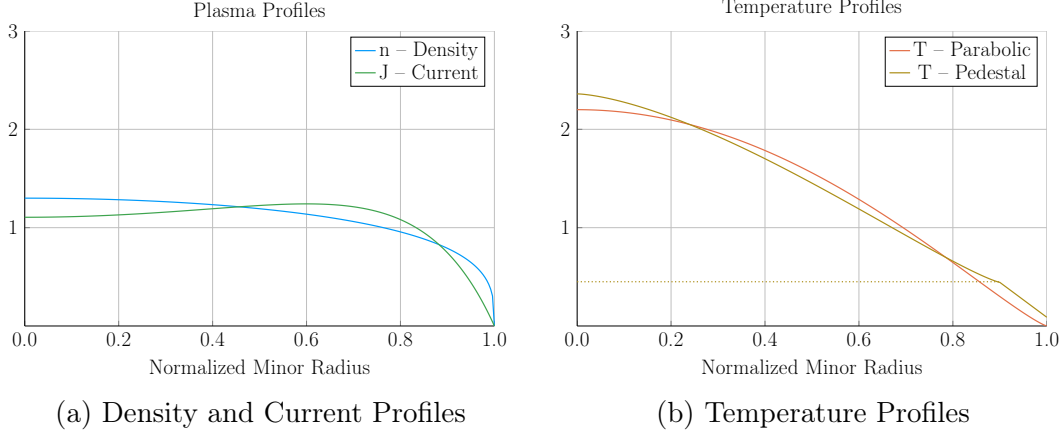


Figure 2-3: Radial Plasma Profiles

The three most fundamental ~~profiles~~^{properties} of a fusion plasma are its temperature, density, and current. These ~~profiles~~ allow the model to reduce from three dimensions to just half of one.

Although not self-consistent, these profiles do capture enough of the physics to approximate relevant phenomenon, such as transport and fusion power.¹¹

The Density Profile

To begin, density has the simplest profile. This is because it is relatively flat, remaining near the average value – \bar{n} – throughout the body of the plasma until quickly decaying to zero near the edge of the plasma.* For this reason, a parabolic profile with a very low peaking factor – ν_n – is well suited.

$$n(\rho) = \bar{n} \cdot (1 + \nu_n) \cdot (1 - \rho^2)^{\nu_n} \quad (2.2)$$

The reason \bar{n} is referred to as the volume-averaged density is because using the volume integral – given by Eq. (E.24) – over the density profile results in that value

*Even in H-Mode plasmas where density profiles have a pedestal,¹² they usually have much less of a peak than temperatures¹³ – especially so in a reactor setting.¹⁴

516 after dividing through by the volume (V):

$$\bar{n} = \frac{\int n(\mathbf{r}) d\mathbf{r}}{V} \quad (2.3)$$

517 A final point to make is this parabolic profile allows for a short closed-form relation
518 for the Greenwald density limit – substantially simplifying this fusion systems model.

519 The Temperature Profile

520 The use of a parabolic profile for the plasma temperature is slightly more dubious.
521 This is because H-Mode plasmas are actually highly peaked at the center, decaying
522 to a non-zero pedestal temperature near the edge before finally dropping sharply to
523 zero. This model chooses to forego this pedestal representation for a simple parabolic
524 one – although the pedestal approach is discussed in Appendix D. Analogous to the
525 density, the profile treats \bar{T} as the average value and ν_T as the peaking parameter.

$$T(\rho) = \bar{T} \cdot (1 + \nu_T) \cdot (1 - \rho^2)^{\nu_T} \quad (2.4)$$

526

527 The Current **Density** Profile

528 The plasma current **density** is the third profile and cannot safely be represented by a
529 simple parabola. This is because having an adequate bootstrap current relies heavily
530 on a profile being peaked off-axis – i.e. at some radius not at the center. This hollow
531 profile can then be modeled with the commonly given plasma internal inductance (l_i).
532 Concretely, the current's hollow profile is described by:

$$J(\rho) = \bar{J} \cdot \frac{\gamma^2 \cdot (1 - \rho^2) \cdot e^{\gamma \rho^2}}{e^\gamma - 1 - \gamma} \quad (2.5)$$

533 The intermediate γ quantity can then be numerically solved for from the plasma
534 internal inductance using the following relations – with b_p representing the normalized

535 poloidal magnetic field. These are derived in Appendix F.

$$l_i = \frac{4\kappa}{1 + \kappa^2} \int_0^1 b_p^2 \rho d\rho \quad (2.6)$$

536

$$b_p(\rho) = \frac{-e^{\gamma\rho^2}(\gamma\rho^2 - 1 - \gamma) - 1 - \gamma}{\rho(e^\gamma - 1 - \gamma)} \quad (2.7)$$

537 Combined, these three geometric parameters and profiles lay the foundation for this
538 zero-dimensional fusion systems model.

539 2.2 Solving the Steady Current

540 As suggested, one of the most important equations in a fusion reactor is current
541 balance. In steady-state operation, all of a plasma's current (I_P) must come from
542 a combination of its own bootstrap current (I_{BS}), as well as auxiliary current drive
543 (I_{CD}). This can be represented mathematically as:

$$I_P = I_{BS} + I_{CD} \quad (2.8)$$

544 The goal is then to write equations for bootstrap current and driven current. This
545 will make heavy use of the Greenwald density limit. The steady current will then
546 ~~be~~Without spoiling too much, the steady current is shown to be only a function of
547 temperature! In other words, this current is independent of a tokamak's geometry
548 and magnet strength. As will be pointed out then, though, a subtlety arises that will
549 bring the two back into the picture – self-consistency in the current drive efficiency
550 (η_{CD}).

551 2.2.1 Enforcing the Greenwald Density Limit

552 The Greenwald density limit is a density limit that applies to all tokamaks
553 ~~in the field of fusion energy~~. It sets a hard limit on the density and how it scales with

554 current and reactor size. Although currently lacking a true first-principles theoretical
 555 explanation, it does have a real meaning within the design context. Operate at too low
 556 a density and run the risk of never entering H-Mode. Run the density too high, and
 557 cause the tokamak's plasma to ~~disrupt~~~~disrupt catastrophically!~~ These conclusions
 558 can be seen in Fig. 2-4.

559 As no theoretical backing exists, the Greenwald density limit can simply be written
 560 (with citation) as:¹⁵

$$\hat{n} = N_G \cdot \left(\frac{I_P}{\pi a^2} \right) \quad (2.9)$$

561 Here, \hat{n} has units of $10^{20} \frac{\text{particles}}{\text{m}^3}$, N_G is the Greenwald density fraction, and I_P is again
 562 the plasma current (measured in mega-amps). ~~and π has its usual meaning(3.141592653...).~~
 563 The final variable is then the minor radius – a – which was previously defined through:

$$a = \epsilon \cdot R_0 \quad (2.1)$$

564 The next step is transforming the *line-averaged* density (\hat{n}) into the *volume-averaged*
 565 version (\bar{n}) used in this model. Harnessing the simplicity of the density's parabolic
 566 profile allows this relation to be written in a closed form as:

$$\hat{n} = \frac{\sqrt{\pi}}{2} \cdot \left(\frac{\Gamma(\nu_n + 2)}{\Gamma(\nu_n + \frac{3}{2})} \right) \cdot \bar{n} \quad (2.10)$$

567 Where $\Gamma(\dots)$ represents the gamma function: the non-integer analogue of the facto-
 568 rial function.

569 Combining these pieces allows the volume-averaged density to be written in standard-
 570 ized units (~~i.e. the ones we use~~) as:

$$\bar{n} = K_n \cdot \left(\frac{I_P}{R_0^2} \right) \quad (2.11)$$

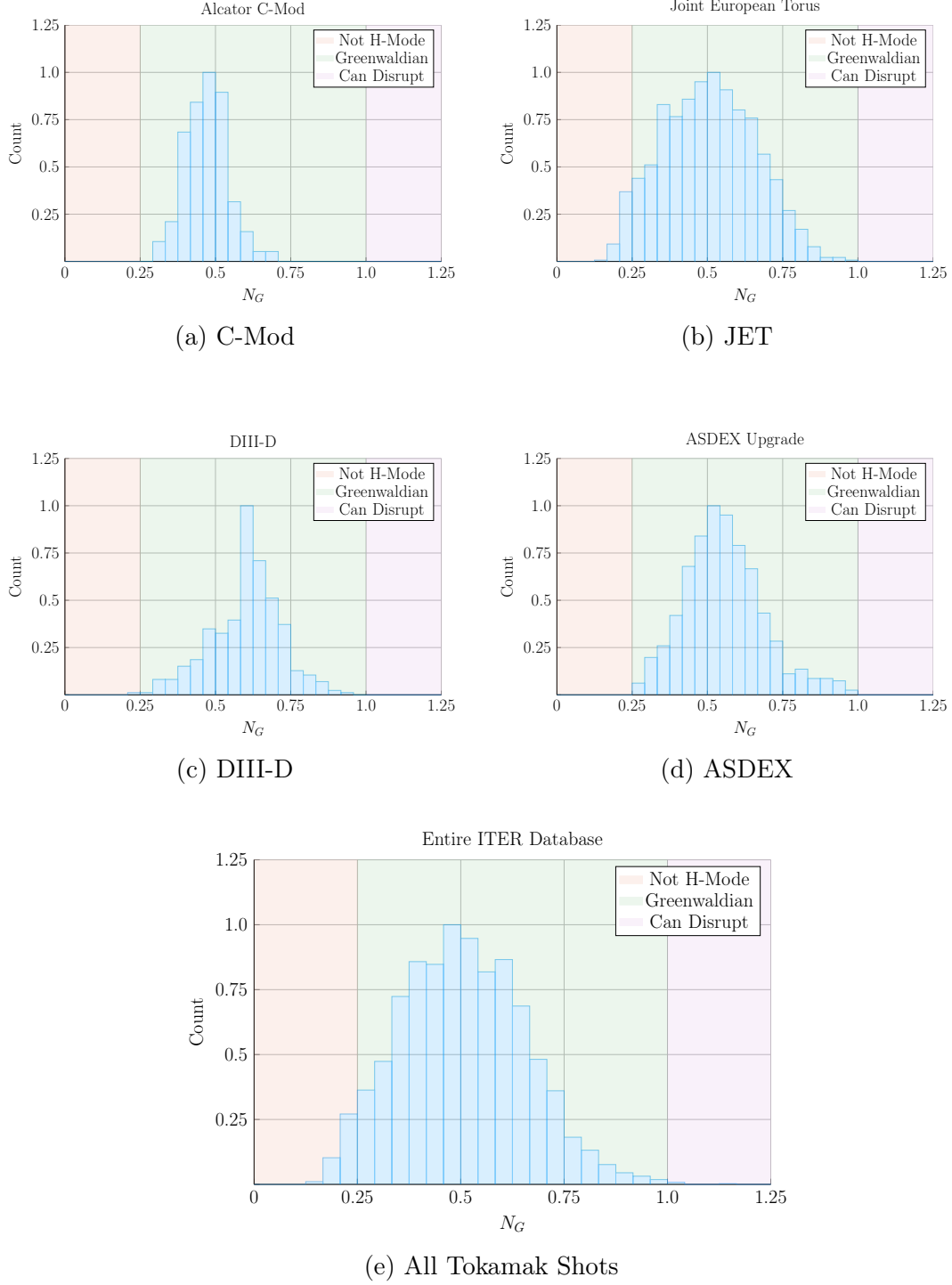


Figure 2-4: Greenwald Density Limit

The Greenwald Density Limit is a robust metric of what densities an H-Mode plasma can attain. Although empirical in nature, it accurately predicts when a tokamak will undergo degraded plasma transport.¹⁵ it is an indicator for good transport regimes.

571

$$K_n = \frac{2N_G}{\epsilon^2 \pi^{3/2}} \cdot \left(\frac{\Gamma(\nu_n + \frac{3}{2})}{\Gamma(\nu_n + 2)} \right) \quad (2.12)$$

572 The format of the previous equation pair will be used throughout the remainder of
 573 the paper. The top equation relates ~~dynamicfloating~~ variables (i.e. \bar{n} , I_P , and R_0),
 574 while the ~~staticfixed~~-value coefficient (K_n) lumps together ~~staticfixed~~ quantities, such
 575 as: N_G , ϵ , 2, π , and ν_n .

576 2.2.2 Declaring the Bootstrap Current

577 The first term to define in current balance, Eq. (2.8), is the bootstrap current. This
 578 bootstrap current is a mechanism of tokamak plasmas that helps supply some of
 579 the current needed to keep a plasma in equilibrium~~stable~~. Its underlying behavior
 580 stems from particles stuck in banana-shaped orbits on the outer edges of the device
 581 propelling the majority species along their helical trajectories around the tokamak.
 582 ~~From a hand-waving perspective, it involves particles stuck in banana-shaped orbits~~
 583 ~~on the outer edges of a tokamak behaving like racing-game style speed boosts that~~
 584 ~~accelerate charged particles along their hooped-shaped race tracks.~~

585 Utilizing the surface integral from Eq. (E.25), the bootstrap current (I_{BS}) can be
 586 written in terms of the temperature and density profiles: ~~To get an equation for~~
 587 ~~bootstrap current, we must first introduce the surface integral—made possible from~~
 588 ~~our previous choice of geometric parameters:—~~

589 ~~Here, Q is an arbitrary function of the normalized radius (ρ) and g is a geometric~~
 590 ~~factor (of order 1):~~

591 ~~This allows the bootstrap current (I_{BS}) to be written in terms of the temperature~~
 592 ~~and density profiles:~~

$$I_{BS} = 2\pi a^2 \kappa g \int_0^1 J_{BS} \rho d\rho \quad (2.13)$$

593

$$\begin{aligned}
J_{BS} &= f\left(n, T, \frac{dn}{d\rho}, \frac{dT}{d\rho}\right) \\
&\equiv -4.85 \cdot n \cdot T \cdot \frac{R_0 \sqrt{\epsilon} \rho}{d\psi/d\rho} \cdot \left(\frac{1}{n} \frac{dn}{d\rho} + 0.54 \frac{1}{T} \frac{dT}{d\rho} \right)
\end{aligned} \tag{2.14}$$

594 The second definition for the bootstrap current density – J_{BS} – comes from using
595 well known theoretical results plus several simplifying assumptions, including the
596 large aspect limit. The value of $d\psi/d\rho$ is given in Appendix F.

597 ~~For a more formal look into this J_{BS} function, check the appendix section on pedestal~~
598 ~~temperatures. The point to make now is that it depends on the the profiles' derivatives,~~
599 ~~leading to one major discrepency in the model.~~

600 As shown later in the results, bootstrap fractions are often under-predicted by this
601 model. This is due to parabolic profiles (i.e. for temperature) having much less steep
602 declines near the edge (i.e. in their derivatives) than characteristic H-Mode profiles
603 with pedestals. This implies that the area most positively impacted by a pedestal
604 profile for temperature would be the bootstrap current derivation. The instructions
605 to do so are given in Appendix D.4.

606 ~~Getting back on track—and without completeness—the bootstrap current can now~~
607 ~~be written in proportionality form as:~~

608 ~~Recognizing that the last term is basically the inverse of the Greenwald density (see~~
609 ~~Eq. 2.11), allows the proportionality to be written in the following form. Note that~~
610 ~~this implies the bootstrap current is only a function of temperature!~~

611 ~~In standardized units, this proportionality can be written as a concrete relation of~~
612 ~~the form:~~

613 Finally, summarizing the results of Appendix F, the bootstrap current is found to be
614 only a function of temperature and static variables! In standardized units, it can be
615 written as:

$$I_{BS} = K_{BS} \cdot \bar{T}$$

(2.15)

616

$$K_{BS} = 4.879 \cdot K_n \cdot \left(\frac{1 + \kappa^2}{2} \right) \cdot \epsilon^{5/2} \cdot H_{BS} \quad (2.16)$$

617

$$H_{BS} = (1 + \nu_n)(1 + \nu_T)(\nu_n + 0.054\nu_T) \int_0^1 \frac{\rho^{5/2} (1 - \rho^2)^{\nu_n + \nu_T - 1}}{b_p} d\rho \quad (2.17)$$

618 Quickly noting, this H_{BS} term serves as the analogue of ~~static~~~~fixed~~-value coefficients
 619 (e.g. K_{BS} and K_n) when they contain an integral. And b_p represents the poloidal
 620 magnet strength given by Eq. 2.7.

621 2.2.3 Deriving the Fusion Power

622 ~~The next segue on our journey to solving for the steady current is deriving the fusion~~
 623 ~~power (P_F), which appears in current drive. This requires a more first-principles~~
 624 ~~approach than those used up until now. As such, a quick background is given to~~
 625 ~~motivate the parameters it adds—i.e. the dilution factor (f_D) and the Bosch-Hale~~
 626 ~~fusion reactivity (σv).~~

627 ~~The natural place to start when talking about fusion is the binding-energy per nucleon~~
 628 ~~plot (see Fig. N). As can be seen, the function reaches a maximum value around the~~
 629 ~~element Iron ($A=56$). What this means at a basic level is: elements lighter than iron~~
 630 ~~can *fuse* into a heavier one (i.e. hydrogens into helium), whereas heavier elements~~
 631 ~~can *fission* into lighter ones (e.g. uranium into krypton and barium). This is what~~
 632 ~~differentiates fission (uranium-fueled) reactors from fusion (hydrogen-fueled) ones.~~
 633 ~~For fusion reactors, the most common reaction in a first-generation tokamak will be:~~
 634 ~~What this reaction describes is two isotopes of hydrogen—i.e. deuterium and tritium~~
 635 ~~—fusing into a heavier element, helium, while simultaneously ejecting a neutron. The~~
 636 ~~entire energy of the fusion reaction (E_F) is then divvied up 80-20 between the neutron~~
 637 ~~and helium, respectively. Quantitatively, the helium (hereafter referred to as an alpha~~
 638 ~~particle) receives 3.5 MeV.~~

639 ~~The final point to make before returning to the fusion power derivation is the main~~
 640 ~~difference between the two fusion products: helium (i.e. the alpha particle) and the~~

neutron. First, neutrons lack a charge—they are neutral. This means they cannot be confined with magnetic fields. As such, they simply move in straight lines until they collide with other particles. As the structure of a tokamak is mainly metal, the neutron is much more likely to collide there than the gaseous plasma, which is orders of magnitude less dense. Conversely, alpha particles are charged—when stripped of their electrons—and can therefore be kept within the plasma using magnets. What this means practically is that of the 17.6 MeV that comes from every fusion reaction, only 3.5 MeV remains inside the plasma (within the helium particle species).

The next segue on our journey to solving for the steady current is deriving the fusion power (P_F), which appears in current drive. A comprehensive introduction to this is given in Appendix C. Summarized, though, a formula for Returning to the problem at hand, the fusion power from a D-T reaction – in megawatts – is given by the following volume integral:⁷ –Jeff Freidberg’s textbook through the following volume integral:–

$$P_F = \int E_F n_D n_T \langle \sigma v \rangle d\mathbf{r} \quad (2.18)$$

$$E_F = 17.6 \text{ MeV} \quad (2.19)$$

The E_F quantity is the energy created from a deuterium-tritium fusion reaction. The n_D and n_T in this equation then represent the density of the deuterium and tritium ions, respectively. Assuming a 50-50 mix of the two, they can be related to the electron density – i.e. the one used in this model – through the dilution factor (f_D). This dilution factor represents the decrease in available fuel from part of the plasma actually being composed of non-hydrogen gasses:

$$n_D = n_T = f_D \cdot \left(\frac{n}{2}\right) \quad (2.20)$$

The fusion reactivity, $\langle \sigma v \rangle$, is then a nonlinear function of the temperature, T , which the model approximates using the Bosch-Hale tabulation (described in the appendix). As this tabulated value appears inside an integral, it seems important to point out that the temperature is now the most difficult dynamicfloating variable to handle –

665 over R_0 , B_0 , \bar{n} , and I_P . This will come into play when the model is formalized next
 666 chapter.

667 The next step in the derivation of fusion power is transforming the three-dimensional
 668 volume integral (see Eq. 2.18) into a zero-dimension averaged value. First, the volume
 669 analogue of the previously given surface-area integral is:

$$Q_V = 4\pi^2 R_0 a^2 \kappa g \int_0^1 Q(\rho) \rho d\rho \quad (2.21)$$

670 Where again, Q is an arbitrary function of ρ and g is a geometric factor approximately
 671 equal to one. The fusion power can now be rewritten as:

$$P_F = \pi^2 E_F f_D^2 R_0 a^2 \kappa g \int_0^1 n^2 \langle \sigma v \rangle \rho d\rho \quad (2.22)$$

672 In standardized units, this becomes:

$$P_F = K_F \cdot \bar{n}^2 \cdot R_0^3 \cdot (\sigma v) \quad (2.23)$$

673

$$K_F = 278.3 \cdot f_D^2 \cdot (\epsilon^2 \kappa g) \quad (2.24)$$

674 Where the standardized fusion reactivity is now,

$$(\sigma v) = 10^{21} (1 + \nu_n)^2 \int_0^1 (1 - \rho^2)^{2\nu_n} \langle \sigma v \rangle \rho d\rho \quad (2.25)$$

675 ~~As mentioned before, this fusion power is divvied up 80-20 between the neutron and~~
 676 ~~alpha particle. These relations will be used shortly. For now, they can be described~~
 677 ~~mathematically as:~~ At this point, the current drive needed for steady-state can now
 678 be defined.

2.2.4 Using Current Drive

As may have been lost along the way, ~~this chapter's the current~~ mission is to define a formula for steady current – from the current balance equation for steady-state tokamaks:

$$I_P = I_{BS} + I_{CD} \quad (2.8)$$

In standardized units, the equation for current drive is often given in the literature as:¹⁶

$$I_{CD} = \eta_{CD} \cdot \left(\frac{P_H}{\bar{n}R_0} \right) \quad (2.26)$$

Here, η_{CD} is the current drive efficiency with units $\left(\frac{\text{MA}}{\text{MW}\cdot\text{m}^2} \right)$ and P_H is the heating power in megawatts driven by LHCD (and absorbed by the plasma).

Let it be known, though, that driving current in a plasma is hard! In fact, pulsed reactor designers (i.e. European fusion researchers) think it is so difficult, they may choose to forego it completely – focusing only on inductive sources that necessitate reactor fatigue and downtime.

A common current drive efficiency (η_{CD}) seen in many designs is 0.3 ± 0.1 in the standard units. It is however inherently a function of all the plasma parameters – with subtlety put off until the discussion of self-consistency. For now it assumed to have some constant/~~static~~~~fixed~~ value.

The remaining step in deriving an equation for driven current (I_{CD}) is a formula for the heating power (P_H). The way fusion systems models – like this one – handle the heating power is through the physics gain factor, Q . Sometimes referred to as big Q , this value represents how many times over the heating power (P_H) is amplified as it is transformed into fusion power (P_F):

$$P_H = \frac{P_F}{Q} \quad (2.27)$$

Now, utilizing the previously defined Greenwald density and fusion power:

$$\bar{n} = K_n \cdot \left(\frac{I_P}{R_0^2} \right) \quad (2.11)$$

$$P_F = K_F \cdot \bar{n}^2 \cdot R_0^3 \cdot (\sigma v) \quad (2.23)$$

The current from LHCD can be written as:

$$I_{CD} = K_{CD} \cdot I_P \cdot (\sigma v) \quad (2.28)$$

$$K_{CD} = (K_F K_n) \cdot \frac{\eta_{CD}}{Q} \quad (2.29)$$

As η_{CD} and Q appear within a ~~staticfixed~~ coefficient, it is implied that both remain constant throughout a solve. This subtlety is lifted when handling η_{CD} self-consistently, which will be discussed shortly. However, even in that context, it proves beneficial to still think of η_{CD} as a sequence of ~~staticfixed~~ variables – set by the model rather than the user.

2.2.5 Completing the Steady Current

~~TheAs hinted along the way, the~~ goal of this ~~chaptersection~~ has been to derive a simple formula for steady current (I_P). The problem started with current balance in a steady-state reactor:

$$I_P = I_{BS} + I_{CD} \quad (2.8)$$

Two equations were then found for the bootstrap (I_{BS}) and driven (I_{CD}) current:

$$I_{BS} = K_{BS} \cdot \bar{T} \quad (2.15)$$

$$I_{CD} = K_{CD} \cdot I_P \cdot (\sigma v) \quad (2.28)$$

Combining these three equations and solving for the total plasma current (I_P) – in

716 mega-amps – yields:

$$I_P = \frac{K_{BS} \bar{T}}{1 - K_{CD}(\sigma v)} \quad (2.30)$$

717 This is the answer we have been seeking!

718 As mentioned before, this simple formula appears to only depend on temperature!*

719 Apparently, the plasma should have the same current at some temperature (i.e. $\bar{T} =$
720 15 keV), regardless of the size of the machine or the strength of its magnets. This
721 has the important corollary that each temperature maps to only one current value.
722 Further, each temperature would then map to a single magnet strength, capital cost,
723 etc. (as shown next chapter).

724 As has become a mantra, though, the subtlety of this behavior lies in the self-
725 consistency of the current-drive efficiency – η_{CD} .

726 2.3 Handling Current Drive Self-Consistently

727 Although a thorough description of the wave theory behind lower-hybrid current
728 drive (LHCD) is well outside the scope of this text, it does motivate the solving of
729 a tokamak’s major radius (R_0) and field strength (B_0). It also shows how what was
730 once a simple problem has now transformed into a rather complex one – a common
731 occurrence with plasmas.

732 The logic behind finding a self-consistent current-drive efficiency is starting at some
733 plausible value (i.e. $\eta_{CD} = 0.3$), solving for the steady current – i.e. $I_P = f(\bar{T})$ – and
734 then somehow iteratively creeping towards a value deemed self-consistent. What this
735 means is that in addition to the solver described in the last section, there needs to
736 be a black-box function that solutions are sent piped through to get better guesses at
737 η_{CD} . The black-box function we use is a variation of the Ehst-Karney model.¹⁷

738 As mentioned, a self-consistent η_{CD} is found once a trip through the Ehst-Karney

*This dependence only on temperature refers to dynamic variables. The plasma current can still be highly volatile to many of the static variables, such as: ϵ , κ , N_G , f_D , ν_n , l_i , etc.

739 black-box results in the same η_{CD} as was ~~sent~~~~ipped~~ in – to some tolerable level of error.

740 This consistency incorporates an explicit dependence on the tokamak configuration.

741 Mathematically,

$$\tilde{\eta}_{CD} = f(R_0, B_0, \bar{n}, \bar{T}, I_P) \quad (2.31)$$

742 As such, to recalculate it after every solution of the steady current requires a value

743 for both B_0 and R_0 – the targets of this model’s primary and ~~limiting~~~~secondary~~

744 constraints. These will be the highlight of the next chapter.

Chapter 3

Formalizing the Systems Model

The goal of this chapter is to take a step back from the steady current derivation and see the larger picture behind reactor design. As such, a more in-depth description of ~~staticfixed~~ and ~~dynamicfloating~~ variables is given. This discussion of ~~dynamicfloating~~ variables will then lend itself to a description of the framework underpinning the fusion systems model. As such, we will now need formulas for the radius and magnet strength of the tokamak. Moving forward, the current will ~~then~~ remain a connecting piece as we ~~redirect focusswitch-gears~~ to pulsed tokamaks and compare ~~the underlying solvers of the two schemes~~.~~the two schemes' underlying solvers.~~

The end result of this analysis will then be equations that allow the density (\bar{n}), current (I_P), major radius (R_0), and magnet strength (B_0) to be written as functions of the temperature (\bar{T}) and static variables (e.g. ν_n , N_G , f_D). These formulas are the product of applying constraints required for all tokamak reactors with several other limiting constraints. The constraints relevant to all tokamak reactors are: the Greenwald limit, current balance, and power balance. Limit constraints then include: the Troyon beta limit, the kink safety factor, the wall loading limit, the maximum power constraint, and the heat loading limit.

Actual methodologies for solving for the five dynamic variables simultaneously – i.e. \bar{T} , \bar{n} , I_P , R_0 , B_0 – are put off until Chapter 5.

765 3.1 Explaining StaticFixed Variables

766 In this model, ~~staticfixed~~ variables are ones that remain constant while solving for
 767 a reactor. These include geometric scalings (i.e. ϵ , δ , κ), profile parameters (i.e. ν_n ,
 768 ν_T , l_i), and a ~~couple dozens~~ of physics constants related to pulsed and steady-
 769 state design (e.g. Q , N_G , f_D). For a complete list of ~~staticfixed~~ variables, consult
 770 ~~Appendix A~~~~the appendix~~. The point to make now is that this model treats ~~staticfixed~~
 771 variables as ~~immutable~~~~second-class~~ objects. As such they often reside in ~~staticfixed~~
 772 coefficients – K_\square – which are treated as constants.

773 3.2 Connecting DynamicFloating Variables

774 ~~DynamicFloating~~ variables – \bar{T} , \bar{n} , I_P , R_0 , B_0 – are the first-class variables of this
 775 fusion systems model. They represent the fundamental properties of a plasma and
 776 tokamak (which constitute a fusion reactor). As such, they will be reintroduced one
 777 at a time, explaining how they fit into the model – and which ~~equations are~~~~equation~~
 778 ~~is~~ capable of representing ~~them~~~~it~~.

Table 3.1: Dynamic Variables

Symbol	Name	Units
I_P	Plasma Current	MA
\bar{T}	Plasma Temperature	keV
\bar{n}	Electron Density	10^{20} m^{-3}
R_0	Major Radius	m
B_0	Magnetic Field	T

779 Bluntly, this fusion systems model is a simple algebra problem: solve five equations
 780 with five unknowns (i.e. \bar{T} , \bar{n} , I_P , R_0 , B_0). Although this naive approach would work,
 781 we can do a little better by ~~collapsing~~~~wrangling~~ these five equations down to just one.
 782 This was already done while deriving the steady current. It just happened that the
 783 current was not directly dependent on the tokamak size (R_0) or magnet strength (B_0).
 784 This will prove more challenging for the generalized current needed for pulsed oper-

785 ation. Even so, this equation will still be ~~reducedboiled-down~~ to one equation with a
786 single unknown – I_P . A solution to which can be solved much faster than the naive
787 5 equation approach. This is one reason the model is so fast.

788 The Plasma Temperature – \bar{T}

789 The plasma temperature, measured in keV (kilo-electron-volts), is one of the most
790 ~~nonlinearfinicky~~ variables in the fusion systems ~~frameworkmodel~~. It first proved trou-
791 blesome when it was shown that a pedestal profile – not a parabolic one used here
792 – would be needed for an accurate calculation of bootstrap current. The ~~black-~~
793 ~~boxunusual~~ tabulation for reactivity – (σv) – which appeared in fusion power only
794 further exposed this nonlinearity.

795 Acknowledging that temperature is the most difficult to handle parameter prompts its
796 use as the scanned variable. What this means practically is scanning temperatures ~~is~~
797 ~~the most straightforward method to produceproduces~~ curves of reactors. By example,
798 a scan may be run over the average temperatures (\bar{T}): 10, 15, 20, 25, and 30 keV –
799 ~~where each correspondseorresponding~~ to its own reactor ~~with its own field strength~~
800 (B_0), plasma current (I_P), etc. In equation form, this becomes:

$$\bar{T} = \text{const.} \quad (3.1)$$

801 The constant value, here, ~~Where the constant~~ happens to be 10 keV in one run, 15
802 keV for the next, and 30 keV in the fifth.

803 The Plasma Density – \bar{n}

804 The Greenwald density limit is a constraint with a simple form that applies to all
805 tokamak reactors. ~~The cornerstone of this fusion systems model has always been the~~
806 ~~application of the Greenwald density limit from square one.~~ It is for this reason – as
807 well as being a good approximation – that a parabolic profile was rationalized over a

808 pedestal (H-Mode) one. Repeated, the Greenwald density limit is:

$$\bar{n} = K_n \cdot \frac{I_P}{R_0^2} \quad (2.11)$$

809 This is an exceptionally simple relationship and why it guided the model. Unlike the
810 next three variables, it is actually used in their derivations. ~~Therefore, any reactor~~
811 ~~found through this model is considered a *Greenwaldian Reactor*—one held at the~~
812 ~~Greenwald density limit.~~

813 **The Plasma Current – I_P**

814 The plasma current is what separates steady-state from pulsed operation. From
815 before, the steady current was found to be:

$$I_P = \frac{K_{BS}\bar{T}}{1 - K_{CD}(\sigma v)} \quad (2.30)$$

816 This was derived by setting the total current equal to the two sources of current:
817 bootstrap and current drive. Or in fractional form,

$$I_P = I_{BS} + I_{CD} \rightarrow 1 = f_{BS} + f_{CD} \quad (3.2)$$

818 This says that the current fractions of bootstrap and current drive must sum to one.
819 As shown next chapter, inductive sources can be included into this current balance:

$$1 = f_{BS} + f_{CD} + f_{ID} \quad (3.3)$$

820

821 This equation shows how steady-state and pulsed operation can coexist (see Fig. 3-1).
822 The final point to make is reducing the model to being purely pulsed – i.e. neglecting
823 the current drive:

$$1 = f_{BS} + f_{ID} \quad (3.4)$$

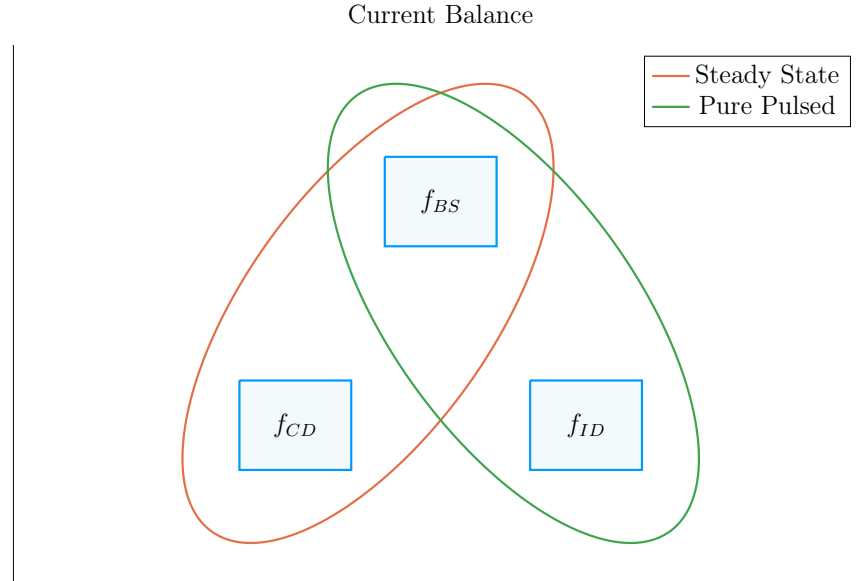


Figure 3-1: Current Balance in a Tokamak

In a tokamak, there needs to be a certain amount of current – and that current has to come from somewhere. All good reactors have an adequate bootstrap current. What provides the remaining current is what distinguishes steady state from pulsed operation.

Therefore, the next chapter will generalize the steady current to allow pulsed operation, and then simplify it to the purely pulsed case. Just as steady current faced self-consistency issues with η_{CD} , this current will also involve its own root solving conundrum – the description of which will be given in the following two chapters.

The Tokamak Magnet Strength – B_0

The tokamak magnet strength has no ~~uniqueobvious~~ equation to eliminate it. With foresight, the one this model ~~useschooses-to-use~~ is the power balance inherent to everyin-a reactor. Similar to current balance, power balance is what separates a reactor from a ~~device incapable of producing net electricitytoaster~~. As such, it is referred throughout this document as: the primary constraint. It will be derived later this chapter.

835 The Tokamak Major Radius – R_0

836 Much like the magnet strength, the major radius has no ~~unique~~~~obvious~~ relation to
837 express it. ~~The model therefore uses this equation to handle a reactor's various~~~~This is~~
838 ~~convenient, because the model still has yet to resolve one of its most pressing issues:~~
839 physical and engineering-based constraints. This ~~laundry~~ list of requirements further
840 restricts reactor space to the curves shown in the results section. Collectively, these
841 are referred to as the ~~limiting~~~~secondary~~ constraints – discussed later this chapter.
842 ~~These~~~~By miraele, these~~ constraints all just happen to depend on the size of the reactor
843 – the reason they are chosen to ~~represent~~~~substitute out~~ the radius.

844 3.3 Enforcing Power Balance

845 What separates a reactor from a ~~device incapable of producing net electricity~~~~toaster~~
846 is power balance. ~~Within a tokamak, it~~~~It~~ accounts for how the power going into
847 a plasma's core exactly matches the power coming out of it. To approximate this
848 conservation equation, two sets of power will be introduced: the sources and the
849 sinks.

850 The sources have mainly been introduced at this point – they include the alpha
851 power (P_α) ~~from fusion reactions~~ and the heating power (P_H), as well as a new ohmic
852 power term (P_Ω). The remaining two powers – the sinks – then appear through the
853 radiation and heat conduction losses, which will be given shortly. In equation form,
854 power balance becomes:

$$\sum_{sources} P = \sum_{sinks} P \quad (3.5)$$

855 or expanded to fit this model:

$$P_\alpha + P_H + P_\Omega = P_{BR} + P_\kappa \quad (3.6)$$

856 For clarity, the left-hand side of this equality are the sources. Whereas the remaining

two are sinks, i.e. Bremsstrahlung radiation (P_{BR}) and heat conduction losses (P_{κ}).

3.3.1 Collecting Power Sources

As suggested, the two dominant sources of power in a tokamak are: alpha power (P_{α}) and auxiliary heating (P_H). From Appendix C, it was determined that alpha particles (i.e. helium nuclei) carry around 20% of the total fusion power; or as we put it mathematically:

$$P_{\alpha} = \frac{P_F}{5} \quad (3.7)$$

Additionally, it was determined that the heating power is what was eventually amplified into fusion power – or through equation:

$$P_H = \frac{P_F}{Q} \quad (3.8)$$

The final source term then is the ohmic power (P_{Ω}). This is identical to how copper wires in a home heat up as current runs through them. From a simple circuits picture, the power across the plasma is related to its current and resistance – in our standardized units – through:

$$P_{\Omega} = 10^6 \cdot I_P^2 \cdot R_P \quad (3.9)$$

~~Here, the resistance of the plasma is unlike any material humans encounter on a daily basis—actually decreasing with temperature. This~~The fusion systems model handles the plasma resistance (R_P) with the neoclassical Spitzer resistivity. Through equation,⁴

$$R_P = \frac{K_{RP}}{R_0 \bar{T}^{3/2}} \quad (3.10)$$

$$K_{RP} = 5.6e-8 \cdot \left(\frac{Z_{eff}}{\epsilon^2 \kappa} \right) \cdot \left(\frac{1}{1 - 1.31\sqrt{\epsilon} + 0.46\epsilon} \right) \quad (3.11)$$

874 Combined with the Greenwald limit, ohmic power can be written more compactly as,

$$P_{\Omega} = K_{\Omega} \cdot \left(\frac{\bar{n}^2 R_0^3}{T^{3/2}} \right) \quad (3.12)$$

875

$$K_{\Omega} = 10^6 \cdot \frac{K_{RP}}{K_n^2} \quad (3.13)$$

876 With the sources defined, we are now in a position to discuss the two sink terms used
877 in this model's power balance.

878 3.3.2 Approximating Radiation Losses

879 All nuclear reactors emit radiation. From a power balance perspective, this means
880 some power has to always be reserved to recoup from its losses – measured in megawatts.
881 In a fusion reactor, the three most important types of radiation are: Bremsstrahlung
882 radiation, line radiation, and synchrotron radiation.

883 ~~This Without going into too much detail, this~~ model chooses to only model Bremsstrahlung
884 radiation – as it usually dominates within the plasma's core. ~~Within most designs,~~
885 ~~Bremsstrahlung radiation outweighs the other two's contribution, to core power bal-~~
886 ~~ance, two-to-one.~~^{2,7} However, adding the effects of line-radiation and synchrotron
887 radiation would drive results closer to real-world experiments. For example, line-
888 radiation would better account for the ~~effects of~~ heavy impurities that ~~are emitted~~
889 ~~from the divertor plate and first wall appear as pieces of a tokamak fall into the plasma.~~
890 For clarity, Bremsstrahlung – or breaking – radiation is what occurs when a charged
891 particle (e.g. an electron) is accelerated by some means. In a tokamak, this happens
892 all the time as ~~electrons collide with the ion species.~~¹⁸~~charged particles are flung~~
893 ~~around and around the machine.~~ This term can be ~~As given in Jeff Freidberg's book,~~
894 ~~this term is~~ described by the volume integral:⁴

$$P_{BR} = \int S_{BR} d\mathbf{r} \quad (3.14)$$

895 ~~Where~~Here, the radiation power density (S_{BR}) is given by:

$$S_{BR} = \left(\frac{\sqrt{2}}{3\sqrt{\pi^5}} \cdot \frac{e^6}{\epsilon_0^2 c^3 h m_e^{3/2}} \right) \cdot (Z_{eff} n^2 T^{1/2}) \quad (3.15)$$

896 The constants in the left set of parentheses all have their usual physics meanings (i.e.
897 c is the speed of light and m_e is the mass of an electron). What is new is the effective
898 charge: Z_{eff} .

899 The effective charge is a scheme for ~~reducing~~collapsing the charge ~~each ion~~that ~~each~~
900 ~~partiele~~ has to a ~~single representative~~collective value. Fundamental charge, here, is
901 what: neutrons lack, electrons and hydrogen have one of, and helium has two. As
902 such, a plasma with a purely deuterium and tritium fuel would have an effective
903 charge of one. This value would then quickly rise if a Tungsten tile – with 74 units
904 of charge – were to fall into the plasma core from the walls of the tokamak.

905 Using the volume integral – seen in the derivation of fusion power – allows the
906 Bremsstrahlung power to be written in standardized units as:

$$P_{BR} = K_{BR} \bar{n}^2 \bar{T}^{1/2} R_0^3 \quad (3.16)$$

907

$$K_{BR} = 0.1056 \frac{(1 + \nu_n)^2 (1 + \nu_T)^{1/2}}{1 + 2\nu_n + 0.5\nu_T} Z_{eff} \epsilon^2 \kappa g \quad (3.17)$$

908 This power term represents the radiation power losses involved in power balance. All
909 that is needed now is a formula for heat conduction losses – ~~one of the most difficult~~
910 ~~plasma behavior~~the ~~hardest plasma behavior~~ to model to date.

911 3.3.3 Estimating Heat Conduction Losses

912 Heat is energy that ~~moves about randomly~~lacks ~~direction~~ on a microscopic level.
913 Macroscopically, it generally moves from hotter areas to colder ones. As hinted by
914 the plasma profile for temperature, heat emanates from the center of a plasma and
915 migrates towards the walls of its tokamak enclosure. It therefore ~~is a critical~~seems ~~an~~

916 ~~important~~ quantity to calculate when balancing power in a plasma's core.

917 The difficulty of estimating heat conduction, though, lies in the ~~nonlinear behavior~~~~chaotic~~
918 ~~nature~~ of plasmas – no theory or ~~quick-running code~~~~computation~~~~today~~ can properly
919 model it. As such, reactor designers have turned towards experimentalists for empir-
920 ical scaling laws based on the dozen or so strongest tokamaks in the world. These are
921 collectively referred to as confinement time scalings, i.e. the ELMy H-Mode Scaling
922 Law.

923 The derivation of this heat conduction loss term (P_κ) starts in a manner similar to
924 the previous powers. To begin, an equation for P_κ ~~can be found using the following~~
925 ~~volume integral:~~⁴~~is given in Jeff Freidberg's book as:~~

$$P_\kappa = \frac{1}{\tau_E} \int U d\mathbf{r} \quad (3.18)$$

926 This volume integral includes two new terms: the confinement time (τ_E) and the
927 internal energy (U). Before explaining these terms, a qualitative description is in
928 order. As mentioned previously, the heat – or microscopically random – energy is
929 captured by the internal energy (U). Then the confinement time (τ_E) is how long
930 it would take for the heat to ~~undergo an e-folding~~~~completely leave the device~~ if the
931 ~~device~~~~system~~ were suddenly turned off.

932 A formula for confinement time will be delayed till the end of this section, when it is
933 needed to solve for the magnetic field (B_0). The internal energy (U), however, can be
934 given now as it has its typical physics meaning. This assumes that all three plasma
935 species are held nearly at the same temperature (T) as the electrons:

$$U = \frac{3}{2} (n + n_D + n_T) T \quad (3.19)$$

936 Here again, n_D and n_T – the density of deuterium and tritium, respectively – are
937 related to the electron density (used in this model) through the dilution factor, which

938 assumes a 50-50 mix of D-T fuel:

$$n_D = n_T = f_D \cdot \left(\frac{n}{2} \right) \quad (3.20)$$

939 ~~After several substitutions,Foregoing the mathematical rigor of previous sections,~~ the
940 equations here can be combined to form an equation for P_κ – the heat conduction
941 losses – in standardized units:

$$P_\kappa = K_\kappa \frac{R_0^3 \bar{n} \bar{T}}{\tau_E} \quad (3.21)$$

942

$$K_\kappa = 0.4744 (1 + f_D) \frac{(1 + \nu_n)(1 + \nu_T)}{1 + \nu_n + \nu_T} (\epsilon^2 \kappa g) \quad (3.22)$$

943 Now that all five terms have been defined in power balance, the next step is expanding
944 it and solving for the tokamak’s toroidal magnetic field strength: B_0 .

945 3.3.4 Writing the Lawson ~~ParameterCriterion~~

946 Before ~~arriving at a formula forlocking in the primary constraint—i.e.~~ the magnet
947 strength (B_0) ~~usingequation from~~ power ~~balance,balancee~~ – it seems appropriate to
948 take a detour and explain an intermediate solution: the Lawson ~~ParameterCriterion~~.
949 Within the fusion community, the Lawson ~~ParameterCriterion~~ is the cornerstone in
950 any argument on the possibility of a ~~tokamak everdesign~~ being used as a ~~reactor.reactore~~
951 ~~(and not just some grandiose toaster).~~

952 An equation for the Lawson ~~ParameterCriterion~~ – sometimes referred to as the *triple*
953 *product* – is easily found in the literature as:

$$n \cdot T \cdot \tau_E = \frac{60}{E_F} \cdot \frac{T^2}{\langle \sigma v \rangle} \quad (3.23)$$

954 Similar to the steady current derived earlier, the right-hand side is only dependent
955 on temperature. Further, as the left-hand side is a measure of difficult to achieve

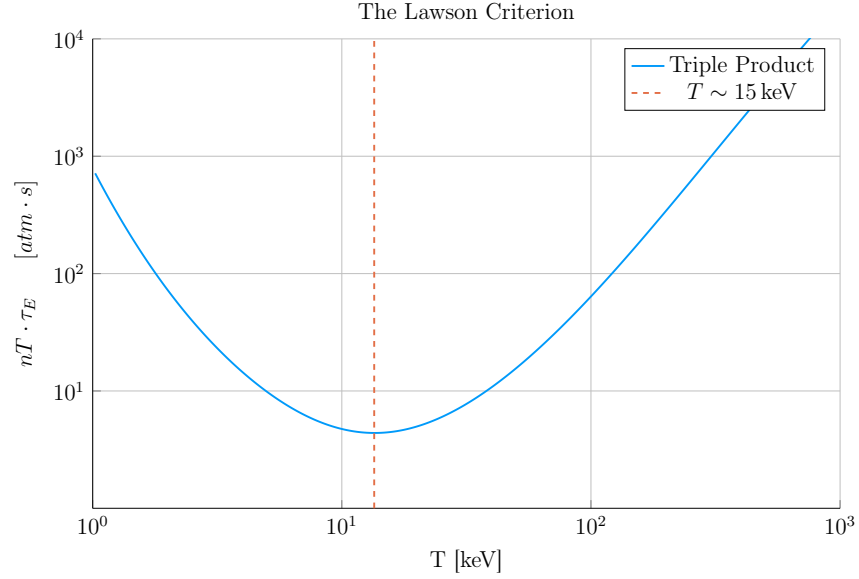


Figure 3-2: Power Balance in a Reactor

Power balance is what differentiates a reactor from a radiator. When cast as the Lawson ~~Parameter Criterion~~ for fusion, it explains why D-T plasmas often have a temperature around 15 keV.

parameters, the goal is to minimize both sides. As shown in Fig. 3-2, this occurs when the plasma temperature is around 15 keV – a fact well known to many fusion engineers. As will be seen, this is a simplified result of our model. This is why $\bar{T} = 15$ keV is not always the optimum temperature – but usually is in the right neighborhood for reasonable reactor designs.

As all the terms in power balance have already been defined, the starting point will be simply repeating the standardized equations for all five included powers.

$$P_{\alpha} = \frac{P_F}{5} \quad (3.7)$$

$$P_H = \frac{P_F}{Q} \quad (3.8)$$

$$P_{\Omega} = K_{\Omega} \cdot \left(\frac{\bar{n}^2 R_0^3}{\bar{T}^{3/2}} \right) \quad (3.12)$$

$$P_{BR} = K_{BR} \bar{n}^2 \bar{T}^{1/2} R_0^3 \quad (3.16)$$

966

$$P_\kappa = K_\kappa \frac{R_0^3 \bar{n} \bar{T}}{\tau_E} \quad (3.21)$$

967 With the fusion power again being,

$$P_F = K_F \cdot \bar{n}^2 \cdot R_0^3 \cdot (\sigma v) \quad (2.23)$$

968 These can then be substituted into power balance:

$$P_\alpha + P_H + P_\Omega = P_{BR} + P_\kappa \quad (3.6)$$

969 After a couple lines of algebra, power balance can be rewritten in a form analogous
970 to the triple product:

$$\bar{n} \cdot \bar{T} \cdot \tau_E = \frac{K_\kappa \bar{T}^2}{\left(K_P (\sigma v) + K_{OH} \bar{T}^{-3/2} \right) - K_{BR} \bar{T}^{1/2}} \quad (3.24)$$

971

$$K_P = K_F \cdot \left(\frac{5 + Q}{5 \times Q} \right) \quad (3.25)$$

972 As expected, this shares a form ~~As can be seen, this is remarkably~~ similar to the simple
973 Lawson ~~Parameter~~ **Criterion**:

$$n \cdot T \cdot \tau_E = \frac{60}{E_F} \cdot \frac{T^2}{\langle \sigma v \rangle} \quad (3.23)$$

974 The main difference is this model does not ignore ohmic power and radiation losses
975 completely. The inclusion of radiation for example sometimes bars a range of temper-
976 atures from being physically realizable.* With this intermediate relation in place, the
977 goal is now to give a formula for the confinement time and solve it for the magnetic
978 field strength (B_0) – thus giving the Primary Constraint.

*The denominator of Eq 3.24 has discontinuities when the $K_{BR} \bar{T}^{1/2}$ term exactly equals the parenthesised one. Therefore, valid reactors only exist outside the discontinuities, when the entire triple product is finite and positive.

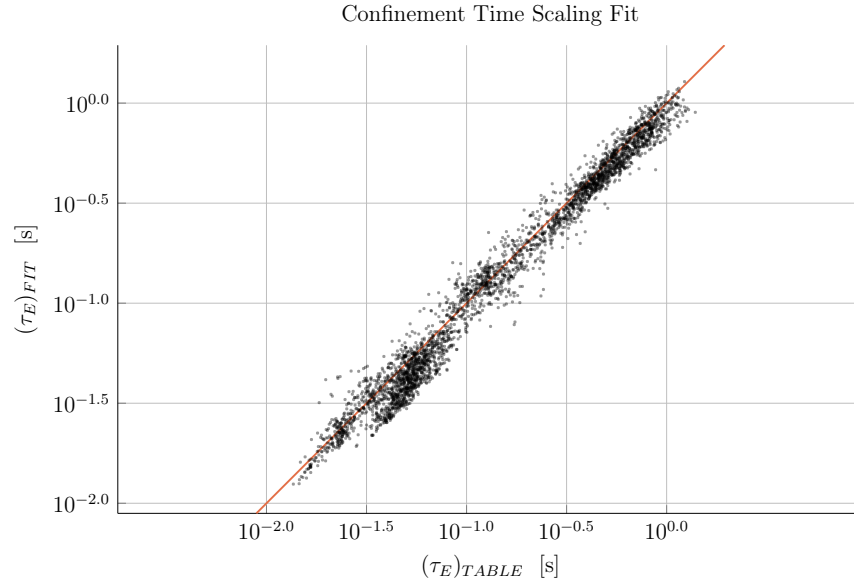


Figure 3-3: H-Mode Confinement Time Scaling

This plot shows how well the ELMy H-Mode Scaling Law does for fitting τ_E to the ITER98 database of global tokamaks. For most values, the fit is at least 80% accurate with the measured value.

3.3.5 Finalizing the Primary Constraint

The goal now is to transform the Lawson ~~Parameter~~~~Criterion~~ into an equation for magnet strength (B_0). This choice to solve the equation for B_0 was motivated by the goals of analysis and how it will fit ~~completely arbitrary, only motivated by the foresight of how it fits~~ into the fusion systems model. To solve the primary constraint, the confinement time scaling law will need to be introduced. At the end, a ~~convoluted~~~~messy~~ – albeit highly useful – relation will be the reward.

The energy confinement time – τ_E – is one of the most ~~difficult to obtain~~~~elusive~~ terms in all of fusion energy. It is an attempt to ~~reduce~~~~boil-down~~ all the ~~nonlinear behavior~~~~chaotic-nature~~ of plasmas into a simple measure of how fast its internal energy would be ejected from the tokamak if the device was instantaneously shut down. As such, reactor designers have turned toward experimentalists for empirical scalings based on the world's tokamaks (see Fig. 3-3). These all share a form similar

992 to:

$$\tau_E = K_\tau H \frac{I_P^{\alpha_I} R_0^{\alpha_R} a^{\alpha_a} \kappa^{\alpha_\kappa} \bar{n}^{\alpha_n} B_0^{\alpha_B} A^{\alpha_A}}{P_{src}^{\alpha_P}} \quad (3.26)$$

993 This ~~regressional fit~~~~mouthful of a formula~~ is how the field actually designs machines
994 (i.e. ITER). Let it be known, though, that ~~fits of this kind~~~~these fits~~ often do remark-
995 able well, having relative errors less than 20% on interpolated data. The new terms
996 in this equation are: P_{src} , K_τ , H , A , and the α_\square factors.

997 First, the loss power is a metric used in the engineering community to quantify the
998 power being transported out of the “core” of the plasma by charged particles (i.e. not
999 the neutrons).⁶ To optimize fits, experimentalists have defined this as a combination
1000 of the source power terms:

$$P_{src} = P_\alpha + P_H + P_\Omega \quad (3.27)$$

1001 ~~However, many have argued that the term should actually be replaced by its correct~~
1002 ~~physics meaning—the conductive heat loss power. As this model uses the ELMy~~
1003 ~~H-Mode scaling law, which is standard in the field, this alternative definition will~~
1004 ~~not be used:~~ Moving on, K_τ is simply a constant fit-makers use in their scalings.
1005 Whereas H is the ~~enhancement factor over the empirical fit.~~~~(H-Mode) scaling factor—~~
1006 ~~the analogue of K_τ used by reactor designers. This H factor can be used to artificially~~
1007 ~~boost the confinement of a machine (i.e. it adds a little bit of magic).~~ Next, Continuing,
1008 A is the average mass number of the fuel source, in atomic mass units. For a 50-50
1009 D-T fuel, this is 2.5, as deuterium weighs two amus and tritium weighs three. Lastly,
1010 the alpha factors (e.g. α_n , α_a , α_P) are fitting parameters that represent each variable’s
1011 relative importance in the scaling.

1012 For ELMy H-Mode, this confinement scaling law can be written as:

$$\tau_E = 0.145 H \frac{I_P^{0.93} R_0^{1.39} a^{0.58} \kappa^{0.78} \bar{n}^{0.41} B_0^{0.15} A^{0.19}}{P_{src}^{0.69}} \quad (3.28)$$

1013 ~~However, similar scaling laws~~~~Where similar ones~~ can be ~~writtengiven~~ for L-Mode,
1014 I-Mode, etc. One final remark to make before moving on is that even these fits
1015 have subtleties. The value of κ , for example, may have a slightly different geometric

1016 meaning from tokamak to tokamak. And the exact definition of loss power – P_{src} –
 1017 introduces an even larger area of discrepancy. ~~Although not actually used, a better~~
 1018 ~~fit for our model might be one from the author:~~

1019 Returning to the problem at hand, though, this model's Lawson ~~Parameter Criterion~~
 1020 (eq. 3.24) can be simplified after expanding the left-hand side using the Greenwald
 1021 density and substituting in a confinement time scaling law. ~~After a few lines of~~
 1022 ~~algebra, this can be transformed~~ ~~Albeit a little cumbersome, this can be wrangled~~
 1023 ~~into a formula~~ ~~an equation~~ for B_0 !

$$B_0 = \left(\frac{G_{PB}}{K_{PB}} \cdot \left(I_P^{\alpha_I^*} R_0^{\alpha_R^*} \right)^{-1} \right)^{\frac{1}{\alpha_B}} \quad (3.29)$$

$$G_{PB} = \frac{\bar{T} \cdot \left(K_P(\sigma v) + K_\Omega \bar{T}^{-3/2} \right)^{\alpha_P}}{\left(K_P(\sigma v) + K_\Omega \bar{T}^{-3/2} - K_{BR} \bar{T}^{1/2} \right)} \quad (3.30)$$

$$K_{PB} = H \cdot \left(\frac{K_\tau K_n^{\alpha_n^*}}{K_\kappa} \right) \cdot (\epsilon^{\alpha_a} \kappa^{\alpha_\kappa} A^{\alpha_A}) \quad (3.31)$$

1026 Where we have added new starred alpha values for the density, current, and major
 1027 radius:

$$\alpha_n^* = 1 + \alpha_n - 2\alpha_P \quad (3.32)$$

$$\alpha_I^* = \alpha_I + \alpha_n^* \quad (3.33)$$

$$\alpha_R^* = \alpha_R + \alpha_a - 2\alpha_n^* - 3\alpha_p \quad (3.34)$$

1030 ~~Again, if the alternate definition for heat loss (\tilde{P}_{abs}) were used, another definition for~~
 1031 ~~G_{PB} would arise. Quickly reemphasizing, though, these tilded values are not actually~~
 1032 ~~used in the model:~~

1033 This equation for B_0 – derived from power balance – is thus the primary constraint
 1034 for reactor designs. It is the first step in connecting the plasma (i.e. \bar{n} , \bar{T} , and I_P) to
 1035 its tokamak enclosure (i.e. B_0 and R_0). The remaining step is finding an equation –

1036 or in this case, equations – for the major radius of the device. These radius equations
 1037 will collectively be referred to as: the ~~limiting constraints.Secondary Constraints.~~
 1038 ~~Before moving onto the Secondary Constraint, it is worth noting that this power~~
 1039 ~~balance equation can be written in a triple product form analogous to the Lawson~~
 1040 ~~ParameterCriterion.~~ For this reason, we will refer to it as the Freidberg Triple
 1041 ~~Product:~~
 1042 ~~As is readily apparent, this has a shape similar to the Lawson ParameterCriterion.~~
 1043 ~~Again, the goal is operate when the right hand side reaches an approximate minimum.~~
 1044 ~~This corresponds to when the left hand side is also minimized — where each term~~
 1045 ~~represents one of the difficult to achieve quantities of a tokamak fusion reactor.~~

1046 3.4 Collecting ~~LimitingSecondary~~ Constraints

1047 As of now, the only missing equation within our list of ~~staticfixed~~ variables – i.e.
 1048 R_0 , B_0 , \bar{T} , \bar{n} , and I_P – is for the major radius of the tokamak. This equation will
 1049 come from around five potential limits, each either physical or engineering-based.
 1050 These limits will then correspond to different curves through reactor space. As will
 1051 be shown, many of these reactors will be invalid (as they violate at least one of the
 1052 other limits). ~~Our analysis is always based on selecting the most stringent criterion.~~
 1053 Before tackling the subject of finding reactors that exist on the fine line of satisfying
 1054 every ~~limitingsecondary~~ constraints, though, it is essential to collect them one-by-one.
 1055 These are: the Troyon Beta Limit, the Kink Safety Factor, the Wall Loading Limit,
 1056 the Power Cap Constraint, and the Heat Loading Limit.
 1057 The goal of this section is to solve for each of these constraints on the major radius. As
 1058 with the primary constraint, this choice of solving for R_0 was ~~not completely unique,~~
 1059 ~~just motivated by physics and engineering concerns.completely arbitrary.~~ It just so
 1060 happens that each limit described here depends on the size of a reactor – which is
 1061 not true for the magnetic field strength.

1062 3.4.1 Introducing the Beta Limit

1063 The Beta Limit is the most important ~~limitingsecondary~~ constraint – especially for
 1064 steady-state reactors. It sets a maximum on the amount of pressure a plasma is
 1065 willing to tolerate. As with future ~~limitingsecondary~~ constraints, literature-based
 1066 equations will be transformed into formulas for R_0 . Each will then contain some
 1067 limiting quantity that can be handled by a ~~staticfixed~~ variable – as β_N will be used
 1068 shortly.

1069 The starting point for the beta limit is to define the important plasma physics quan-
 1070 tity: β – the plasma beta. This value is a ratio between a plasma’s internal pressure
 1071 and the pressure exerted on it by the tokamak’s magnetic configuration. Mathemat-
 1072 ically,⁴

$$\beta = \frac{\text{plasma pressure}}{\text{magnetic pressure}} = \frac{\bar{p}}{\left(\frac{B_0^2}{2\mu_0}\right)} \quad (3.35)$$

1073 Using this model’s temperature and density profiles, the volume-averaged pressure
 1074 (\bar{p}) can be written in units of atmospheres (i.e. atm) as:

$$\bar{p} = 0.1581 (1 + f_D) \frac{(1 + \nu_n)(1 + \nu_T)}{1 + \nu_n + \nu_T} \bar{n} \bar{T} \quad (3.36)$$

1075 Moving forward, the final step is plugging this definition for plasma beta into the
 1076 ~~physics-based~~ Troyon Beta Limit derived using standard MHD stability analysis. ~~Limit.~~
 1077 ~~Although outside the scope of this text, it is a stability limit set by treating plasmas~~
 1078 ~~as charge-carrying fluids.~~ This equation can be written in the following form, where
 1079 β_N is the normalized plasma beta – i.e. a ~~staticfixed~~ variable usually set between 2%
 1080 and 4%.¹⁹

$$\beta = \beta_N \frac{I_P}{aB_0} \quad (3.37)$$

1081 Substituting the plasma β from eq. 3.35, into this relation results in the model’s first
 1082 equation for tokamak radius:

$$R_0 = \frac{K_{TB}\bar{T}}{B_0} \quad (3.38)$$

$$K_{TB} = 4.027 \times 10^{-2} \cdot \left(\frac{K_n \epsilon}{\beta_N} \right) \cdot (1 + f_D) \cdot \frac{(1 + \nu_n)(1 + \nu_T)}{1 + \nu_n + \nu_T} \quad (3.39)$$

As mentioned, this is often the dominating constraint in a steady-state reactor. The often dominating constraint for pulsed designs – the kink safety factor – will be the focus of the next subsection.

3.4.2 Giving the Kink Safety Factor

Just like how the Troyon Beta Limit set a fluids-based maximum on plasma pressure, the Kink Safety Factor sets one on the plasma's current. This constraint usually only appears in pulsed designs, as it is assumed that getting to this high a current in steady-state (with only LHCD) would prove extremely impractical.

The starting point, again, is an equation from the literature for the kink condition:^{6,20}

$$q_{*95} = 5\epsilon^2 \cdot \frac{R_0 B_0}{I_P} \cdot \left(\frac{1 + \kappa^2 \cdot (1 + 2\delta^2 - 1.2\delta^3)}{2} \right) \quad (3.40)$$

Here the safety factor – q_{*95} – ~~is subscripted by 95, an identifier that this value is taken at the 95% flux surface (i.e. near the statistically drawn edge of the plasma).~~ It typically has values around 3. ~~Next, the f_q variable is a geometric scaling factor:⁶~~

Combined, the kink safety factor can now be written in standardized units as:

$$R_0 = \frac{K_{SF} I_P}{B_0} \quad (3.41)$$

$$K_{SF} = \frac{q_{*95}}{5\epsilon^2} \cdot \left(\frac{2}{1 + \kappa^2 \cdot (1 + 2\delta^2 - 1.2\delta^3)} \right) \quad (3.42)$$

This relation is the ~~limitingsecondary~~ constraint important for most pulsed reactor designs. As with the Beta Limit, the two are derived through plasma physics alone. The remaining ~~limitingsecondary~~ constraints, however, are engineering-based in origin – these include: the Wall Loading Limit, the Power Cap Constraint, and the Heat Loading Limit. Each will be defined shortly.

1102 3.4.3 Working under the Wall Loading Limit

1103 The first engineering-based ~~limiting~~~~secondary~~ constraint – the wall loading limit –
1104 will prove to be an important quantity when determining the magnet strength at
1105 which reactor costs ~~begin~~~~first-start~~ to increase. As hinted, its definition originates
1106 from nuclear engineering concerns: it is a measure of the maximum neutron damage
1107 a tokamak’s walls can take over the lifetime of the machine.*

1108 The first step in deriving a ~~limiting~~~~secondary~~ constraint for wall loading is a de-
1109 scription of the problem it models. In a reactor, fusion reactions typically make
1110 high-energy neutrons – with around 14.1 MeV of kinetic energy – that ~~collide with~~
1111 ~~the tokamak enclosure. continually blast the inner wall of the tokamak.~~ Therefore a
1112 ~~simple~~~~quick-and-dirty~~ metric would be limiting the amount of neutron power that
1113 can be unloaded on the surface area of a tokamak. This can be written as:²¹

$$P_W = \frac{P_n}{S_P} \quad (3.43)$$

1114

$$S_P = 4\pi^2 a R_0 \cdot \frac{(1 + \frac{2}{\pi} (\kappa^2 - 1))}{\kappa} \quad (3.44)$$

1115 Here, S_P is the surface area of the tokamak’s inner wall and P_n is the neutron power
1116 derived in the subsection on fusion power. The quantity, P_W , then serves a role
1117 analogous to β_N for the beta limit and q_{*95} for the kink safety factor – it is a ~~static~~~~fixed~~
1118 variable representing the maximum allowed wall loading. For fusion reactors, P_W is
1119 assumed to be around 2-4 $\frac{\text{MW}}{\text{m}^2}$. It will be shown that the wall loading limit is important
1120 in any tokamak – regardless of operating mode (i.e. steady-state or pulsed).

1121 Finishing this ~~limiting~~~~secondary~~ constraint, the Wall Loading limit can be written in
1122 standardized units as:

$$R_0 = K_{WL} \cdot I_P^{\frac{2}{3}} \cdot (\sigma v)^{\frac{1}{3}} \quad (3.45)$$

1123

$$K_{WL} = \left(\frac{K_F K_n^2}{5\pi^2 P_W} \cdot \frac{\kappa}{\epsilon} \cdot \frac{1}{1 + \frac{2}{\pi} \cdot (\kappa^2 - 1)} \right)^{\frac{1}{3}} \quad (3.46)$$

*For clarity, the wall loading limit should actually be a energy fluence limit. It is converted to an instantaneous power limit for ease of design purposes.

1124 3.4.4 Setting a Maximum Power Cap

1125 As opposed to the previous three ~~limitingsecondary~~ constraints, the maximum power
1126 cap is more of a ~~constraint set by economic competitiveness.rule-of-thumb~~. Because
1127 no reactor – coal, solar, or otherwise – has a 4000 MW reactor, neither should fusion.*
1128 It makes sense from a practical position after realizing the long history of tokamaks
1129 being delayed, underfunded, or completely canceled. Mathematically, this has the
1130 simple form:

$$P_E \leq P_{CAP} \quad (3.47)$$

1131 Here, P_{CAP} is the maximum allowed power output of the reactor. Similar to the other
1132 limiting quantities, P_{CAP} is treated as a ~~staticfixed~~ variable (i.e. set to 4000 MW).
1133 The electrical power output of the reactor (P_E) is then related to the fusion power
1134 through:⁴

$$P_E = 1.273 \eta_T \cdot P_F \quad (3.48)$$

1135 ~~The constant in front (i.e. 1.273) represents some extra power the reactor makes~~
1136 ~~as more fuel is bred when the fusion neutrons pass through a tokamak (inside its~~
1137 ~~still-undiscussed blanket region).~~ The variable η_T is the thermal efficiency of the
1138 reactor – which is usually found to be around 40%. ~~And the constant in front (i.e.~~
1139 ~~1.273) represents some extra power the reactor makes as fuel is bred by the fusion~~
1140 ~~neutrons passing through a tokamak's lithium-filled blanket. Explicitly this results~~
1141 ~~from including the energy released by lithium-6 as it undergoes neutron capture (E_{Li}).~~

1142

$$1.273 = \frac{E_F + E_{Li}}{E_F} \quad (3.49)$$

1143

$$E_{Li} = 4.8 \text{ MeV} \quad (3.50)$$

*Note that this 4000 MW (electric) is a maximum. A 1000 MW reactor would obviously not violate this constraint. Instead it would likely be pressing on either the kink or beta limit.

1144 Substituting in fusion power and solving for the major radius results in:

$$R_0 = K_{PC} \cdot I_P^2 \cdot (\sigma v) \quad (3.51)$$

1145

$$K_{PC} = K_F K_n^2 \cdot \left(\frac{1.273 \eta_T}{P_{max}} \right) \quad (3.52)$$

1146 This ~~limitingsecondary~~ constraint can be used to create curves of reactors, although
1147 it is mainly used as a stopping point for designs – i.e. if you get to the power-cap
1148 regime, you have gone too far. This is different than the next constraint, which is
1149 ~~fundamentally an unsolved problem withinbasically a glorified warning sign in~~ the
1150 ~~moderneontemporary~~ tokamak design paradigm.²²

1151 3.4.5 Listing the Heat Loading Limit

1152 ~~Fusion plasmas~~Plasmas are hot. The commonly given ~~relationfact~~ is one electron volt
1153 is around 20,000 °F – ~~which makes 15 keV around a quarter-billion Fahrenheit.~~Although
1154 ~~slightlya tad~~ deceptive, ~~heat damage to~~melting a tokamak is an all too real concern.
1155 The problem is there is currently no solution to the problem. Although researchers
1156 have explored various types of heat divertors, none have been shown to withstand the
1157 ~~gigawatts-per-square-meter~~ of heat emitted from a reactor-size tokamak.²²~~Further,~~
1158 ~~as it is not as glamorous as plasma physics, attempts to tackle the problem head-on~~
1159 ~~have often gone unfunded.~~²²

1160 As such, this model takes an approach similar to the research community, calculating
1161 it at the end as a manual check on the difficulty of building such a device – but not
1162 using it to explicitly guide design.~~As such, this model takes the approach that we are~~
1163 ~~no worse than the rest of the field.~~ We almost completely ignore the heat loading limit
1164 ~~and just refer to it at the end, saying "and then this magic divertor will have to deal~~
1165 ~~with solar corona levels of heat." After which, discussion will quickly be redirected~~
1166 ~~to happier concerns.~~ For completeness~~thoroughness~~ though, a ~~limitingsecondary~~ con-
1167 straint will still be derived. The first step is giving the heat load limit commonly

1168 found in the literature:²¹

$$q_{DV} = \frac{K_{DV}}{K_F} \cdot \frac{P_F I_P^{1.2}}{R_0^{2.2}} \quad (3.53)$$

1169

$$K_{DV} = \frac{18.31 \times 10^{-3}}{\epsilon^{1.2}} \cdot K_P \cdot \left(\frac{2}{1 + \kappa^2} \right)^{0.6} \quad (3.54)$$

1170 This is the heat load that impinges on an extended leg, double null divertor – primarily
1171 from the outer midplane of the plasma core. After a simple rearrangement and
1172 substitution for fusion power, this becomes:

$$R_0 = K_{DH} \cdot I_P \cdot (\sigma v)^{\frac{1}{3.2}} \quad (3.55)$$

1173

$$K_{DH} = \left(\frac{K_{DV} K_n^2}{q_{DV}} \right)^{\frac{1}{3.2}} \quad (3.56)$$

1174 At this point all the ~~limitingsecondary~~ constraints have been defined. The next step
1175 is taking a step back and motivating the derivation of a current equation suitable for
1176 pulsed tokamaks.

1177 3.5 Summarizing the Fusion Systems Model

1178 ~~Stepping back, this~~This chapter focused on the bigger picture behind designing a
1179 zero-dimension fusion systems model. It started with a description of various design
1180 parameters and then ~~moved onto~~~~segued into~~ explaining the five relations needed to
1181 close the model – i.e. for \bar{T} , \bar{n} , I_P , B_0 , and R_0 .

1182 Before ~~moving onto~~ generalizing the steady current to ~~allow modeling~~model pulsed
1183 reactors, ~~though~~, a quick recap of the equations will prove beneficial. The first variable
1184 ~~described~~~~tackled~~ was temperature – i.e. scan five evenly-spaced \bar{T} values between 10
1185 and 30 keV. This was then quickly followed by the Greenwald density limit – the ~~a~~
1186 ~~simple relation assumed to apply to all fusion reactors.~~cornerstone of this framework.

1187 Through equations, these two were written as:

$$\bar{T} = \text{const.} \quad (3.1)$$

1188

$$\bar{n} = K_n \cdot \frac{I_P}{R_0^2} \quad (2.11)$$

1189 The next variable handled was the steady current:

$$I_P = \frac{K_{BS}\bar{T}}{1 - K_{CD}(\sigma v)} \quad (2.30)$$

1190 As was mentioned then, this only directly depends on temperature, but is strongly af-
1191 fected by a tokamak's configuration – R_0 and B_0 - through the current drive efficiency
1192 (η_{CD}). For pulsed reactors, this equation proves too simple as it ignores inductive
1193 current. To remedy the situation, current balance will be revisited next chapter. The
1194 main point to make now, though, is that the R_0 and B_0 dependence will be made
1195 explicit.

1196 Moving on, the remaining equations were the primary and ~~limitingsecondary~~ con-
1197 straints for B_0 and R_0 , respectively. It was through these relations that a tokamak's
1198 configuration was brought back into the fold. The choice of solving the two con-
1199 straints for their respective variables was ~~not completely uniquecompletely-arbitrary~~
1200 – motivated only by the foresight of how they fit into the model. Repeated below,
1201 they served as the proper vehicles for closing the system of equations. ~~The next step~~
1202 ~~now is to learn how to generalize the current formula and design a pulsed tokamak~~
1203 ~~reactor.~~

$$B_0 = \left(\frac{G_{PB}}{K_{PB}} \cdot \left(I_P^{\alpha_I^*} R_0^{\alpha_R^*} \right)^{-1} \right)^{\frac{1}{\alpha_B}} \quad (3.29)$$

$$R_0 = \frac{K_{TB}\bar{T}}{B_0} \quad (3.38)$$

1204

$$R_0 = \frac{K_{SF}I_P}{B_0} \quad (3.41)$$

$$R_0 = K_{WL} \cdot I_P^{\frac{2}{3}} \cdot (\sigma v)^{\frac{1}{3}} \quad (3.45)$$

1205

$$R_0 = K_{PC} \cdot I_P^2 \cdot (\sigma v) \quad (3.51)$$

1206

$$R_0 = K_{DH} \cdot I_P \cdot (\sigma v)^{\frac{1}{3.2}} \quad (3.55)$$

1207 The next step now is to learn how to generalize the current formula and design a
 1208 pulsed tokamak reactor (see Chapter 4). After this is done, Chapter 5 will pick up
 1209 where this chapter leaves off – transforming this fusion systems model into a simple
 1210 reactor solver.

1211 Chapter 4

1212 Designing a Pulsed Tokamak

1213 Pulsed tokamaks are the flagship of the European fusion reactor design effort. As such,
1214 this paper's model will now be generalized to accommodate this mode of operation.
1215 Fundamentally, this involves transforming current balance into flux balance – adding
1216 inductive (pulsed) sources to stand alongside the LHCD (steady-state) ones.

1217 The first step in generalizing current balance will be understanding the problem from
1218 a basic electrical engineering perspective – i.e. with circuit analysis. The resulting
1219 equation will then be transformed into the flux balance seen in other models from
1220 the literature. All that will need to be done then is solving the problem for plasma
1221 current (I_P) and simplifying it for various situations – e.g. steady-state operation.

1222 This generalized plasma current will then be found to be a function of the other
1223 dynamic variables (i.e. R_0 , B_0 , and \bar{T}). This, of course, is more difficult to handle
1224 computationally than the steady current, which only directly depended on tempera-
1225 ture (\bar{T}). Discussion about solving this new root solving problem will be the topic of
1226 the next chapter.

1227 4.1 Modeling Plasmas as Circuits

1228 Although it may have been lost along the way, what makes plasmas so interesting and
1229 versatile – in comparison to gases – is their ability to respond to electric and magnetic
1230 fields. It seems natural then to model plasma current from a circuits perspective (i.e.
1231 with resistors, voltage sources, and inductors). By name, this circuit is referred to as
1232 a transformer where: the plasma is the secondary and the yet-to-be discussed central
1233 solenoid (of the tokamak) is the primary.

1234 The first step in deriving a current equation is to determine the circuit equations
1235 that govern pulsed operation in a tokamak. This will be done in two steps. First, we
1236 will draw a circuit diagram and write the equations that describe it. Next, we will
1237 use a simple schematic for how current evolves in a transformer to boil the resulting
1238 differential equations into simple algebraic ones – as is the hallmark of our model.

1239 4.1.1 Drawing the Circuit Diagram

1240 Understanding a circuit always starts with drawing a simple diagram, see Fig. 4-1.
1241 This figure depicts the transformer governing pulsed reactor. The left sub-circuit
1242 is the transformer’s primary – the central solenoid component of the tokamak that
1243 provides most of the inductive current. Whereas, the right sub-circuit is the plasma
1244 acting as the transformer’s secondary. The central solenoid, here, is then a helically-
1245 spiraled metal coil that fits within the inner ring of the doughnut. For now, every
1246 other flux source (besides this central solenoid) is neglected.

1247 This is described by the standard circuits involving voltage sources, resistors, and
1248 ~~inductors: Hopefully without scaring the reader too much, the circuit equations—~~
1249 ~~when only modeling voltage sources, resistors, and inductors—are described by:~~

$$V_i = \sum_j^n \frac{d}{dt} (M_{ij} I_j) + I_i R_i \quad , \quad \forall i = 1, 2, \dots, n \quad (4.1)$$

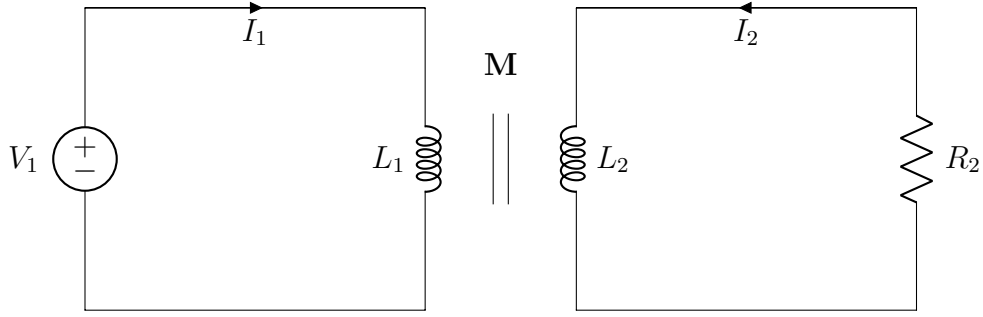


Figure 4-1: A Simple Plasma Transformer Description

A plasma transformer consists of a solenoid primary (left) and a plasma secondary (right). They are connected by their mutual inductance, M . Note that the two currents – I_1 and I_2 – travel in opposite directions.

Without going into the inductances (M) and resistances (R), the variable n is the number of sub-circuits, here being 2. Whereas, the variables i and j are the indices of sub-circuits (i.e. 1 for the primary, 2 for the secondary). For illustrative purposes, this would boil down to the following relation for a battery attached to a lightbulb:

$$V = IR \quad (4.2)$$

Back to the transformer diagram, the equations for the two subcircuits can be expanded and greatly simplified. Besides ignoring every inductive source other than the central solenoid, the next powerful assumption is treating the solenoid as a superconductor (i.e. with negligible resistance). Lastly, the inductances between components and themselves are held constant – independent of time. This allows the coupled transformer equations to be written as:

$$V_1 = L_1 \dot{I}_1 - M \dot{I}_2 \quad (4.3)$$

$$-I_2 R_P = L_2 \dot{I}_2 - M \dot{I}_1 \quad (4.4)$$

With I_1 and I_2 going in opposite directions. Note, here, that the subscript on M has been dropped, as there are only two components. This was done in conjunction

1262 to adding internal (self-)inductance terms. Mathematically, the mapping between
 1263 variables is:

$$M = M_{12} = M_{21} \quad (4.5)$$

1264

$$L_1 = M_{11} \quad (4.6)$$

1265

$$L_2 = M_{22} \quad (4.7)$$

1266 Repeated, the one subscript represents the primary – the central solenoid – and the
 1267 two stands for the plasma as the transformer’s secondary. Exact definitions for the
 1268 inductances will be put off till the end of the next subsection.

1269 4.1.2 Plotting Pulse Profiles

1270 Up until now, little has been discussed that has a time dependence. For steady-state
 1271 tokamaks, this did not occur because it is an extreme case where pulses **could last**
 1272 **weeks or months.basically last the duration of the machine’s lifespan (i.e. around**
 1273 **50 years).** By definition, though, a pulsed machine has pulses – with around ten
 1274 scheduled per day. For this reason, a fusion pulse is now investigated in detail.

1275 Transformer pulses between the central solenoid and the plasma occur on the timescale
 1276 of hours. **During this time, a plasma is brought up to some quasi-steady-state current**
 1277 **(I_P^*) for several~~around an~~ hour and then ramped back down using the available flux in**
 1278 **the solenoid (measured in volt-seconds).** For clarity, each pulse is subdivided into four
 1279 phases: ramp-up, flattop, ramp-down, and dwell. Pictorially represented in Fig. 4-2,
 1280 these divisions allow a simple scheme for transforming the coupled circuit differential
 1281 equations – from Eqs. (4.3) and (4.4) – into simple algebraic formulas.

1282 Along the way, we will approximate derivatives with linear piecewise functions. Using
 1283 t_i to represent the initial time and t_f as the final one, these can be written as:

$$\dot{I} = \frac{I(t_f) - I(t_i)}{t_f - t_i} \quad (4.8)$$

Tokamak Circuit Profiles

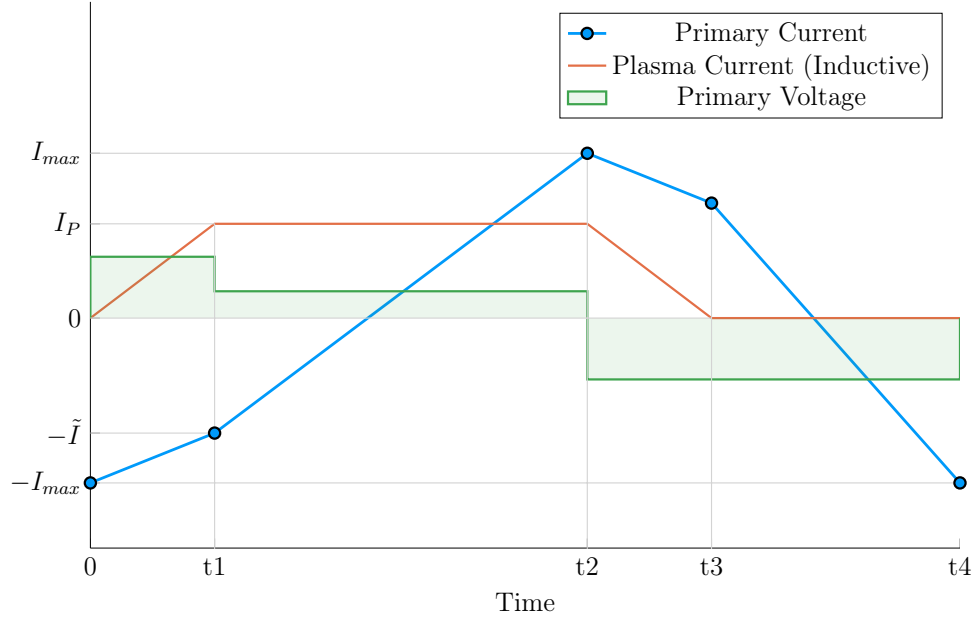


Figure 4-2: Time Evolution of Circuit Profiles

A circuit pulse involves four phases: (1) Ramp-Up, (2) Flattop, (3) Ramp-Down, and (4) Dwell. In reality, flattop can last more than 90% of the pulse.⁷ This makes the slope of the primary current during this phase much shallower than shown.

1284 In tabular form, the data from Fig. 4-2 can be written in this piecewise fashion as:

Table 4.1: Piecewise Linear Scheme for Pulsed Operation

(a) Currents			(b) Voltage			
Time	I_1	I_2	Phase	t_i	t_f	V_1
0	$-I_{max}$	0	Ramp-Up	0	t_1	$+V_{max}$
t_1	$-\tilde{I}$	I_P^*	Flattop	t_1	t_2	$+\tilde{V}$
t_2	$+I_{max}$	I_P^*	Ramp-Down	t_2	t_3	$-V_{max}$
t_3	$+\tilde{I}$	0	Dwell	t_3	t_4	$-V_{max}$
t_4	$-I_{max}$	0				

1285 The exact definitions for the plasma's inductive current (I_P^*) and the maximum volt-
 1286 age in the central solenoid (V_{max}) will be put off until the end of the section.

1287 The Ramp-Up Phase – RU

1288 The first phase in every plasma pulse is the ramp-up. During ramp-up, the central
1289 solenoid starts discharging from its fully charged values, as the plasma is brought to
1290 its quasi-steady-state current. As this occurs on the timescale of minutes – not hours
1291 – resistive effects of the plasma can safely be ignored. This results in the ramp-up
1292 equations becoming:

$$V_{max} = \frac{1}{\tau_{RU}} \cdot \left(L_1 \cdot (I_{max} - \tilde{I}) - M \cdot I_{ID} \right) \quad (4.9)$$

$$0 = \frac{1}{\tau_{RU}} \cdot \left(M \cdot (I_{max} - \tilde{I}) - L_2 \cdot I_{ID} \right) \quad (4.10)$$

1293 Simplifying these equations will be done shortly, for now the new terms are what
1294 is important. The maximum voltage of the solenoid is V_{max} – usually measured in
1295 kilovolts. Next, I_{max} is the solenoid’s current at the beginning of ramp-up. Whereas
1296 \tilde{I} is the magnitude of the current once the plasma is at its flattop inductive-drive
1297 current – I_{ID} . The τ_{RU} quantity, then, is the duration of time it takes to ramp-
1298 up (i.e. RU). Again, L_1 and L_2 are the microhenry-scale internal inductances of the
1299 solenoid and plasma, respectively, and M is the mutual inductance between them.

1300 The last step in discussing ramp-up is giving the two important formulas that come
1301 from it:

$$\tilde{I} = I_{max} - I_{ID} \cdot \left(\frac{L_2}{M} \right) \quad (4.11)$$

1302

$$\tau_{RU} = \frac{I_{ID}}{V_{max}} \cdot \left(\frac{L_1 L_2 - M^2}{M} \right) \quad (4.12)$$

1303 The Flattop Phase – FT

1304 The most important phase in any reactor’s pulse is flattop – the quasi-steady-state
1305 time when the tokamak is making ~~electricity, electricity (and money)~~. Flattops are
1306 assumed to last a couple of hours for a profitable machine, during which the central

1307 solenoid completely discharges to overcome a plasma's resistive losses – keeping it
 1308 in a quasi-steady-state mode of operation. In a steady-state reactor, this phases
 1309 constitutes the entirety of the pulse.

1310 Although the resistance cannot be safely neglected for flattop – as it was for ramp-up –
 1311 the plasma's inductive current (I_{ID}) is assumed constant. This leads to its derivative
 1312 in equations cancelling out! Mathematically,

$$\tilde{V} = \frac{L_1}{\tau_{FT}} \cdot (I_{max} + \tilde{I}) \quad (4.13)$$

$$I_{ID}R_P = \frac{M}{\tau_{FT}} \cdot (I_{max} + \tilde{I}) \quad (4.14)$$

1313 As with ramp-up, the simplifications will be given shortly. The new terms here,
 1314 however, are an intermediate voltage for the central solenoid (\tilde{V}), and the duration
 1315 of the flattop (τ_{FT}). The resistance term was given in Eq. (3.10). Solutions can then
 1316 be found by substituting \tilde{I} – from Eq. (4.11) – into the flattop equations:

$$\tilde{V} = I_{ID}R_P \cdot \left(\frac{L_1}{M} \right) \quad (4.15)$$

1317

$$\tau_{FT} = \frac{I_{max} \cdot 2M - I_{ID} \cdot L_2}{I_{ID}R_P} \quad (4.16)$$

1318 The Ramp-Down Phase – RD

1319 Due to the simplicity – and symmetry – of this model's reactor pulse, ramp-down is
 1320 the exact mirror of ramp-up. It takes the same amount of time and results in the
 1321 same algebraic equations. For brevity, this will just be represented as:

$$\tau_{RD} = \tau_{RU} \quad (4.17)$$

1322 For clarity, this is the time when a plasma's current is brought down from its flattop
 1323 value to zero.

1324 The Dwell Phase – DW

1325 Where the first three phases had little ambiguity, the dwell phase changes definition
1326 from model to model. For now, it is assumed to be the time it takes the central
1327 solenoid to reset after a plasma has been completely ramped-down to an off-mode.
1328 To get a more realistic duty factor for cost estimates, it could include an evacuation
1329 time, set to last around thirty minutes. During this evacuation, a plasma is vacuumed
1330 out of a device as it undergoes some inter-pulse maintenance.

1331 Ignoring evacuation for now, the dwell phase involves resetting the central solenoid
1332 when the plasma's current is negligible. This ~~fundamentally~~ means the secondary of
1333 the transformer is ~~an open circuit~~~~nonexistent~~ – ~~fundamentally~~ the central solenoid is
1334 the ~~only component~~~~entire circuit~~. In equation form,

$$V_{max} = \frac{L_1}{\tau_{DW}} \cdot (I_{max} + \tilde{I}) \quad (4.18)$$

1335 Or substituting in \tilde{I} and solving for τ_{DW} ,

$$\tau_{DW} = \frac{L_1}{M} \cdot \frac{(I_{max} \cdot 2M - I_{ID} \cdot L_2)}{V_{max}} \quad (4.19)$$

1336 4.1.3 Specifying Circuit Variables

1337 The goal now is to collect the results from the four phases and introduce the induc-
1338 tance, resistance, voltage, and current terms relevant to our model. This will motivate
1339 recasting the problem as flux balance in a reactor – the form commonly used in the
1340 literature (and discussed next section).

1341 First, collecting the phase durations in one place:

$$\tau_{RU} = \frac{I_{ID}}{V_{max}} \cdot \left(\frac{L_1 L_2 - M^2}{M} \right) \quad (4.12)$$

$$\tau_{FT} = \frac{I_{max} \cdot 2M - I_{ID} \cdot L_2}{I_{ID} R_P} \quad (4.16)$$

$$\tau_{RD} = \tau_{RU} \quad (4.17)$$

$$\tau_{DW} = \frac{L_1}{M} \cdot \frac{(I_{max} \cdot 2M - I_{ID} \cdot L_2)}{V_{max}} \quad (4.19)$$

1342 These can be used in the definition of the duty-factor: the fraction of time a reactor
1343 is putting electricity on the grid. Formulaically,

$$f_{duty} = \frac{\tau_{FT}}{\tau_{pulse}} \quad (4.20)$$

$$\tau_{pulse} = \tau_{RU} + \tau_{FT} + \tau_{RD} + \tau_{DW} \quad (4.21)$$

1345 As will turn out, the solving of pulsed current actually only involves Eq. (4.16).
1346 What is interesting about this, is that there is no explicit dependence on ramp-down
1347 or dwell! Whereas ramp-up passes \tilde{I} to the flattop phase, the other two are just
1348 involved in calculating the duty factor.

1349 The remainder of this subsection will then be defining the following circuit variables:
1350 I_{ID} , I_{max} , V_{max} , L_1 , L_2 , and M . Again, the resistance was defined last chapter as:

$$R_P = \frac{K_{RP}}{R_0 \bar{T}^{3/2}} \quad (3.10)$$

1351 **The Inductive Current – I_{ID}**

1352 The inductive current is the source of current that separates pulsed from steady-state
1353 operation. Quickly fitting it into the previous definitions of current balance – see
1354 Eq. (3.3):

$$I_{ID} = I_P - (I_{BS} + I_{CD}) \quad (4.22)$$

1355 As before, I_P is the total plasma current in mega-amps, I_{BS} is the bootstrap current,
 1356 and I_{CD} is the current from LHCD (i.e. lower hybrid current drive). For this model,
 1357 the relation can be rewritten as:

$$I_{ID} = I_P \cdot \left(1 - K_{CD}(\sigma v)\right) - K_{BS} \bar{T} \quad (4.23)$$

1358 **The Central Solenoid Maximums – V_{max} and I_{max}**

1359 For this simple model, the central solenoid has two maximum values: the voltage and
 1360 current. The voltage is the easier to give value. Literature values have this around:⁵

$$V_{max} \approx 5 \text{ kV} \quad (4.24)$$

1361 The maximum current, on the other hand, can be defined through Ampere's Law on
 1362 a helically-shaped central solenoid:¹⁰

$$I_{max} = \frac{B_{CS} h_{CS}}{N \mu_0} \quad (4.25)$$

1363 Here, B_{CS} is a magnetic field strength the central solenoid is assumed to operate at
 1364 (i.e. 12 T), h_{CS} is the height of the solenoid, N is the number of loops, and μ_0 has
 1365 its usual physics meaning (i.e. $40 \pi \frac{\mu\text{H}}{\text{m}}$). As will be seen, the value of N does not
 1366 directly affect the model, as it cancels out in the final flux balance. The height of
 1367 the central solenoid will be the focus of an upcoming section on improving tokamak
 1368 geometry.

1369 **The Central Solenoid Inductance – L_1**

1370 For a central solenoid with circular cross-sections of finite thickness (d), the inductance
 1371 can be written as:¹⁹

$$L_1 = G_{LT} \cdot \left(\frac{\mu_0 \pi N^2}{h_{CS}} \right) \quad (4.26)$$

1372

$$G_{LT} = \frac{R_{CS}^2 + R_{CS} \cdot (R_{CS} + d) + (R_{CS} + d)^2}{3} \quad (4.27)$$

1373 Note that R_{CS} is the inner radius of the central solenoid and $(R_{CS} + d)$ is the outer
 1374 one. In the limit where d is negligible, this says that the inductance is quadratically
 1375 dependent on the radius of the central solenoid:

$$\lim_{d \rightarrow 0} G_{LT} = G_{LT}^\dagger = R_{CS}^2 \quad (4.28)$$

1376 The formulas for both R_{CS} and d will be defined in a few sections.

1377 The Plasma Inductance – L_2

1378 The plasma inductance is a composite of several different terms, but overall scales
 1379 with radius. Through equation,

$$L_2 = K_{LP} R_0 \quad (4.29)$$

1380 This ~~static~~fixed coefficient – K_{LP} – then combines three inductive behaviors of the
 1381 plasma. The first is its own self inductance (through l_i).⁴ The next is a resistive
 1382 component through the Ejima coefficient, C_{ejima} , which is usually set to $\sim \frac{1}{3}$.⁶ And
 1383 lastly, a geometric component – involving ϵ and κ – is given by the Hirshman-Neilson
 1384 model.²³ Mathematically,

$$K_{LP} = \mu_0 \cdot \left(\frac{l_i}{2} + C_{ejima} + \frac{(b_{HN} - a_{HN})(1 - \epsilon)}{(1 - \epsilon) + \kappa d_{HN}} \right) \quad (4.30)$$

1385 Here the HN values come from the 1985 Hirshman-Neilson paper:

$$a_{HN}(\epsilon) = 2.0 + 9.25\sqrt{\epsilon} - 1.21 \epsilon \quad (4.31)$$

1386

$$b_{HN}(\epsilon) = \ln(8/\epsilon) \cdot (1 + 1.81\sqrt{\epsilon} + 2.05 \epsilon) \quad (4.32)$$

1387

$$d_{HN}(\epsilon) = 0.73\sqrt{\epsilon} \cdot (1 + 2\epsilon^4 - 6\epsilon^5 + 3.7\epsilon^6) \quad (4.33)$$

1388 The Mutual Inductance – M

1389 The mutual inductance – M – represents the coupling between the solenoid primary
1390 and the plasma secondary. A common method for treating this mutual inductance is
1391 through a coupling coefficient, k, that links the two self-inductances. Formulaically,

$$M = k\sqrt{L_1L_2} \quad (4.34)$$

1392 The value of the coupling coefficient, k, is always less than (or equal to) 1, but usually
1393 has a value around one-third. With all the equations defined, we are now at a position
1394 to explain one of the larger nuances of this fusion systems framework: declaring the
1395 pulse length of a tokamak.

1396 4.1.4 ConstructingReasoning the Pulse Length

1397 This subsection focuses on a quantitative estimate for how to select a pulse length.
1398 As no fusion reactor exists in the world today, the writers believe this is an acceptable
1399 calculation. Further, the resulting length of two hours matches the durations of other
1400 studies in the literature.

1401 Starting at the end, our goal is to find the pulse length of a tokamak reactor in
1402 seconds – as dictated by cyclical stress concerns. The first piece of information is
1403 the expected lifetime of the central solenoid, $N \approx 10$ years. The next is the desired
1404 number of ~~pulses~~shots the central solenoid will have to last: ~~machine will likely have,~~
1405 $M \approx 50,000$ pulses.* This gives the roughballpark estimate of around 10 pulses a
1406 day – or a flattop pulse length of two hours.

1407 With the pulse length defined, we are now in a position to justify neglecting the duty
1408 factor for pulsed reactors in this model. Using expectedballpark reactor values – while

*This 50,000 pulses is based on the values from the ITER design specifications.²⁴

1409 assuming the central solenoid has around 4000 turns – leads to the following scalings:

$$\tau_{FT} \sim \tau_{pulse} \sim \text{O}(\text{hours}) \quad (4.35)$$

1410

$$\tau_{RU} \sim \tau_{RD} \sim \tau_{DW} \sim \text{O}(\text{mins}) \quad (4.36)$$

1411 As such, even pulsed tokamak reactors should have a duty factor of around unity:

$$f_{duty} \approx 1 \quad (4.37)$$

1412 This analysis of course would change if the central solenoid became an inexpensive
 1413 component to replace. For example, if a tokamak had a new one installed annually,
 1414 the pulse length could shorten to be on the order of minutes.

1415 Now that all the terms in a pulsed circuit have been explored, we will move on to
 1416 rearranging the flattop equation to reproduce flux balance. This will then naturally
 1417 lead to a generalized current equation – which is the main result of the chapter.

1418 4.2 Producing Salvaging Flux Balance

1419 The goal of this section is to arrive at a conservation equation for flux balance that
 1420 mirrors the ones in the literature. The fusion systems model this one attempts to
 1421 follow most is the PROCESS code.⁶ In a manner similar to power balance, flux
 1422 balance can be written as:

$$\sum_{sources} \Phi = \sum_{sinks} \Phi \quad (4.38)$$

1423 4.2.1 Rearranging the Circuit Equation

1424 The way to arrive at flux balance from the circuit equation is to rearrange the flattop
 1425 phase's duration equation:

$$\tau_{FT} = \frac{I_{max} \cdot 2M - I_{ID} \cdot L_2}{I_{ID} R_P} \quad (4.16)$$

1426 Multiplying by the right-hand side's denominator and moving the negative term over
 1427 yields:

$$2MI_{max} = I_{ID} \cdot (L_2 + R_P\tau_{FT}) \quad (4.39)$$

1428 This equation is flux balance, where the left-hand side are the sources (e.g. the central
 1429 solenoid), and the other terms are the sinks (i.e. ramp-up and flattop). The source
 1430 term can currently be encapsulated in:

$$\Phi_{CS} = 2MI_{max} \quad (4.40)$$

1431 The sinks, namely the ramp-up inductive losses (Φ_{RU}) and the flattop resistive losses
 1432 (Φ_{FT}), are what drain up the flux. Again, ramp-down and dwell are not included as
 1433 sinks because flux balance only tracks till the end of flattop. They come into play
 1434 when measuring the cost of electricity – through the duty factor from Eq. (4.20).

1435 Relabeling terms, flux balance can now be rewritten as:

$$\Phi_{CS} = \Phi_{RU} + \Phi_{FT} \quad (4.41)$$

1436 With the ramp-up and flattop flux given respectively by:

$$\Phi_{RU} = L_2 \cdot I_{ID} \quad (4.42)$$

1437

$$\Phi_{FT} = (R_P\tau_{FT}) \cdot I_{ID} \quad (4.43)$$

1438 On comparing these quantities to the ones from the PROCESS team, Φ_{RU} and Φ_{FT}
 1439 are exactly the same. The source terms, on the other hand, are off for two reasons
 1440 – both related to the central solenoid being the only source term in flux balance.
 1441 This can partially be remedied by adding the second most dominant source of flux
 1442 a posteriori – i.e. the PF coils. The second, and inherently limiting factor, is the
 1443 simplicity of the current model. All that can be shown to this regard is that the Φ_{CS}
 1444 terms does reasonably predict the values from the PROCESS code.

1445 4.2.2 AddingImporting Poloidal Field Coils

1446 Adding the effect of PF coils – belts of current driving plates on the outer edges of
1447 the tokamak – leads to as much as a 50% improvement^{6,7}~~a second-order improvement~~
1448 over relying solely on the central solenoid for flux generation. From the literature,
1449 this can be modeled as:¹⁹

$$\Phi_{PF} = \pi B_V \cdot (R_0^2 - (R_{CS} + d)^2) \quad (4.44)$$

1450 Where again R_{CS} and d are the inner radius and thickness of the central solenoid,
1451 respectively. These will be the topic of the next section.

1452 Moving forward, the vertical field – B_V – is a magnetic field oriented up-and-down
1453 with the ground. It is needed to prevent a tokamak plasma from drifting radially~~spinning~~
1454 out of the machine. From the literature, the magnitude of this vertical field (valid for
1455 a circular plasma) is given by:⁶

$$|B_V| = \frac{\mu_0 I_P}{4\pi R_0} \cdot \left(\ln \left(\frac{8}{\epsilon} \right) + \beta_p + \frac{l_i}{2} - \frac{3}{2} \right) \quad (4.45)$$

1456 Analogous to the previously covered plasma beta, the poloidal beta can be represented
1457 by:²⁵

$$\beta_p = \frac{\bar{p}}{\left(\frac{\overline{B_p}^2}{2\mu_0} \right)} \quad (4.46)$$

1458 Where the average poloidal magnetic field comes from a simple application of Am-
1459 pere's law:

$$\overline{B_p} = \frac{\mu_0 I_P}{l_p} \quad (4.47)$$

1460 The variable l_p is then the perimeter of the tokamak's cross-sectional halves:

$$l_p = 2\pi a \cdot \sqrt{g_p} \quad (4.48)$$

1461 Here, g_p is another geometric scaling factor,

$$g_p = \frac{1 + \kappa^2(1 + 2\delta^2 - 1.2\delta^3)}{2} \quad (4.49)$$

1462 ~~After a few lines of algebra~~Boiled down, this relation for the magnitude of the vertical
1463 magnetic field can be written in standardized units as:

$$|B_V| = \left(\frac{1}{10 \cdot R_0} \right) \cdot (K_{VI} I_P + K_{VT} \bar{T}) \quad (4.50)$$

1464

$$K_{VT} = K_n \cdot (\epsilon^2 g_P) \cdot (1 + f_D) \frac{(1 + \nu_n)(1 + \nu_T)}{1 + \nu_n + \nu_T} \quad (4.51)$$

1465

$$K_{VI} = \ln \left(\frac{8}{\epsilon} \right) + \frac{l_i}{2} - \frac{3}{2} \quad (4.52)$$

1466 For clarity, this will be plugged into the new PF coil flux contribution (Φ_{PF}):

$$\Phi_{PF} = \pi B_V \cdot (R_0^2 - (R_{CS} + d)^2) \quad (4.44)$$

1467 Which then gets plugged into a more complete flux balance:

$$\Phi_{CS} + \Phi_{PF} = \Phi_{RU} + \Phi_{FT} \quad (4.53)$$

1468 The R_{CS} and d terms found in Φ_{PF} will now be discussed as they are needed for this
1469 more sophisticated tokamak geometry.

1470 4.3 Improving Tokamak Geometry

1471 From before, this fusion systems model has been said to depend on the major and
1472 minor radius – R_0 and a , respectively – and along the way, various geometric param-
1473 eters have been defined (e.g. ϵ , κ , δ) to describe the geometry further. Now three
1474 more thicknesses will be added: b , c , and d . Additionally, two fundamental dimension
1475 corresponding to the solenoid will be given: the radius (R_{CS}) and height (h_{CS}). These

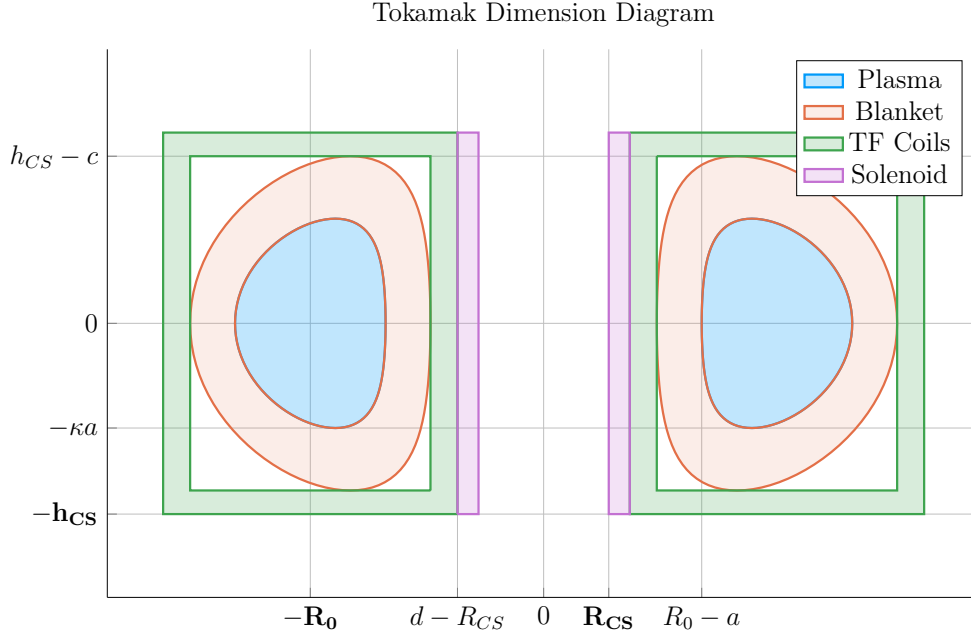


Figure 4-3: Dimensions of Tokamak Cross-Section

are the topics of this section.

4.3.1 Defining Central Solenoid Dimensions

The best way to conceptualize tokamak geometry is through cartoon – see Fig. E-2. What this says is there is a gap at the very center of a tokamak. This gap extends radially outwards to R_{CS} meters where the ~~spiraledslinky-shaped~~ central solenoid – of thickness d – begins. Between the outer edge of the solenoid and the wall of the torus (i.e. the doughnut) are the blanket and toroidal field (TF) coils.

The blanket and TF coils have thicknesses of b and c , respectively. Before defining b , c , and d , though, it proves fruitful to relate all the quantities in equations for the inner radius (R_{CS}) and height (h_{CS}) of the central solenoid.

$$R_{CS} = R_0 - (a + b + c + d) \quad (4.54)$$

$$h_{CS} = 2 \cdot (\kappa a + b + c) \quad (4.55)$$

1487 Again, this relation is pictorially represented in Fig. E-2. The next step is defining:
1488 b , c , and d – to close the variable loop.

1489 4.3.2 CalculatingMeasuring Component Thicknesses

1490 In between the inner surface of the central solenoid and the major radius of the
1491 tokamak are four thicknesses: a , b , c , and d . This subsection will go over them
1492 one-by-one.

1493 The Minor Radius – a

1494 The minor radius was the first of these thicknesses we encountered. To calculate it,
1495 we introduced the inverse aspect ratio (ϵ) to relate it to the major radius (R_0):

$$a = \epsilon \cdot R_0 \quad (2.1)$$

1496 The Blanket Thickness – b

1497 The blanket is an area between the TF coils and the torus that is **strongly** composed
1498 **mainly** of lithium **steel**. It serves to both: protect the superconducting magnet struc-
1499 tures from neutron damage, as well as breed **a-little** more tritium fuel from stray
1500 fusion neutrons. In equation form, the blanket thickness is given by:²¹

$$b = 1.23 + 0.074 \ln P_W \quad (4.56)$$

1501 ~~Here, the constant term (i.e. 1.23) is approximately the mean-free-path of fusion~~
1502 ~~neutrons through lithium-7—the thickness of lithium needed to reduce the population~~
1503 ~~of neutrons by $\sim 65\%$. Here, P_W While the second term, which includes P_W , is a~~
1504 ~~correction to account for extra wall loading (as discussed in Section 3.4.3the secondary~~
1505 ~~constraint section).~~

1506 Moving forward, the remaining two thicknesses – c and d – are handled differently,

1507 estimating structural steel portions as well as magnetic current-carrying ones.

1508 The Toroidal Field Coil Thickness – c

1509 The thickness of the TF coils – c – is a little beyond the scope of this paper. It does,
 1510 however, have a form that combines a structural steel component with a magnetic
 1511 portion. From ~~a previous model~~~~one of Jeff's previous models~~, this can be given as:²¹

$$c = G_{CI}R_0 + G_{CO} \quad (4.57)$$

$$G_{CI} = \frac{B_0^2}{4\mu_0\sigma_{TF}} \cdot \frac{1}{(1 - \epsilon_b)} \cdot \left(\frac{4\epsilon_b}{1 + \epsilon_b} + \ln \left(\frac{1 + \epsilon_b}{1 - \epsilon_b} \right) \right) \quad (4.58)$$

$$G_{CO} = \frac{B_0}{\mu_0 J_{TF}} \cdot \frac{1}{(1 - \epsilon_b)} \quad (4.59)$$

1514 The critical stress – σ_{TF} in G_{CI} implies it depends on the structural component,
 1515 whereas the maximum current density – J_{TF} – implies a magnetic predisposition
 1516 in G_{CO} . The use of G_{\square} in these quantities, instead of K_{\square} is because they include
 1517 the toroidal magnetic field strength – B_0 . For this reason, they are referred to as
 1518 ~~dynamicfloating~~ coefficients. Lastly, the term ϵ_b represents the blanket inverse aspect
 1519 ratio that combines the minor radius with the blanket thickness:

$$\epsilon_b = \frac{a + b}{R_0} \quad (4.60)$$

1520 The Central Solenoid Thickness – d

1521 Finishing this discussion where we started, the central solenoid's thickness – d – has
 1522 a form similar to the TF coil's (i.e. c). In mathematical form, this can be represented
 1523 as:²¹

$$d = K_{DR}R_{CS} + K_{DO} \quad (4.61)$$

$$K_{DR} = \frac{3B_{CS}^2}{6\mu_0\sigma_{CS} - B_{CS}^2} \quad (4.62)$$

1525

$$K_{DO} = \frac{6B_{CS}\sigma_{CS}}{6\mu_0\sigma_{CS} - B_{CS}^2} \cdot \left(\frac{1}{J_{OH}} \right) \quad (4.63)$$

1526 Here, the use of K_{\square} for the coefficients signifies their use as ~~static~~fixed coefficients.
 1527 Therefore, B_{CS} must be treated as a ~~static~~fixed variable representing the magnetic
 1528 field strength in the central solenoid. For prospective solenoids using high temperature
 1529 superconducting (HTS) tape, B_{CS} may be around 20 T. The values of σ_{CS} and J_{CS}
 1530 have similar meanings to the ones for TF coils. These are collected in a table below
 1531 with example values representative of our model.

Table 4.2: Example TF Coils and Central Solenoid Critical Values

(a) Stresses [MPa]			(b) Current Densities [MA/m ²]		
Item	Symbol	Limit	Item	Symbol	Limit
Solenoid	σ_{CS}	600 300	Solenoid	J_{CS}	100 50
TF Coils	σ_{TF}	600	TF Coils	J_{TF}	200

1532 Before moving on, it seems important to say that although K_{DI} and K_{DO} do not
 1533 depend on ~~dynamic~~floating variables, R_{CS} most definitely does. This is what makes
 1534 the central solenoid's thickness difficult.

1535 4.3.3 Revisiting Central Solenoid Dimensions

1536 Now that the various thicknesses have been defined (i.e. a , b , c , and d), the equations
 1537 for the solenoid's dimensions (i.e. R_{CS} and h_{CS}), can now be revisited and simplified.
 1538 From before,

$$R_{CS} = R_0 - (a + b + c + d) \quad (4.54)$$

1539

$$h_{CS} = 2 \cdot (\kappa a + b + c) \quad (4.55)$$

Utilizing the four thicknesses from before, these can now be expanded to simple formulas. Repeating the thicknesses:

$$a = \epsilon \cdot R_0 \quad (2.1)$$

$$b = 1.23 + 0.074 \ln P_W \quad (4.56)$$

$$c = G_{CI}R_0 + G_{CO} \quad (4.57)$$

$$d = K_{DR}R_{CS} + K_{DO} \quad (4.61)$$

Plugging these into the central solenoid's dimensions results in:

$$h_{CS} = 2 \cdot (R_0 \cdot (\epsilon\kappa + G_{CI}) + (b + G_{CO})) \quad (4.64)$$

$$R_{CS} = \frac{1}{1 + K_{DR}} \cdot (R_0 \cdot (1 - \epsilon - G_{CI}) - (K_{DO} + b + G_{CO})) \quad (4.65)$$

1540 These are the complete central solenoid dimension formulas. To make them more
1541 tractable to the reader, they will now be simplified one step at a time. (The same
1542 simplification exercise will be done again after the generalized current is derived later
1543 this chapter.)

1544 The first simplification to make while estimating central solenoid dimensions is to
1545 neglect the magnetic current-carrying portions of the central solenoid and TF coils.
1546 This results in:

$$\lim_{\substack{G_{CO} \rightarrow 0 \\ K_{DO} \rightarrow 0}} h_{CS} = h_{CS}^\dagger = 2R_0 \cdot (K_{EK} + \epsilon_b + G_{CI}) \quad (4.66)$$

$$\lim_{\substack{G_{CO} \rightarrow 0 \\ K_{DO} \rightarrow 0}} R_{CS} = R_{CS}^\dagger = \frac{R_0}{1 + K_{DR}} \cdot (1 - \epsilon_b - G_{CI}) \quad (4.67)$$

1548 The new ~~static~~~~fixed~~ coefficient, here, is:

$$K_{EK} = \epsilon \cdot (\kappa - 1) \quad (4.68)$$

1549 The next simplification is ignoring the TF coil thickness – and thus magnetic field

1550 dependence – altogether:

$$\lim_{G_{CI} \rightarrow 0} h_{CS}^{\dagger} = h_{CS}^{\ddagger} = 2R_0 \cdot (K_{EK} + \epsilon_b) \quad (4.69)$$

1551

$$\lim_{G_{CI} \rightarrow 0} R_{CS}^{\dagger} = R_{CS}^{\ddagger} = \frac{R_0}{1 + K_{DR}} \cdot (1 - \epsilon_b) \quad (4.70)$$

1552 These oversimplifications will be used later this chapter while simplifying the gener-
 1553 alized current equation to something more tractable. For now, they highlight how the
 1554 dimensions change as different components are neglected. The next step is bringing
 1555 plasma physics back into the flux balance equation and solving for the generalized
 1556 current.

1557 4.4 Piecing Together the Generalized Current

1558 The goal of this section is to quickly expand flux balance using all the defined quan-
 1559 tities and then massage it into an equation for plasma current – which is suitable for
 1560 root solving. This starts with a restatement of flux balance in a reactor:

$$\Phi_{CS} + \Phi_{PF} = \Phi_{RU} + \Phi_{FT} \quad (4.53)$$

1561

$$\Phi_{CS} = 2MI_{max} \quad (4.40)$$

1562

$$\Phi_{PF} = \pi B_V \cdot (R_0^2 - (R_{CS} + d)^2) \quad (4.44)$$

1563

$$\Phi_{RU} = L_2 \cdot I_{ID} \quad (4.42)$$

1564

$$\Phi_{FT} = (R_P \tau_{FT}) \cdot I_{ID} \quad (4.43)$$

1565 The first step is realizing that the central solenoid flux can now be rewritten using
 1566 the new geometry in a standardized form:

$$\Phi_{CS} = K_{CS} \cdot \sqrt{R_0 G_{LT} h_{CS}} \quad (4.71)$$

1567

$$K_{CS} = 2kB_{CS} \cdot \sqrt{\frac{\pi K_{LP}}{\mu_0}} \quad (4.72)$$

1568 Next, we will slightly simplify the PF coil flux using a **dynamicfloating** variable coef-
1569 ficient:

$$\Phi_{PF} = G_V \cdot \frac{K_{VI}I_P + K_{VT}\bar{T}}{R_0} \quad (4.73)$$

1570

$$G_V = \frac{\pi}{10} \cdot (R_0^2 - (R_{CS} + d)^2) \quad (4.74)$$

1571 This allows us to rewrite the generalized current as:

$$I_P = \frac{(K_{BS} + G_{IV}/G_{IP}) \cdot \bar{T}}{1 - K_{CD}(\sigma v) - G_{ID}/G_{IP}} \quad (4.75)$$

1572

$$G_{IV} = K_{VT}G_V + K_{CS}R_0^{3/2} \cdot \frac{\sqrt{h_{CS}G_{LT}}}{\bar{T}} \quad (4.76)$$

1573

$$G_{ID} = K_{VI}G_V \quad (4.77)$$

1574

$$G_{IP} = K_{LP}R_0^2 + \frac{K_{RP}\tau_{FT}}{\bar{T}^{3/2}} \quad (4.78)$$

1575 As we will show in the next section, this form not only has a form remarkably similar
1576 to the steady current – it reduces to it in the limit of infinitely long pulses!

1577 4.5 Simplifying the Generalized Current

1578 This section focuses on making various simplifications to the generalized current:

$$I_P = \frac{(K_{BS} + G_{IV}/G_{IP}) \cdot \bar{T}}{1 - K_{CD}(\sigma v) - G_{ID}/G_{IP}} \quad (4.75)$$

1579 As promised, this will start with the trivial simplification of the generalized current
1580 into steady state. Next it will move on to a basic simplification for the purely pulsed
1581 case. These two activities should shed some light on how to interpret the equation in
1582 the more complicated hybrid case.

1583 4.5.1 Recovering the Steady Current

1584 The place to start with the steady current is the ~~dynamic~~~~floating~~ coefficient, G_{IP} :

$$G_{IP} = K_{LP} R_0^2 + \frac{K_{RP} \tau_{FT}}{\bar{T}^{3/2}} \quad (4.78)$$

1585 As can be seen, as $\tau_{FT} \rightarrow \infty$, so does the coefficient,

$$\lim_{\tau_{FT} \rightarrow \infty} G_{IP} = \infty \quad (4.79)$$

1586 Because G_{IU} and G_{ID} remain constant, their contribution to plasma current becomes
1587 insignificant in this limit. Concretely,

$$\lim_{\tau_{FT} \rightarrow \infty} I_P = \frac{K_{BS} \bar{T}}{1 - K_{CD}(\sigma v)} \quad (4.80)$$

1588 This is precisely the steady current given by Eq. (2.30)! The generalized current
1589 automatically works when modeling steady-state tokamaks.*

1590 4.5.2 Extracting the Pulsed Current

1591 For pulsed reactors, we have to ~~resolve a similar problem~~~~play a similar game~~ – except
1592 now τ_{FT} is expected to be a reasonably sized number (i.e. 2 hours).

1593 With an aim at intuition, the reactor is first treated as purely pulsed – having no
1594 current drive assistance:

$$\lim_{\eta_{CD} \rightarrow 0} I_P = \frac{(K_{BS} + G_{IU}/G_{IP}) \cdot \bar{T}}{1 - (G_{ID}/G_{IP})} \quad (4.81)$$

1595 Next, for simplicity-sake, the PF coil contribution to flux balance is assumed negligi-

*It should be noted that this is much harder when setting τ_{FT} to a large, but finite number – as η_{CD} still needs to be solved self-consistently.

1596 ble, as it was always just a correction term:

$$\lim_{\Phi_{PF} \ll \Phi_{CS}} G_{IU} = K_{CS} R_0^{3/2} \cdot \frac{\sqrt{h_{CS} G_{LT}}}{\bar{T}} \quad (4.82)$$

1597

$$\lim_{\Phi_{PF} \ll \Phi_{CS}} G_{ID} = 0 \quad (4.83)$$

1598 Piecing this altogether, we can write a new current for this highly simplified case,

$$I_P^\dagger = K_{BS} \bar{T} + \frac{K_{CS} R_0^{3/2} \cdot \sqrt{h_{CS} G_{LT}}}{K_{LP} R_0^2 + K_{RP} \tau_{FT} \bar{T}^{-3/2}} \quad (4.84)$$

1599 As this is not quite simple enough, these previous simplifications will be incorporated:

$$G_{LT}^\dagger = R_{CS}^2 \quad (4.28)$$

1600

$$h_{CS}^\dagger = 2R_0 \cdot (K_{EK} + \epsilon_b) \quad (4.69)$$

1601

$$R_{CS}^\dagger = \frac{R_0}{1 + K_{DR}} \cdot (1 - \epsilon_b) \quad (4.70)$$

1602 Taking these into consideration results in the following current formula:

$$I_P^\dagger = K_{BS} \bar{T} + \left(\frac{K_{CS} R_0^3}{K_{LP} R_0^2 + K_{RP} \tau_{FT} \bar{T}^{-3/2}} \cdot \frac{(1 - \epsilon_b) \cdot \sqrt{2(K_{EK} + \epsilon_b)}}{1 + K_{DR}} \right) \quad (4.85)$$

1603 In the limit that the pulse length drops to zero (and bootstrap current is negligible),

$$\lim_{\tau_{FT} \rightarrow 0} I_P^\dagger = R_0 \cdot \left(\frac{K_{CS}}{K_{LP}} \cdot \frac{(1 - \epsilon_b) \cdot \sqrt{2(K_{EK} + \epsilon_b)}}{1 + K_{DR}} \right) \quad (4.86)$$

1604 This implies that a purely pulsed current scales with major radius to leading order.

1605 4.5.3 Rationalizing the Generalized Current

1606 From the previous two subsections, we arrived at equations for infinitely large and
 1607 infinitely small pulse lengths:

$$\lim_{\tau_{FT} \rightarrow \infty} I_P = \frac{K_{BS} \bar{T}}{1 - K_{CD}(\sigma v)} \quad (4.80)$$

1608

$$\lim_{\tau_{FT} \rightarrow 0} I_P^\dagger = R_0 \cdot \left(\frac{K_{CS}}{K_{LP}} \cdot \frac{(1 - \epsilon_b) \cdot \sqrt{2(K_{EK} + \epsilon_b)}}{1 + K_{DR}} \right) \quad (4.86)$$

1609 What these imply at an intuitive level is that at small pulses, current scales with the
 1610 major radius. While for long pulses, current scales with plasma temperature. In the
 1611 general case, of course, the problem becomes much harder to predict. – as shown by
 1612 the code’s results using Eq. (4.75).

Chapter 5

Completing the Systems Model

As opposed to previous chapters, this one will focus on the numerics behind the fusion systems model. A simple algebra will lead to a generalized solver for exploring reactor space for low cost and interesting machines. This will then naturally segue into a discussion of how plots are made and should be interpreted. The remaining chapters will then decouple the presentation of results from their analytic conclusions.

5.1 Describing a Simple Algebra

In essence, ~~Boiled-down~~, the systems model used here is a simple algebra problem – given five equations, solve for five unknowns. The goal is then to pick the five equations that best represent modern fusion reactor design (as shown in Fig. 5-1). This selection should also be done in such a way that actually reduces the system of equations to a simple univariate root solving equation (i.e. one equation with one unknown). As will be shown in the results, this model does reasonably ~~remarkably~~ well: matching ~~other~~ ~~year-long~~ modeling campaigns in seconds.

The logical place to start in a discussion of this algebra problem is with the three equations fundamental to all reactor-grade tokamaks – both in steady-state and pulsed operation. These are: the Greenwald density limit, power balance, and current bal-

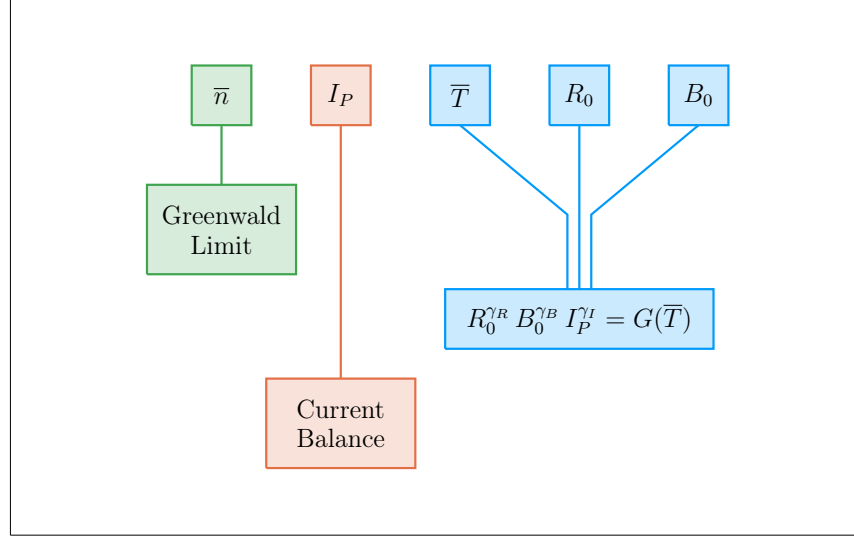


Figure 5-1: Equation Selection for Fusion System

The goal of this fusion system is to create a set of equations that model the five dynamic variables. These are the Greenwald limit for density, current balance for the plasma current, and three generalized formulas for the temperature, major radius, and toroidal field strength.

1631 ance. The Greenwald density's importance was hinted early on when it was used to
1632 simplify every equation derived thereafter.

$$\bar{n} = K_n \cdot \frac{I_P}{R_0^2} \quad (2.11)$$

1633 The two balance equations ~~proved to be~~prove slightly more complicated.~~dubious.~~ As
1634 was ~~shown, shown previously,~~ current balance ~~—the stability requirement for tokamaks~~
1635 ~~— was the more difficult of the two — bringing most peculiar. It brought~~ forth the notion
1636 of self-consistency for steady-state machines and a highly-coupled multi-root equation
1637 for pulsed ones. As such, ~~current balance this equation~~ stands as the ~~equation one~~
1638 everything ~~is substituted else will be substituted~~ into to ~~do a final setup for a~~ univariate
1639 root solve.

$$I_P = \frac{(K_{BS} + G_{IV}/G_{IP}) \cdot \bar{T}}{1 - K_{CD}(\sigma v) - G_{ID}/G_{IP}} \quad (4.75)$$

1640 Although slightly buried in Eq. (4.75), the right-hand side actually depends on all the
1641 quantities (including I_P through the ~~wall loading term in~~ blanket thickness). Through

1642 equation,

$$I_P = f(I_P, \bar{T}, R_0, B_0) \quad (5.1)$$

1643 The remaining equation common to all reactor-grade tokamaks is power balance –
1644 the relation that ~~quantifies its net electricity production capabilities.separates power~~
1645 ~~plants from toasters.~~ Due to the use of the ELMy H-Mode scaling law for modeling
1646 the diffusion coefficient, this had the complicated form of:

$$R_0^{\alpha_R^*} \cdot B_0^{\alpha_B} \cdot I_P^{\alpha_I^*} = \frac{G_{PB}}{K_{PB}} \quad (5.2)$$

1647 Although being rather cumbersome, this equation actually remains relatively simple
1648 in that all three quantities on the left-hand side are separable. To close the system,
1649 two more equations of this form are needed. These have the following form and will
1650 be described next.

$$R_0^{\gamma_R} \cdot B_0^{\gamma_B} \cdot I_P^{\gamma_I} = G(\bar{T}) \quad (5.3)$$

1651 5.2 Generalizing Previous Equations

1652 Where the equations defined up to this point in the chapter are shared among all fusion
1653 reactors, the remaining two equations – needed to close the system – must be **partially**
1654 chosen by the user. These ~~user-supplied~~ equations come in three ~~varieties:flavors:~~
1655 limits, ~~intermediatederived~~ quantities, and ~~dynamicfloating~~ variables. By convention,
1656 we enforce that at least one limit must be used. The other constraint can then come
1657 from any of the three defined collections, which we will refer to as the closure equation.

1658 5.2.1 Including Limiting Constraints~~Rehashing the Limits~~

1659 The limits category is ~~composed of the limiting constraints given in Chapter 3.simply~~
1660 ~~a rebranding of the secondary constraints given previously.~~ These include the physics
1661 derived limits from MHD theory – i.e. the beta limit (β_N) and the kink safety fac-

1662 tor (q_{*95}) – which for clarity, set maximums on the allowed plasma pressure and
 1663 ~~current, velocity~~, respectively. Additionally, there were several engineering limits also
 1664 described: wall loading, heat loading, and maximum power capacity. For this paper,
 1665 wall loading from neutrons (P_W) is assumed to be important, whereas the other two
 1666 engineering limits are not allowed to explicitly guide designs.
 1667 Combined all these limits, as well as the yet to be defined ~~dynamic float~~ and ~~intermediate derived~~
 1668 equations, are given in Table 5.1. These share a remarkably similar form to power

Table 5.1: Main Equation Bank

To close the system of equations for potential reactors, different equations can be used to
 lock down tokamak designs. These include physics and engineering limits (L), as well as
 ways to set ~~dynamic (D) floating (F)~~ or ~~intermediate (I) derived (D)~~ variables to constant
 values.

Variable	Category	$G(\bar{T})$	γ_R	γ_B	γ_I
Power Balance	-	G_{PB}/K_{PB}	α_R^*	α_B	α_I^*
Beta (β_N)	L	$K_{TB}\bar{T}$	1	1	0
Kink (q_{*95})	L	K_{KF}	1	1	-1
Wall Loading (P_W)	L	$K_{WL}(\sigma v)^{1/3}$	1	0	$-2/3$
Power Cap (P_E)	L	$K_{PC}(\sigma v)$	1	0	-2
Heat Loading (q_{DV})	L	$K_{DV}(\sigma v)^{1/3.2}$	1	0	-1
Major Radius (R_0)	D	$(R_0)_{const}$	1	0	0
Magnet Strength (B_0)	D	$(B_0)_{const}$	0	1	0
Plasma Current (I_P)	D	$(I_P)_{const}$	0	0	1
Plasma Temperature (\bar{T})	D	$(\bar{T})_{const}/\bar{T}$	0	0	0
Electron Density (\bar{n})	D	$(\bar{n})_{const}/K_n$	-2	0	1
Plasma Pressure (\bar{p})	I	$(\bar{p})_{const}/K_n K_{nT} \bar{T}$	-2	0	1
Bootstrap Current (f_{BS})	I	$(f_{BS})_{const}/K_{BS} \bar{T}$	0	0	-1
Fusion Power (P_F)	I	$(P_F)_{const}/K_F K_n^2(\sigma v)$	-1	0	2
Magnetic Energy (W_M)	I	$(W_M)_{const}/K_{WM}$	3	2	0
Cost per Watt (C_W)	I	$(C_W)_{const} \cdot (K_F K_n^2(\sigma v)/K_{WM})$	4	2	-2

1669 balance when put into a generalized, separable state. This hints at why the major
1670 radius (R_0), the toroidal field strength (B_0), and the plasma current (I_P) can easily
1671 be separated and substituted out of the current balance equation.

1672 Before moving on, it proves useful to explain the two limits not used to explicitly guide
1673 reactor design – divertor heat loading and the maximum power capacity. The simpler
1674 of the two to reason is the heat loading limit. Although removing the gigawatts-per-
1675 square-meter of heat is extremely difficult, it remains an unsolved problem worthy of
1676 its own research machine.²² ~~machine, but currently neglected financially.~~ As such, it is
1677 only kept to provide a human-interpreted measure of difficulty. The power cap, on the
1678 other hand, is just handled informally. If a reactor surpasses it (i.e. $P_E > 4000MW$),
1679 it is considered invalid.

1680 While the maximum power cap informally sets a maximum major radius for a ma-
1681 chine, there also exists an implicit minimum major radius. This minimum occurs due
1682 to the hole-size constraint – i.e. at some point there is no longer enough room on the
1683 inside of the machine to store the central solenoid, blanket, and TF coils.

1684 At this point, we can now explain how various quantities in the systems model
1685 can be set to user-given constant values. This basically allows users to treat one
1686 ~~dynamicfloating~~ variable as a ~~staticfixed~~ one (e.g. the temperature and bootstrap
1687 fraction).

1688 5.2.2 Minimizing ~~IntermediateDerived~~ Quantities

1689 Whereas the limits from the previous section represented constraints with real physics
1690 and engineering repercussions, the ~~intermediatederived~~ quantities here are just used
1691 to find when reactors reach certain user-supplied values. Most notable are the capital
1692 cost (through the magnetic energy – W_M) and the cost-per-watt (C_W). The model
1693 also, however, allows easily setting values for the bootstrap fraction, plasma pressure,
1694 and fusion power. As mentioned previously, they are given in Table 5.1 through a

1695 generalized representation of the form:

$$R_0^{\gamma_R} \cdot B_0^{\gamma_B} \cdot I_P^{\gamma_I} = G(\bar{T}) \quad (5.3)$$

1696 What this collection of variables is really useful for, though, is finding minimum cost
1697 reactors – both in a capital context as well as a cost-per-watt one. ~~ThisWithout~~
1698 ~~boring the reader, this~~ is done in a three stage process. The first of which is to find
1699 a valid reactor – i.e. one that satisfies every limiting constraint. Practically, this is
1700 done by searching over a range of scanned temperatures. ~~First, some valid reactor is~~
1701 ~~found: it does not matter if it is good, just valid. This of course can be found by~~
1702 ~~systematically throwing darts at a dart board—see ??.~~

1703 After a valid reactor is found, its cost is recorded leading to a drill-down stage. In
1704 this step, the cost is continuously halved until a valid reactor cannot be found. Once
1705 this invalid reactor is reached, it sets a bound on the minimum cost reactor. As such,
1706 the final stage is a simple bisection step where the minimum cost is honed down to
1707 some acceptable margin of error – see Fig. 5-2.

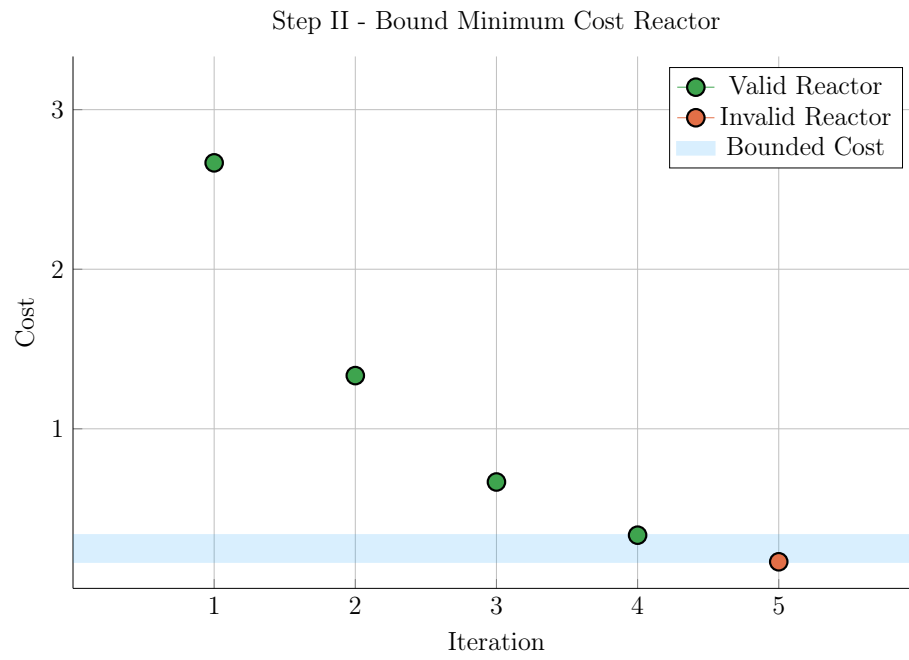
1708 5.2.3 Pinning ~~DynamicFloating~~ Variables

1709 The remaining collection of closure equations is for the five ~~dynamicfloating~~ variables
1710 in the systems model: R_0 , B_0 , \bar{n} , \bar{T} , and I_P . As we are making equations of the
1711 following form, the formulas for R_0 , B_0 , and I_P are trivial.

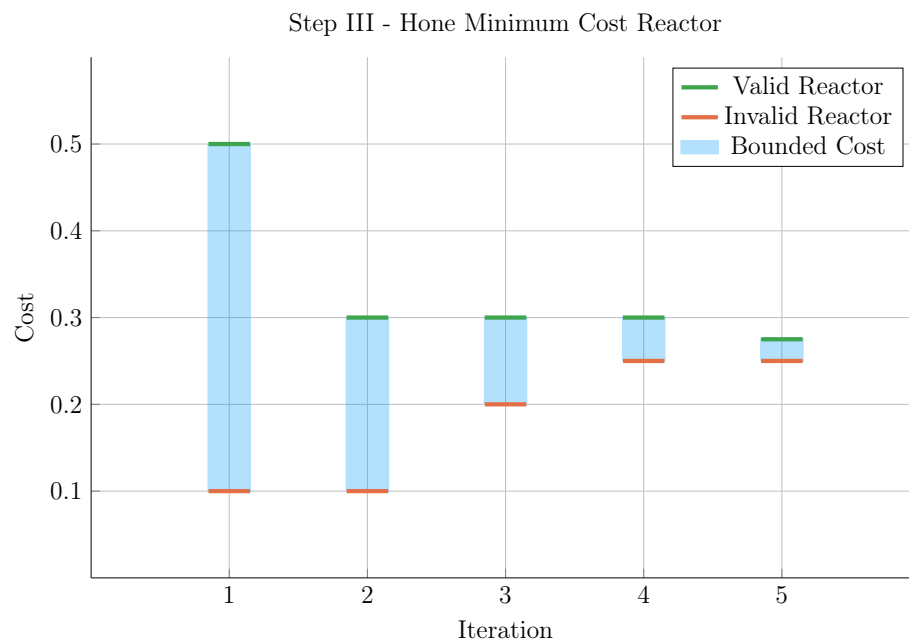
$$R_0^{\gamma_R} \cdot B_0^{\gamma_B} \cdot I_P^{\gamma_I} = G(\bar{T}) \quad (5.3)$$

1712 Next, the equation for \bar{n} – shown in Table 5.1 – is just a simple undoing of the Green-
1713 wald density limit. The remaining equation is then from the original temperature
1714 equation:

$$\bar{T} = const. \quad (3.1)$$



(a) Minimize Step II



(b) Minimize Step III

Figure 5-2: Minimize Cost Step II/III – Optimize Reactor

1715 As was assumed earlier, this is sort of a default equation for the systems model. By
 1716 this, we mean reactor curves can be created by scanning over temperatures, i.e. set
 1717 $\bar{T} = 5$ keV in one run, 10 in the next, etc. This temperature equation also brings up
 1718 a difficulty for the algebraic solver, as it does not depend on: ~~subtlety of the model, as~~
 1719 ~~it does not depend on~~ current, radius, or magnet strength. Overcoming this difficulty
 1720 is discussed next subsection.

1721 5.2.4 Detailing the Equation Solver

1722 The algorithm that motivated this generalized equation approach most notably bi-
 1723 furcates in the situation where the closure equation does not depend on R_0 , B_0 , or I_P
 1724 (i.e. ~~for~~ the temperature equation). The two scenarios are given in Eqs. (5.4) to (5.10)
 1725 – where at least R_0 and B_0 are substituted out of the system. In the temperature
 1726 case, I_P is not needed to be explicitly removed.

1727 Concretely, the root solve for the temperature scenario is for the current, whereas it
 1728 is for the temperature in all other cases. The nomenclature in the code is a *match*
 1729 for Scenario I (i.e. root solving for plasma temperature), and a *solve* for Scenario II
 1730 (i.e. root solving for plasma current).

1731 Scenario I – Match for \bar{T}

$$R_0(\bar{T}) = \left(G_1^{(\gamma_{B,2} \gamma_{I,3} - \gamma_{B,3} \gamma_{I,2})} \cdot G_2^{(\gamma_{B,3} \gamma_{I,1} - \gamma_{B,1} \gamma_{I,3})} \cdot G_3^{(\gamma_{B,1} \gamma_{I,2} - \gamma_{B,2} \gamma_{I,1})} \right)^{\frac{1}{\gamma_{RBI}}} \quad (5.4)$$

$$B_0(\bar{T}) = \left(G_1^{(\gamma_{I,2} \gamma_{R,3} - \gamma_{I,3} \gamma_{R,2})} \cdot G_2^{(\gamma_{I,3} \gamma_{R,1} - \gamma_{I,1} \gamma_{R,3})} \cdot G_3^{(\gamma_{I,1} \gamma_{R,2} - \gamma_{I,2} \gamma_{R,1})} \right)^{\frac{1}{\gamma_{RBI}}} \quad (5.5)$$

$$I_P(\bar{T}) = \left(G_1^{(\gamma_{R,2} \gamma_{B,3} - \gamma_{R,3} \gamma_{B,2})} \cdot G_2^{(\gamma_{R,3} \gamma_{B,1} - \gamma_{R,1} \gamma_{B,3})} \cdot G_3^{(\gamma_{R,1} \gamma_{B,2} - \gamma_{R,2} \gamma_{B,1})} \right)^{\frac{1}{\gamma_{RBI}}} \quad (5.6)$$

$$\begin{aligned} \gamma_{RBI} = & (\gamma_{R,1} \gamma_{B,2} \gamma_{I,3} + \gamma_{R,2} \gamma_{B,3} \gamma_{I,1} + \gamma_{R,3} \gamma_{B,1} \gamma_{I,2}) - \\ & (\gamma_{R,1} \gamma_{B,3} \gamma_{I,2} + \gamma_{R,2} \gamma_{B,1} \gamma_{I,3} + \gamma_{R,3} \gamma_{B,2} \gamma_{I,1}) \end{aligned} \quad (5.7)$$

1734 **Scenario II – Solve for I_P**

$$R_0(\bar{T}) = \left(G_1^{\gamma_{B,2}} \cdot G_2^{-\gamma_{B,1}} \cdot I_P^{(\gamma_{B,1} \gamma_{I,2} - \gamma_{B,2} \gamma_{I,1})} \right)^{\frac{1}{\gamma_{RBT}}} \quad (5.8)$$

1735

$$B_0(\bar{T}) = \left(G_1^{-\gamma_{R,2}} \cdot G_2^{\gamma_{R,1}} \cdot I_P^{(\gamma_{I,1} \gamma_{R,2} - \gamma_{I,2} \gamma_{R,1})} \right)^{\frac{1}{\gamma_{RBT}}} \quad (5.9)$$

1736

$$\gamma_{RBT} = \gamma_{R,1} \gamma_{B,2} - \gamma_{R,2} \gamma_{B,1} \quad (5.10)$$

1737 5.3 Wrapping up the Logic

1738 As stated at the beginning of the chapter, this systems model basically ~~reducesboils~~
 1739 ~~down~~ to a simple 5 equation/5 unknown algebra problem. The Greenwald density was
 1740 implicitly used in the initial derive to simplify the logic. The current balance was then
 1741 delegated to be the root solve equation. Lastly, three equations were needed to remove
 1742 the major radius and magnet strength, as well as either the current or temperature.
 1743 These 16 equations were given in Table 5.1 with the generalized solution given in
 1744 Eqs. (5.4) to (5.10).

1745 This now sets the stage for the most interesting part of the document – the results.
 1746 ~~TheseIn true Dickens fashion, they~~ will come in several forms. The first result type
 1747 ~~we will encounter~~ will be temperature ~~scans thatseans. These~~ allow us to validate the
 1748 model ~~against otherby comparing it to several~~ designs from the literature. ~~These are~~
 1749 ~~created usingThese will use~~ the Scenario II solver.

1750 ~~TheMoving onto examples of the~~ Scenario I matcher ~~will then be used to createare~~
 1751 sensitivity studies and Monte Carlo samplings. The simple one variable sensitivities
 1752 will reveal local trends from sweeping various ~~staticfixed~~ (i.e. input) variables – namely
 1753 H , κ , B_{CS} , etc. – ~~one at a time~~. Whereas the samplings will highlight global trends
 1754 as many ~~staticfixed~~/input variables are allowed to vary simultaneously.

1755 These Scenario I ~~matchersflavors~~ are further subdivided in regards to the nature of
 1756 their closure equation. The first ~~typeflavor~~ comes from finding so called two limit
 1757 solutions, which live at the point where the beta and kink (or wall) limits are just

marginally satisfied. The second main type is then minimum cost reactors – measured
in either a capital cost or cost-per-watt context. These will be used in depth next
chapter.

1761 Chapter 6

1762 Presenting the Code Results

1763 Now that our fusion systems model has been formulated and completed, the next
1764 logical step is to ~~build a codebase and explore reactor space. code it up and run it to~~
1765 ~~produce interesting data.~~ To this, the code encompassing this document's model ~~for~~
1766 ~~this document~~ – Fussy.jl – is available at git.io/tokamak (with a short guide given in
1767 Appendix B). ~~The results from this chapter will be divided into~~ ~~The results will be~~
1768 ~~given shortly.~~

1769 ~~Before accosting the reader with some twenty plots and tables, though, it makes sense~~
1770 ~~to first warn them what they are getting into. This chapter has~~ three sections. The
1771 first is an attempt to test how ~~accurate~~ ~~good~~ the model is by comparing it with other
1772 codes in the field.^{1,5,6} ~~The next will be two prototypes developed to fairly compare~~
1773 ~~pulsed and steady state reactors, the initial motivation for this project. Next, we will~~
1774 ~~develop two prototype reactors that pit steady state against pulsed operation on a~~
1775 ~~levelized playing field.~~

1776 This chapter will then conclude with a discussion on how best to lower ~~reactor~~
1777 ~~costs. the costs of a tokamak reactor.~~ In line with the MIT mission, this will highlight
1778 how using stronger magnets leads to more compact, ~~economic~~ ~~efficient~~ machines. The
1779 new piece of insight, then, is how to optimally incorporate high-temperature super-
1780 conducting (HTS) tape technology – the ~~assumed technological advancement~~ ~~miracle~~
1781 found in the ARC design family.

1782 Succinctly,~~Without spoiling too much for the reader,~~ we will show that HTS tape
1783 should be used in the TF coils for steady-state tokamaks (i.e. B_0), whereas it should
1784 only be appear in the central solenoid (i.e. B_{CS}) for pulsed ones. This is a fundamen-
1785 tally new result!

1786 6.1 Testing theValidating Code againstwith other Mod- 1787 els

1788 After developing a new model, the first next step is to make sure its results are
1789 sensical.~~When you develop a new model, the first thing you have to do is check~~
1790 ~~that it makes sensical results.~~ The goal, however,~~goal~~ is to not ~~to~~ go too far, i.e.
1791 ~~overboard, though,~~ by: comparing it with too many models or requiring perfect
1792 matches with ~~all~~ their results. To this, we will compare Fussy.jl with five designs
1793 ~~coming from the literature~~~~three separate research teams~~ – hopefully casting a wide
1794 enough net through reactor-space to prove sufficient. It should be noted that for how
1795 simple this model is, it does a remarkable job matching ~~the other group's~~~~these~~ more
1796 sophisticated frameworks. It also highlights how discrepancies arise in this highly
1797 non-linear computational problem.

1798 The first reactor design that will provide a basis for comparison is the ARC reactor.⁵
1799 As it was also designed by MIT researchers, the fit is shown to be almost exact. This
1800 of course probably involves a fair amount of inherent biases stemming from ~~shared~~
1801 ~~scientific philosophies and knowledge base.~~~~how this ecosystem operates and produces~~
1802 ~~engineers—most notably as the core of this code comes from Jeff's ongoing interest~~
1803 ~~in the problem.~~

1804 The next set of reactor designs come from the ARIES four-act study.² This ARIES
1805 team is a United States effort to reevaluate the problem of designing a fusion reac-
1806 tor around once a decade. The most recent study focused on how tokamaks ~~would~~
1807 ~~lookshape-up~~ as you assume optimistic and conservative ~~values for~~ physics and engi-

neering parameters. Although our model recovers their results, it does highlight one peculiarity of their algorithm – reliance on the minimum achievable value of H .

The final series of reactors comes from the major codebase used among European fusion systems experts: PROCESS.⁶ As such, this group actually gives an example for pulsed vs. steady-state tokamaks. Although these designs have the most discrepancies with our model, discussion will be given that remedy some of the shortcomings. These basically ~~amount to~~ ~~boil down~~ to: alternative definitions for heat loss appearing in the ELMy H-Mode Scaling, as well as the simplified nature of our flux balance equation – which only accounts for central solenoid and PF coil source terms.

The most important detail to take from the comparisons done in Tables 6.1 to 6.4, however, is that each steady state design from the literature has H factors and Greenwald densities (N_G) that violate standard values (i.e. 1.0). What this means, practically, is steady-state reactors are not possible in the current tokamak paradigm – some technological advancement is needed.

6.1.1 Comparing with the PSFC Arc Reactor

As mentioned, this model matches the results from the ARC design almost ~~perfectly – see Table 6.1 and Fig. 6-2.~~ ~~perfectly.~~ This probably stems from how both models were developed within the MIT community. ~~Two notable discrepancies between the models, however, are in~~ ~~The points to make now, though, is even with how well the results match, there are two notable discrepancies:~~ the fusion power (P_F) and bootstrap current fraction (f_{BS}). These ~~discrepancies likely~~ ~~mainly~~ arise from the use of simple parabolic profiles for temperature and, thus, can be seen in the subsequent model comparisons. ~~temperature.~~

Before moving on, though, it is important to explain how the plots and table used for this comparison are made. First, a list of temperatures between 1 and 40 keV is scanned to produce a set of reactors – each with their own size (R_0), magnet strength (B_0), etc. These reactors are then turned into the two curves shown in Fig. 6-2 by

1835 mapping to their respective values. Note that R_0 vs. B_0 is then a measure of the
1836 accuracy in the tokamak's engineering, while I_P vs \bar{T} is a measure on its plasma's
1837 physics.

1838 Once these curves are created, a design point is chosen on them that has the least
1839 distance to the marked point (from the original model's paper). These two points – or
1840 reactors – are then compared in detail in Table 6.1. Note that the input variables are
1841 shared between the original model and this model's input file. The output between
1842 the two is what is different. For clarity, V is the volume of a tokamak in cubic
1843 meters, and the dash on the inductive current fraction f_{ID} implies it makes up 0% of
1844 the current.

1845 The use of a dash for β_N brings up the final piece of information needed to understand
1846 the plots and table creation process – limiting constraints. Note that in Fig. 6-2, the
1847 solid curve has two portions: **beta** and **wall**. These are the portions where the beta
1848 limit and the wall loading limit are the driving constraints, respectively. For example
1849 at $B_0 = 5\text{T}$, the wall loading (P_W) will be much less than the maximum allowed
1850 2.5MW/m^2 . This is why the dash is next to β_N in Table 6.1, as it is held at the
1851 maximum allowed value (i.e. $\beta_N = 0.026$.)

1852 Finally, the reason there is a dashed **pulsed** curve and a solid **steady** one is because
1853 this reactor was run in both modes of operation. The pulsed label is actually a
1854 slight misnomer as it implies the generalized current balance formula is used (over
1855 the simple steady current from Eq. (2.30)). Because pulses are set to 50 years, they
1856 are functionally steady-state regardless. The real reason the two curves diverge is
1857 because the steady current has a self-consistent current drive efficiency (η_{CD}).

1858 6.1.2 Contrasting with the Aries Act Studies

1859 Moving on, the Aries Act study focuses on how steady-state reactors would look under
1860 both a conservative and optimistic perspective. This is highlighted in Fig. 6-1, which
1861 shows how costs decreases as the H factor is allowed to increase. Notice that for every

1862 value of H , the ACT I study (i.e. the optimistic act) has a lower cost than the design
 1863 from ACT II (i.e. the conservative one).

1864 This figure also highlights another peculiarity of the ARIES study – a reliance on the
 1865 minimum possible value of H . Note that just left of the reactor point on both plots is a
 1866 highly erratic portion of the curve. As such, if even a slightly smaller value of H were
 1867 used in either case, a quite distinct reactor would occur. This is not a robust way to
 1868 design machines. A better approach would be to build with some safety factor – i.e
 1869 at a slightly more ~~optimistic value~~~~magical-version~~ of H . This can be seen in ARC's
 1870 H-Sweep.

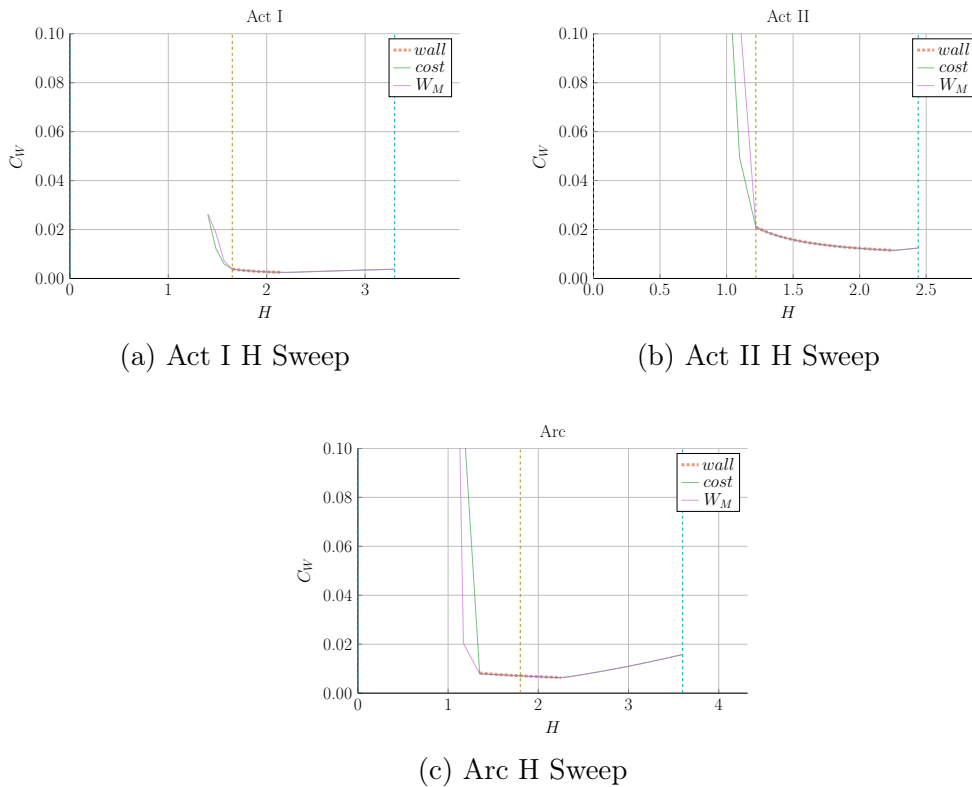


Figure 6-1: Act Studies Cost Dependence on the H Factor

1871 Act I – Advanced Physics and Engineering

1872 Act 1 is the ARIES study that assumes advanced physics and engineering design
1873 parameters. Although this paper’s model does a ~~fair job recovering~~~~good job matching~~
1874 the results from their paper, it does show what optimistic design really means. As
1875 can be seen, this design actually only surpasses the minimum possible toroidal field
1876 strength by as less than a Tesla! Practically, this means ~~their~~~~the~~ reactor is barely
1877 realizable. ~~Trying to build a 5T device would not be possible using their stated reactor~~
1878 ~~input parameters.~~

1879 Act II – Conservative Physics and Engineering

1880 ARIES more conservative design – Act II – is much more like ARC in nature. From
1881 the plots, it is obvious the paper’s model is basically right on top of the reactor curve
1882 made using Fussy.jl. Much like ARC, too, it shows how the model overestimates fusion
1883 power and underestimates bootstrap fraction due to their selection of a pedestal profile
1884 for plasma temperature.

1885 6.1.3 Benchmarking with the Process DEMO Designs

1886 The PROCESS team’s prospective designs for successors to ITER constitute the
1887 final set of model comparisons: the steady-state and pulsed DEMO reactors. As
1888 this paper is designed to compare these modes of operation, this study proves most
1889 ~~informative.~~~~fruitful.~~ It also highlights how common model decisions can dramatically
1890 alter what reactors come out of the solvers.

1891 The first discrepancy is how the PROCESS team defines the loss term in the ELMy H-
1892 Mode scaling law. As shown in their paper, they actually subtract out a Bremsstrahlung
1893 component, while leaving the fitting coefficients the same.⁶ After modifying Fussy.jl
1894 to incorporate this definition, the steady-state reactor is easily reproducible in R_0 –

1895 B_0 slice of reactor space.

$$P_L^{DEMO} = P_{src} - P_{BR} \quad (6.1)$$

1896 Unlike the steady-state case, however, the modified power loss term does not fix the
1897 pulsed case, as it actually draws the reactor curves further from the design in their
1898 paper. As such, it is flux balance that is now the main culprit for discrepancies
1899 between the two models. This makes sense, as this model uses highly simplified
1900 source terms – namely neglecting anything but the central solenoid and PF coils (as
1901 well as ignoring crucial physics for these two components). Even acknowledging the
1902 differences between the two models, Fussy.jl still does ~~reasonably~~~~remarkably~~ well at
1903 reproducing their much more sophisticated coding framework.

1904 The final point to make is about selecting optimum points to build as the ~~dynamic~~~~floating~~
1905 variables are allowed to make curves through reactor space. Up to this point, only
1906 steady-state tokamak designs have been explored. In every single one of these, though,
1907 the paper values have been very close to the point where the beta curves and wall
1908 loading curves cross. This is because they all result in the minimum cost-per-watt.
1909 For pulsed designs, on the other hand, kink curves start to appear for low magnetic
1910 field strengths. Just as beta-wall intersections were optimum places to design for low
1911 cost-per-watt (C_W) reactors, these beta-kink intersections will prove to be the place
1912 where minimum capital cost (W_M) reactors usually occur. ~~This is discussed in more~~
1913 ~~detail in Section 6.3.1.~~

1914 DEMO Steady – A Steady-State ITER Successor

1915 ~~Hands down, this DEMO Steady reactor is the worst modeled reactor using Fussy.jl.~~
1916 ~~As mentioned previously, though, some of the discrepancy was removed by using the~~
1917 ~~PROCESS team’s modified version of heat loss. This heavily corrected the R_0 — B_0~~
1918 ~~curve, but had no effect on the I_P — \bar{T} one. An interesting aside is that these curves~~
1919 ~~actually show how steady current is independent of limiting secondary constraint (as~~
1920 ~~noted).~~

1921 As shown in Fig. 6-5 and Table 6.4, the DEMO steady reactor is the design captured
1922 worst by the Fussy.jl model. Some discrepancy, however can be removed by using
1923 the PROCESS team’s modified version of heat loss, as given by Eq. (6.1).⁶ Although
1924 not supported by the official ITER database fit,²⁶ the PROCESS team reduces the
1925 absorbed power by the Bremsstrahlung power²⁷ – which can lengthen τ_E by more
1926 than 25%.⁷

1927 With this correction, the $R_0 - B_0$ curve is drawn to be right on top of their model’s
1928 design. The same cannot be said for the $I_P - \bar{T}$ curve as steady current was shown to
1929 have little dependence on tokamak configuration (R_0 and B_0) and, correspondingly,
1930 the limiting constraint (e.g. beta and wall).

1931 Note that the labels of modified and pulsed are slightly obscure in this context.
1932 Pulsed, for starters, is actually the generalized solver that does not rely on self-
1933 consistent current drive (i.e. in η_{CD}). The modified label is then when the pulsed
1934 solver uses the P_L^{DEMO} value in approximating heat conductive losses.

1935 DEMO Pulsed – A Pulsed ITER Successor

1936 This pulsed version of DEMO is the only reactor in our collection that is not run in
1937 steady-state. As such, it may be the most important one (i.e. it is the only pulsed
1938 reactor). The first observation from Fig. 6-6~~thing that is abundantly clear~~ is that this
1939 design actually has no valid wall loading portion – only a kink and beta curve exist!
1940 Even so, the results match pretty well. It should be noted, though, that this current
1941 drive is treated as an input and not solved self-consistently.

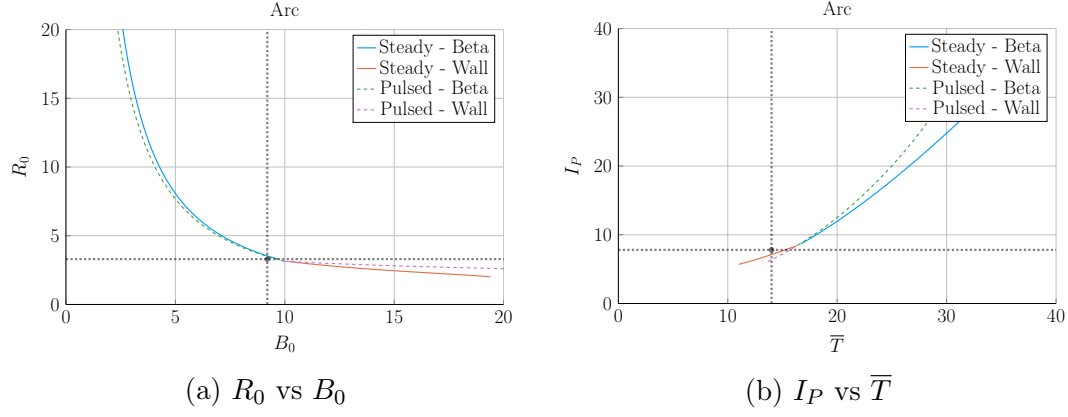


Figure 6-2: Arc Model Comparison

Table 6.1: Arc Variables

(a) Input Variables

Input	Value
H	1.8
Q	13.6
N_G	0.67
ϵ	0.333
κ_{95}	1.84
δ_{95}	0.333
ν_n	0.385
ν_T	0.929
l_i	0.670
A	2.5
Z_{eff}	1.2
f_D	0.9
τ_{FT}	1.6e9
B_{CS}	12.77

(b) Output Variables

Output	Original	Fussy.jl
R_0	3.3	3.4
B_0	9.2	9.5
I_P	7.8	8.8
\bar{n}	1.3	1.3
\bar{T}	14.0	16.8
β_N	0.026	-
q_{95}	7.2	6.1
P_W	2.5	2.2
f_{BS}	0.63	0.56
f_{CD}	0.37	0.44
f_{ID}	-	-
V	141	157
P_F	525	726
η_{CD}	0.321	0.316

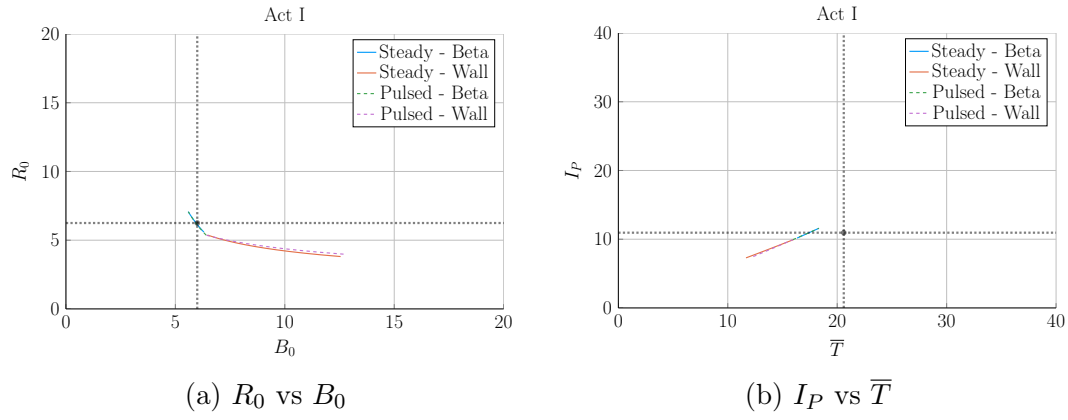


Figure 6-3: Aries Act I Model Comparison

Table 6.2: Act I Variables

(a) Input Variables

Input	Value
H	1.65
Q	42.5
N_G	1.0
ϵ	0.25
κ_{95}	2.1
δ_{95}	0.4
ν_n	0.27
ν_T	1.15
l_i	0.359
A	2.5
Z_{eff}	2.11
f_D	0.75
τ_{FT}	1.6e9
B_{CS}	12.77

(b) Output Variables

Output	Original	Fussy.jl
R_0	6.25	6.23
B_0	6.0	6.0
I_P	10.95	10.78
\bar{n}	1.3	1.3
\bar{T}	20.6	17.2
β_N	0.0427	-
q_{95}	4.5	4.0
P_W	2.45	2.00
f_{BS}	0.91	0.91
f_{CD}	0.09	0.09
f_{ID}	-	-
V	582.0	621.4
P_F	1813	1865
η_{CD}	0.188	0.185

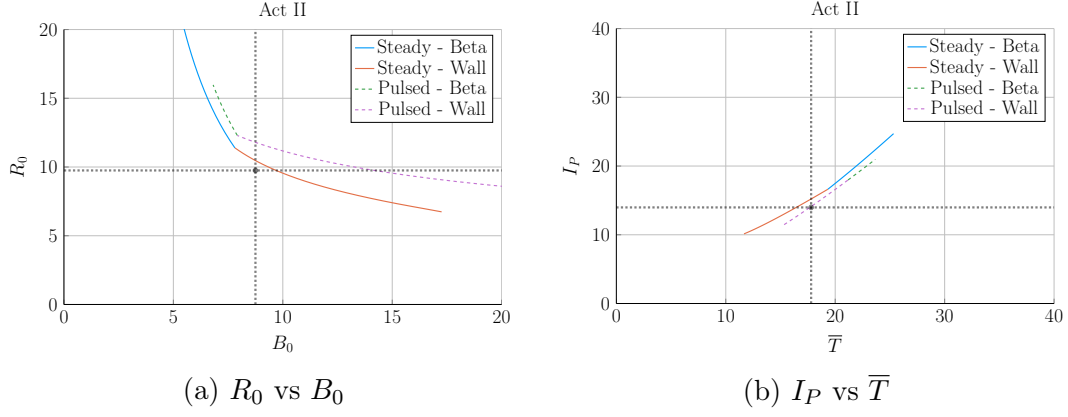


Figure 6-4: Aries Act II Model Comparison

Table 6.3: Act II Variables

(a) Input Variables

Input	Value
H	1.22
Q	25.0
N_G	1.3
ϵ	0.25
κ_{95}	1.964
δ_{95}	0.42
ν_n	0.41
ν_T	1.15
l_i	0.603
A	2.5
Z_{eff}	2.12
f_D	0.74
τ_{FT}	1.6e9
B_{CS}	12.77

(b) Output Variables

Output	Original	Fussy.jl
R_0	9.75	10.22
B_0	8.75	9.05
I_P	13.98	14.84
\bar{n}	0.86	0.82
\bar{T}	17.8	17.4
β_N	0.026	0.023
q_{95}	8.0	6.6
P_W	1.46	-
f_{BS}	0.77	0.66
f_{CD}	0.23	0.34
f_{ID}	-	-
V	2209	2559
P_F	2637	3460
η_{CD}	0.256	0.307

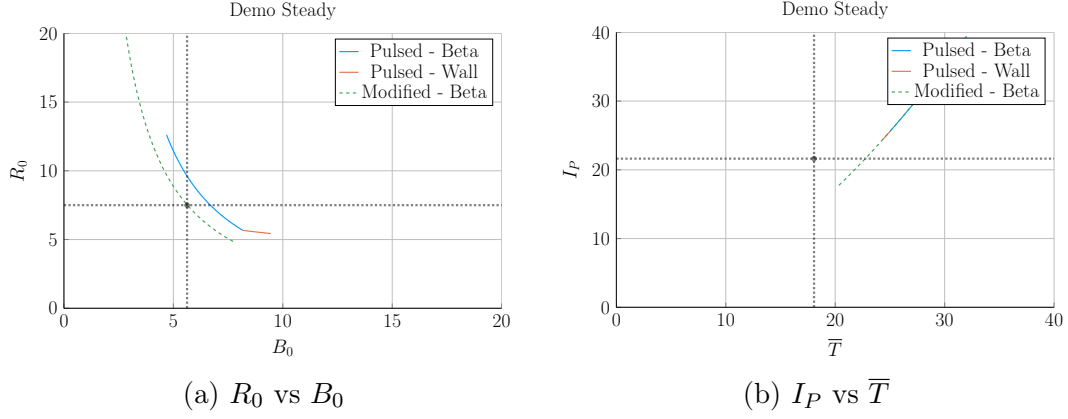


Figure 6-5: Demo Steady Model Comparison

Table 6.4: Demo Steady Variables

(a) Input Variables

Input	Value
H	1.4
Q	24.46
N_G	1.2
ϵ	0.385
κ_{95}	1.8
δ_{95}	0.333
ν_n	0.3972
ν_T	0.9187
l_i	0.900
A	2.856
Z_{eff}	4.708
f_D	0.7366
τ_{FT}	1.6e9
B_{CS}	12.85

(b) Output Variables

Output	Original	Fussy.jl	Modified
R_0	7.5	8.2	7.6
B_0	5.627	6.307	5.577
I_P	21.63	30.93	22.05
\bar{n}	0.875	1.048	0.855
\bar{T}	18.07	27.83	23.00
β_N	0.038	-	-
q_{95}	4.405	3.761	4.360
P_W	1.911	4.151	2.281
f_{BS}	0.611	0.424	0.492
f_{CD}	0.389	0.576	0.508
f_{ID}	-	-	-
V	2217	2879	2351
P_F	3255	8971	4306
η_{CD}	0.4152	-	-

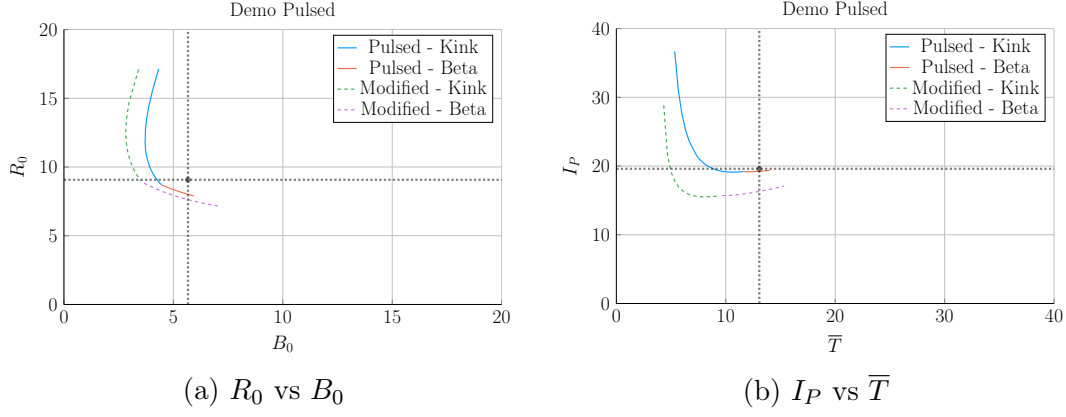


Figure 6-6: Demo Pulsed Model Comparison

Table 6.5: Demo Pulsed Variables

(a) Input Variables

Input	Value
H	1.1
Q	39.86
N_G	1.2
ϵ	0.3226
κ_{95}	1.59
δ_{95}	0.333
ν_n	0.27
ν_T	1.094
l_i	1.155
A	2.735
Z_{eff}	2.584
f_D	0.7753
τ_{FT}	7273
B_{CS}	12.77

(b) Output Variables

Output	Original	Fussy.jl	Modified
R_0	9.07	8.10	7.61
B_0	5.67	5.48	5.71
I_P	19.6	19.3	16.3
\bar{n}	0.7983	0.9795	0.9384
\bar{T}	13.06	13.28	13.00
β_N	0.0259	-	-
q_{95}	3.247	2.853	3.303
P_W	1.05	1.47	1.23
f_{BS}	0.348	0.164	0.190
f_{CD}	0.096	0.106	0.103
f_{ID}	0.557	0.730	0.707
V	2502	1751	1452
P_F	2037	2376	1756
η_{CD}	0.2721	-	-

6.2 Developing Prototype Reactors

Now that the model used in Fussy.jl has been tested against other fusion systems codes in the field, we will develop our own prototype reactors. Because this paper is about making a levelized comparison of pulsed and steady-state tokamaks, we will develop middle-of-the-road reactors that only differ by operating mode. The parameters for these two designs are captured in Tables 6.6 and 6.7.

To compare the two modes of operation, the steady-state prototype, Charybdis, is the obvious choice to start with – as the model was tested against four of these typed reactors. It was also pointed out that the model did remarkably well when recreating ARC. As the authors share many of the ARC team’s philosophies, Charybdis uses ~~static~~fixed parameters very similar to them.⁵

Next, although led to believe Charybdis’ pulsed twin reactor – Proteus – would be created by a simple flip of the switch, it was a slight oversimplification. The first difference is that the pulsed twin, Proteus, is assumed to be purely pulsed: $\eta_{CD} = 0$. Further, the bootstrap current is much less important than it was for steady-state tokamaks. This corresponds to a current profile peaked at the origin – i.e. a parabola. Numerically, this is done by raising l_i from around ~~0.5555~~ to 0.66.

The final difference creates the largest change in the twin reactors: the choice of ~~necessary technological advancement~~~~miracle~~. As ~~mentioned~~hinted several times before, the H factor is a common way designers artificially boost the confinement of their machines. This H value will thus be the technological advancement needed~~miracle~~ for Charybdis, the steady-state prototype. Next, as the main conclusion of this paper is to state the advantages of high magnetic field, ~~an inexpensive way to strengthen thea~~~~free way to boost a~~ central solenoid – through B_{CS} – will be employed using HTS coils.

~~Opposite the order of how they were designed, the goal now is to lock down a value of B_{CS} for Proteus and then use it to set the H factor for Charybdis. This selection algorithm is depicted in Fig. 6-7. For Proteus, the point locked down was $B_{CS} = 20$ T,~~

1970 which occurred at a fusion power (P_F) of around 1250 MW. As shown in the cost
1971 curve, this was at a point where the ratio between the minimum capital cost and
1972 the minimum cost-per-watt saturated. This choice of a 1250 MW reactor then led to
1973 Charybdis having an H factor of 1.7.

1974 The goal now is to impose a constraint on a reactor's economic competitiveness by
1975 setting the fusion power to a relatively low value for both designs – i.e. 1250 MW.
1976 As Fig. 6-7 shows, this results in Charybdis having an H factor of 1.7 and Proteus
1977 having a B_{CS} of around 20T. As shown in the Proteus cost curve, this was at a point
1978 where the ratio between the minimum capital cost and the minimum cost-per-watt
1979 leveled off.

1980 Note that these technological advancements (in H and B_{CS}) are necessary to get
1981 economic – or even physically realizable – reactors. This is the same reason why all
1982 the literature reactors used values for H and N_G that violate standard values.

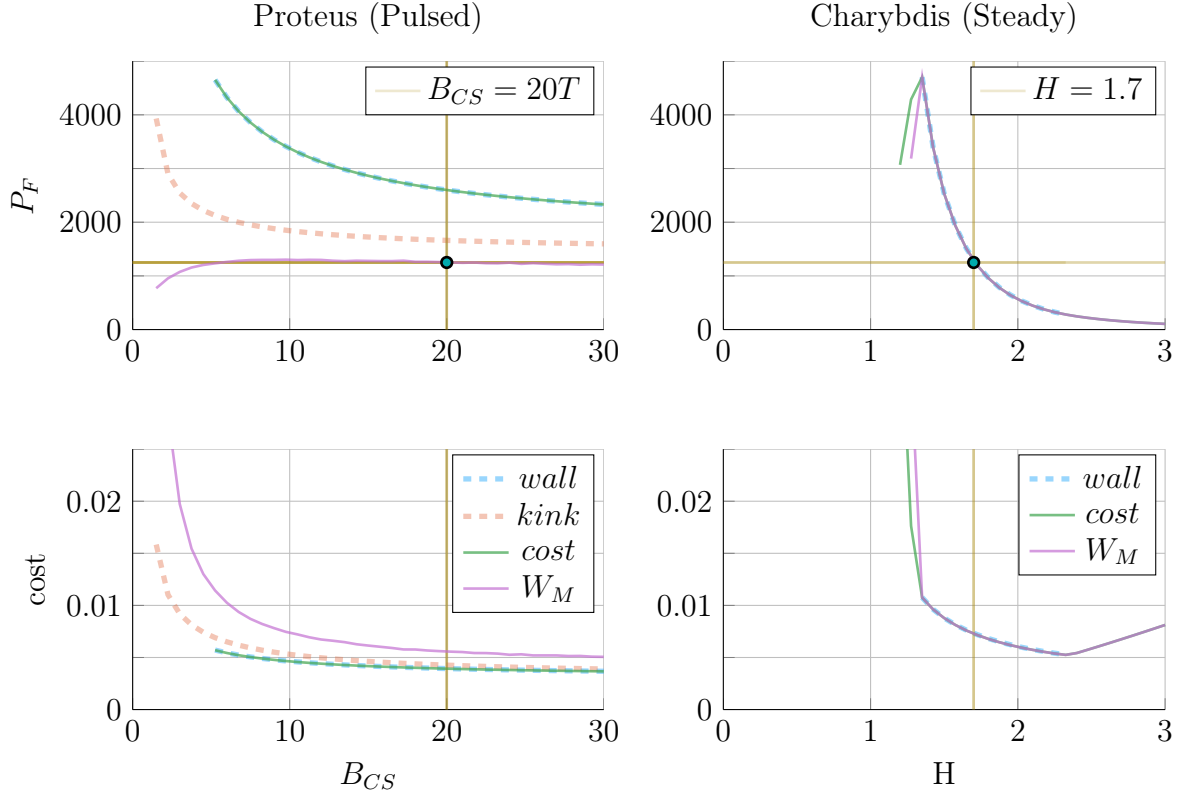


Figure 6-7: ~~Designing Reactor Prototypes~~How to Build a Fusion Reactor

As is convention in fusion engineering, designs are built using one assumed technological advancement. ~~a good design only relies on one miracle.~~ For steady-state reactors, we assume ~~a method for improving~~~~we can get better~~ confinement – by increasing H . While in the pulsed case, the advancement is inexpensive magnet technology for stronger fields ~~in miracle is assuming strong magnets for~~ the central solenoid – B_{CS} .

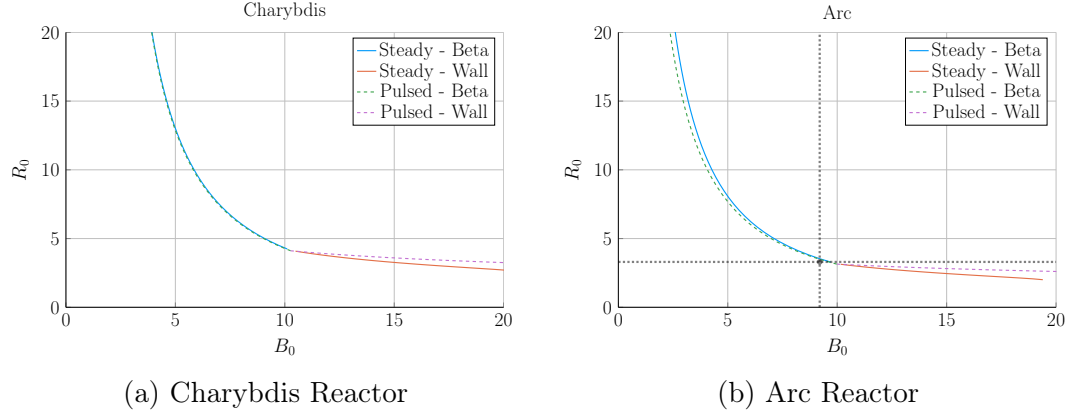


Figure 6-8: Steady State Prototype Comparison

Table 6.6: Charybdis Variables

(a) Input Variables

Input	Value
H	1.7
Q	25.0
N_G	0.9
ϵ	0.3
κ_{95}	1.8
δ_{95}	0.35
ν_n	0.4
ν_T	1.1
l_i	0.558
A	2.5
Z_{eff}	1.75
f_D	0.9
τ_{FT}	1.6e9
B_{CS}	12.0

(b) Output Variables

Output	Value
R_0	4.13
B_0	10.28
I_P	8.98
\bar{n}	1.47
\bar{T}	15.81
β_N	0.028
q_{95}	6.089
P_W	3.003
f_{BS}	0.723
f_{CD}	0.277
f_{ID}	0.0
V	225.5
P_F	1294
η_{CD}	0.291

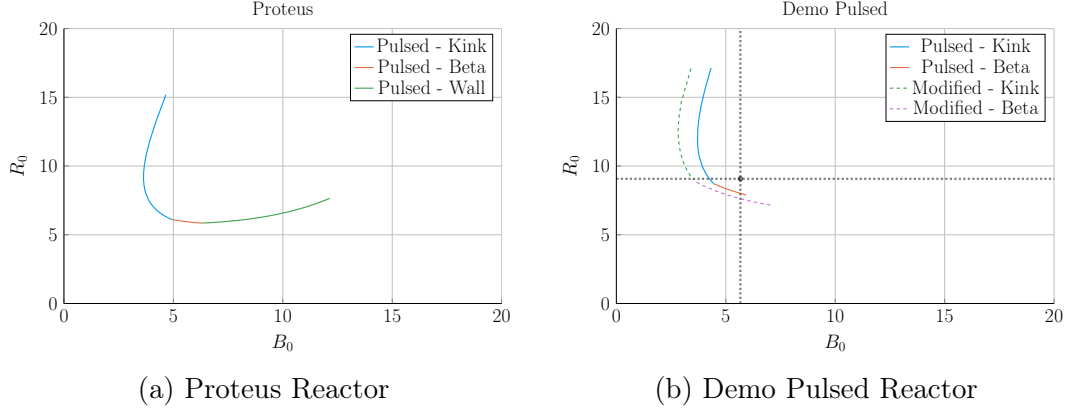


Figure 6-9: Pulsed Prototype Comparison

Table 6.7: Proteus Variables

(a) Input Variables

Input	Value
H	1.0
Q	25.0
N_G	0.9
ϵ	0.3
κ_{95}	1.8
δ_{95}	0.35
ν_n	0.4
ν_T	1.1
l_i	0.633
A	2.5
Z_{eff}	1.75
f_D	0.9
τ_{FT}	7200
B_{CS}	20.0

(b) Output Variables

Output	Value
R_0	6.11
B_0	4.93
I_P	15.54
\bar{n}	1.16
\bar{T}	11.25
β_N	0.028
q_{95}	2.5
P_W	1.763
f_{BS}	0.2675
f_{CD}	0.0
f_{ID}	0.7325
V	732.6
P_F	1667
η_{CD}	0.0

1983 6.2.1 Navigating around Charybdis

1984 The Charybdis reactor is the steady-state twin developed for this paper. As men-
1985 tioned, its parameters are similar to the ARC design. This is shown in Fig. 6-8, where
1986 the two $R_0 - B_0$ curves are almost interchangeable. Before moving on, it proves useful
1987 to note that the optimum place to build on these curves is where the two portions
1988 intersect – as it minimizes costs. These cost curves are shown in Fig. 6-11.

1989 6.2.2 Pinning down Proteus

1990 The pulsed twin reactor, Proteus, highlights the effects of a high field central solenoid.
1991 When compared to the Pulsed Demo design, the $R_0 - B_0$ curve looks far more favor-
1992 able – i.e. each machine built at a certain magnet strength would be more compact
1993 (and cheaper). An interesting facet of Proteus is that it exhibits all three used limits:
1994 kink safety factor, Troyon beta, and wall loading. Cost curves are shown in Fig. 6-12.

1995 6.2.3 Highlighting Operation Differences

1996 Before moving onto general conclusions taken from the data, a quick investigation
1997 into the pulsed vs steady-state twin results is in order. A comparison between the
1998 two is best abridged in Table 6.8.

1999 Most apparently, pulsed reactors are typically larger than steady-state ones and are
2000 meant to be run at higher plasma currents. The former behavior was seen with
2001 the DEMO designs,^{6,7} whereas the latter was already mentioned in discussing how
2002 steady-state reactors never saw a kink (current limiting) regime. Additionally pulsed
2003 machines can be run at much lower temperatures because their higher current im-
2004 proves confinement.

2005 These combined effects lead to the minimum cost reactors for steady-state operation
2006 having much higher toroidal field strengths than their pulsed counterparts. This is
2007 discussed in Section 6.3.2 when explaining optimum use of HTS tape.

Table 6.8: Proteus and Charybdis Comparison

(a) Charybdis		(b) Proteus	
Output	Value	Output	Value
R_0	4.13	R_0	6.11
B_0	10.28	B_0	4.93
I_P	8.98	I_P	15.54
\bar{n}	1.47	\bar{n}	1.16
\bar{T}	15.81	\bar{T}	11.25

2008 **6.3 Learning from the Data**

2009 Now that the model has been properly vetted and prototypes designed, we can explore
2010 how pulsed and steady-state tokamaks scale. ~~This will lead to Fitting with the Dickens~~
2011 ~~theme, there will be~~ three mostly independent results. The first result will explore
2012 how to minimize costs for a reactor by choosing optimum design points. The next will
2013 be an argument for how to properly utilize the HTS magnet technology in component
2014 design. Lastly, we will take a cursory look at the other parameters capable of lowering
2015 machine costs.

2016 **6.3.1 Picking a Design Point**

2017 With more than twenty design parameters, finding the most ~~economic~~~~efficient~~ re-
2018 actor is ~~computationally intractable~~~~a fool's errand~~. Intuition building aside, finding
2019 ~~optimum~~~~good~~ reactors becomes much more feasible when only focusing on ~~dynamic~~~~floating~~
2020 variables – i.e. when keeping ~~static~~~~fixed~~ variables constant. This method, for exam-
2021 ple, is how all the $R_0 - B_0$ curves have been produced this chapter. Once these
2022 curves are produced, it is up to the user to choose which reactor on them to build.
2023 However, the guiding metric usually involves lowering some cost, either: capital cost
2024 or cost-per-watt.

2025 Regardless of reactor type, most ~~economic~~~~efficient~~ tokamaks operate near the beta
2026 limit – where plasma pressure is greatest. Besides being a regime highly sensitive
2027 to magnetic field strength, the beta limit is a constraint that occurs on every reac-

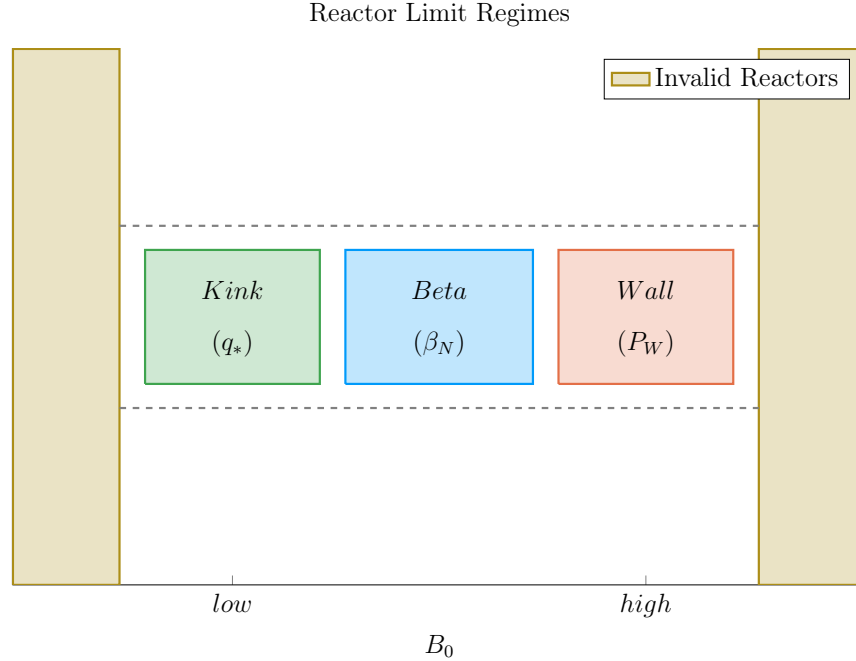


Figure 6-10: Limiting Constraint Regimes as function of B_0

At a simple level, a reactor has around three regimes of design limiting constraints. At low fields, the kink safety factor – through q_* and Eq. (3.41) – drives design. Then at high fields, wall loading – through P_W and Eq. (3.45) – guide reactors. And between the two, the beta limit – through β_N and Eq. (3.38) – are the limiting constraint.

tor (seen by the authors). This beta limit (β_N) is usually nested between the kink limit (q_*) to lower B_0 values and wall loading (P_W) to higher ones. Understanding these regimes is the first step towards building an intuition favoring economic efficient machines – see Fig. 6-10.

Now that the beta limit curve has been designated as the most economic efficient regime to operate in (usually), the goal is to select which reactor on it is the best one to build. Starting with the easier of the two, the optimum design point for steady-state reactors is the point where wall loading first starts to dominate the design. Due to the wall loading relation (see Eq. (3.45)), this causes Here, engineering concerns cause the reactor to start increasing in size and cost – which is bad. This conclusion is justified by the cost curves for all five reactors in Fig. 6-11. As these show, it is also where these reactor designers pinned down their tokamaks.*

*Simply stated, the optimum reactor for steady-state tokamaks is one that just barely satisfies the

2040 The problem of selecting an optimum design is more difficult for the pulsed case. This
 2041 is mainly due to ~~there being a regime where the kink safety factor can actually be a~~
 2042 ~~guiding limiting constraint.the kink limit regime being actually achievable.~~ Following
 2043 the conclusion from steady-state reactors would be an oversimplification because there
 2044 are actually two costs relevant to a reactor: capital cost and cost-per-watt. These
 2045 beta-wall reactors are actually the points often best for minimizing cost-per-watt
 2046 (i.e. your rate of return). The new beta-kink reactors, then, lead to cheap to build
 2047 machines – as they minimize capital cost. These conclusions are shown in Fig. 6-12.
 2048 Summarizing the conclusions of this subsection, the beta limit is usually the best
 2049 constraint to operate at. For lowering the cost-per-watt, a reactor should always be
 2050 run at the highest magnetic field strength (B_0) that ~~has the beta limit at its maximum~~
 2051 ~~allowed value.satisfies the beta limit.~~ This most often occurs when wall loading takes
 2052 over (for steady-state reactors) or reactors start being physically unrealizable (for
 2053 pulsed ones). Building cheap to build reactors – i.e. minimizing capital cost – then
 2054 actually proved to make pulsed design one of trade-offs. This is because the beta-kink
 2055 curve intersection produces a low capital cost reactor, but at the price of operating
 2056 at a subpar cost-per-watt. Designers should therefore balance the two cost ~~metrics~~
 2057 ~~when pinning down a pulsed reactor.metrics.~~

beta and wall loading limit simultaneously – i.e. where the two curves intersect.

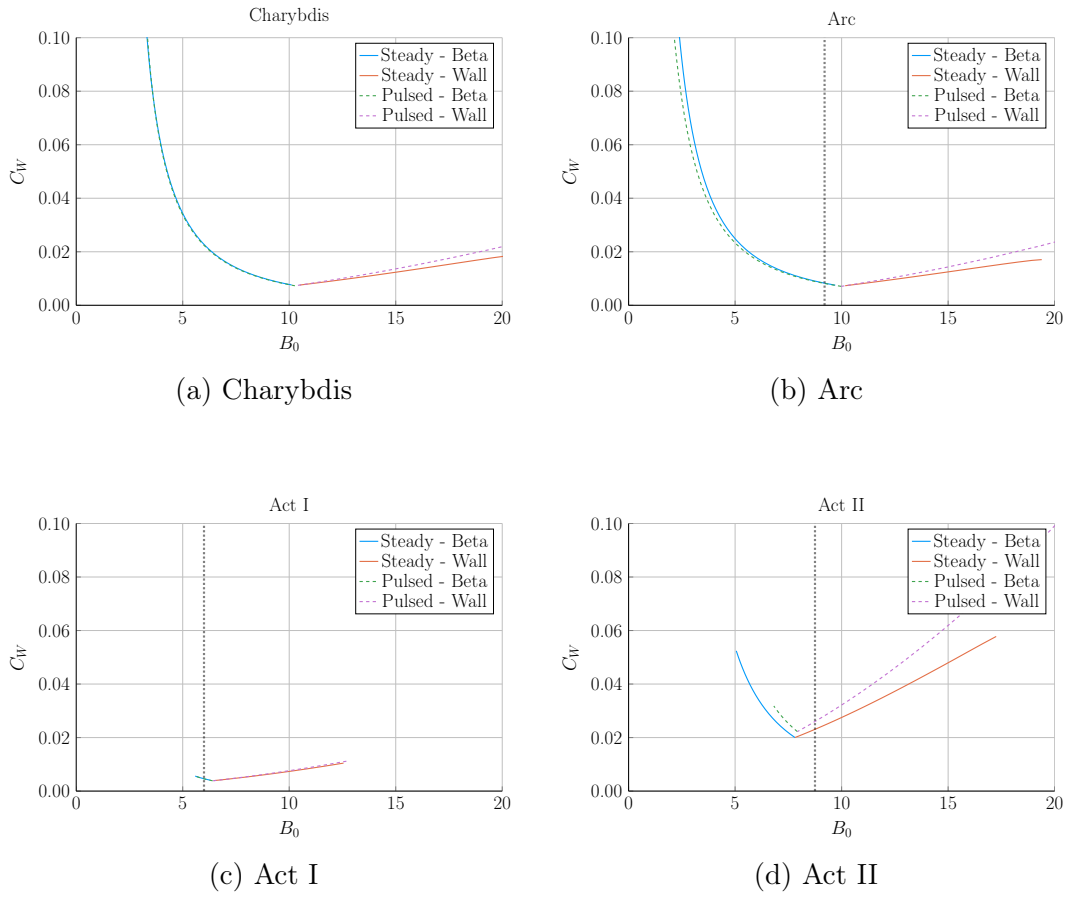


Figure 6-11: Steady State Cost Curves

Steady state reactors typically have two regimes – a lower magnet strength **beta** limiting one and a high field **wall** loading one. As shown, each steady state scan produces a minimum cost reactor at the point where the two regimes meet.

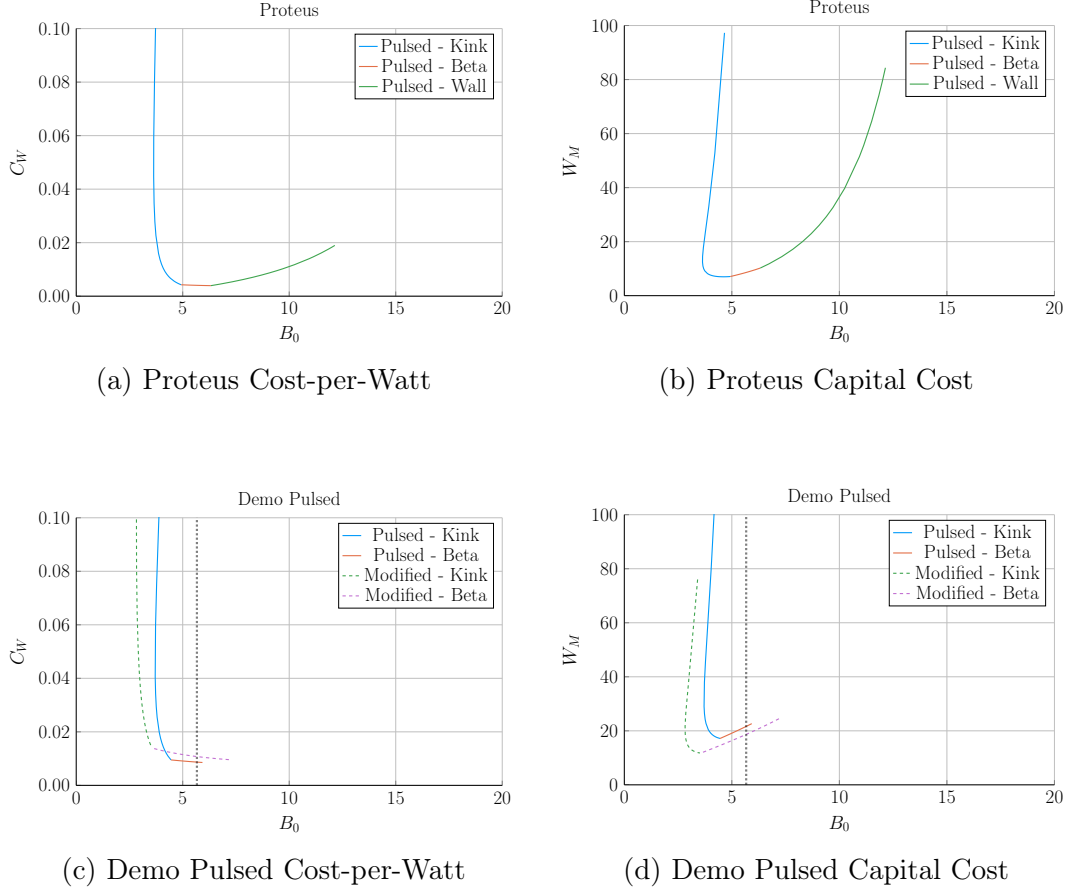


Figure 6-12: Pulsed Cost Curves

Pulsed reactor design is slightly more ambiguous than steady-state in terms of selecting an operating point. These plots show that the cost-per-watt is reduced at the highest field strength available to **beta** regime reactors. The minimum capital cost then occurs when the **beta** and **kink** limit are both just marginally satisfied.

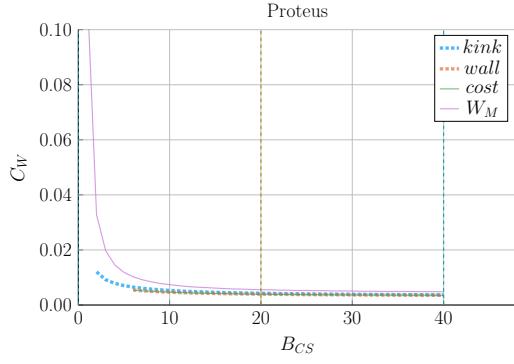
2058 6.3.2 Utilizing High Field Magnets

2059 The main conclusion for this paper is that high field magnets are the way to go to
2060 build an ~~economicefficient~~, compact fusion reactor. In line with the MIT ARC effort,
2061 these high fields will be built with high-temperature superconducting (HTS) tape.
2062 This innovation is set to ~~nearly~~ double the strength of conventional magnets. The
2063 real question is how best to use this technology.

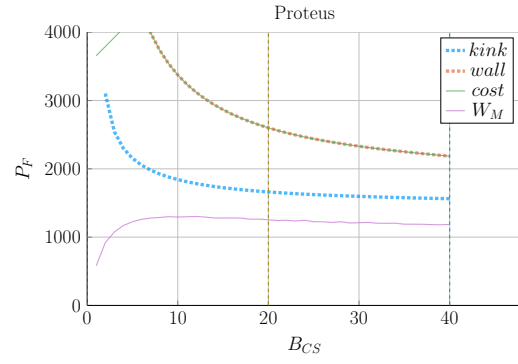
2064 At a very simple level, there are two main places strong magnets can be employed:
2065 the toroidal fields (B_0) and the central solenoid (B_{CS}). The easier mode of operation
2066 to start with is steady-state. This is because steady-state tokamaks do not rely on
2067 a central solenoid ~~to run their functionally infinite length pulses for the profitability~~
2068 ~~of their machines~~. Further, the cost curves in Fig. 6-11 show that all these designs
2069 would benefit from toroidal fields (B_0) not achievable with conventional magnets –
2070 which can only reach around ~~13 T.10 T on a good day.~~

2071 The more interesting result is that pulsed reactors gain no real benefit from using
2072 HTS toroidal field magnets – ~~as mentioned previously in Section 6.2.3~~. Within the
2073 modern paradigm (i.e. D-T fuel, H-Mode, etc), pulsed reactors never have to exceed
2074 the limits of ~~less expensive LTS magnets.inexpensive, copper magnets~~. The place
2075 HTS can really help is with the central solenoid, which governs how long a pulse
2076 can last. Further, ~~improvements to the effect of improving~~ the central solenoid ~~have~~
2077 ~~diminishing returns past saturates within~~ the range accessible to HTS tape. Again,
2078 HTS would be more than adequate for the modern paradigm. These conclusions are
2079 shown in Figs. 6-13 and 6-14.

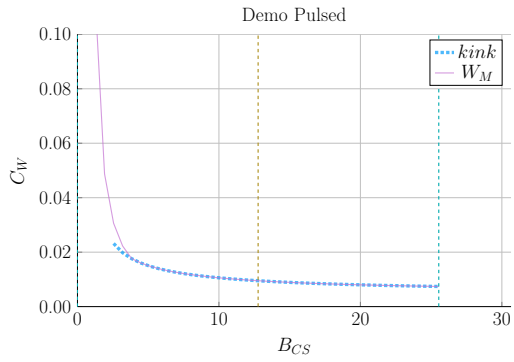
2080 ~~Summarizing this subsection,Rehashing this section,~~ HTS tape is ~~one of~~ the best
2081 ~~waysway~~ to lower the cost of fusion reactors at a commercial scale. For steady-state
2082 reactors, HTS works best in the toroidal field coils (B_0), while the tape would fare
2083 better in the central solenoid (B_{CS}) of pulsed reactors. Further, both effects saturate
2084 within the range of this HTS tape, rendering more sophisticated magnetic technology
2085 unnecessary. HTS is ~~thus one technological advancement that could help usher in an~~



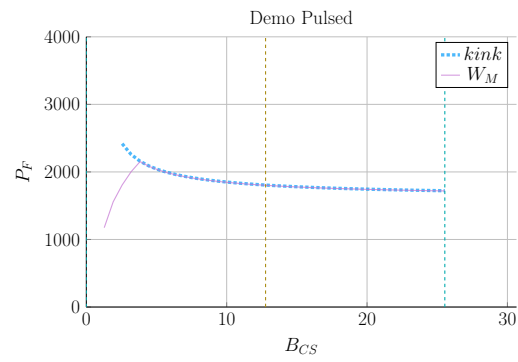
(a) Proteus Cost-per-Watt



(b) Proteus Fusion Power

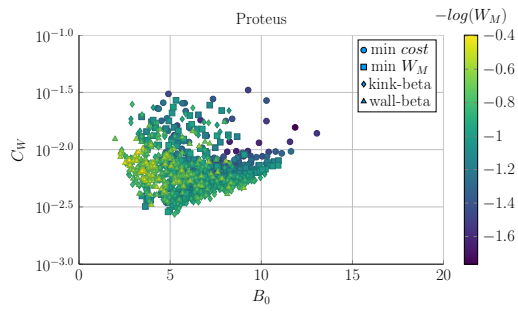


(c) Demo Pulsed Cost-per-Watt

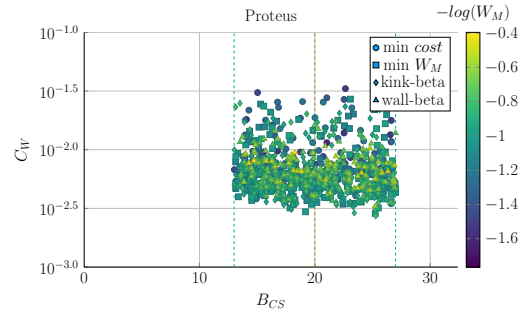


(d) Demo Pulsed Fusion Power

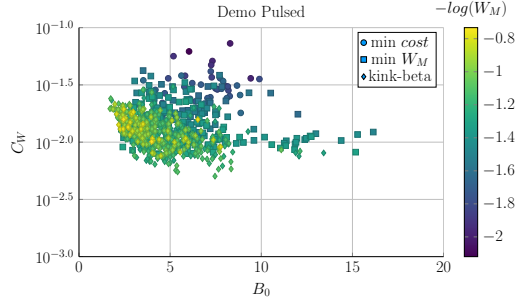
Figure 6-13: Pulsed B_{CS} Sensitivity



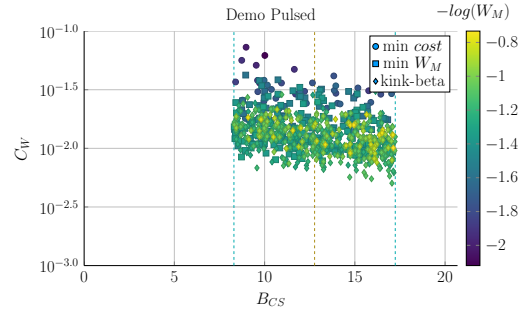
(a) Proteus B_0 Sampling



(b) Proteus B_{CS} Sampling



(c) Demo Pulsed B_0 Sampling



(d) Demo Pulsed B_{CS} Sampling

Figure 6-14: Pulsed Monte Carlo Sampling

era of ~~truly the answer to~~ affordable fusion energy.

6.3.3 Looking at Design Alternatives

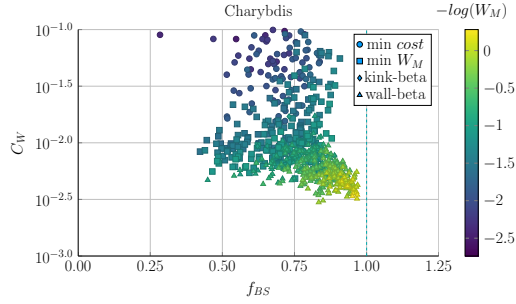
Even in this relatively simple fusion model, there are more than twenty ~~static~~~~fixed~~/input variable knobs a designer can tune to improve reactor feasibility. Many have practical limits, such as being physically realizable or fitting within the ELMY H-Mode database. Thus, the goal of this subsection is to investigate some of the more interesting results. Although many more plots are available in the appendix.

Capitalizing the Bootstrap Current

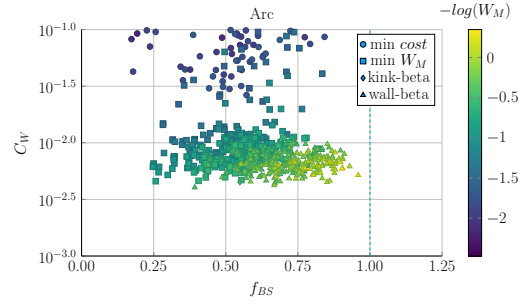
Besides artificially enhancing a plasmas confinement with the H-factor, steady-state reactor designers may also heavily rely on high bootstrap currents. This is because bootstrap current is the portion of current you do not have to pay for. The research ~~group~~~~seamp~~ most focused on this ~~technological advancement are~~~~miracle is~~ General Atomic's DIII-D in San ~~Diego~~ and PPPL's NSTX-U in New Jersey.~~Diego~~. This ~~advancement~~~~miracle~~ relies on tailoring current profiles to be ~~much more~~~~extremely~~ hollow.

Quickly reasoning this ~~seamp's~~ thought process are two sets of plots. The first plot (Fig. 6-15) highlights how the cheapest possible steady-state designs have bootstrap fractions approaching unity – they use almost no current drive. This makes sense as current drive is extremely cost prohibitive (i.e. why people consider pulsed tokamaks).

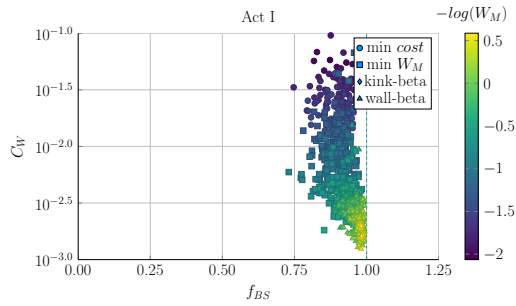
The next plot (Fig. 6-16) is the parameter that determines a current profile's peak radius: l_i . As can be seen, the current peak approaches the outer edge of the plasma as l_i decreases. This in turn boosts the bootstrap fraction closer to one – leading to inexpensive reactors.



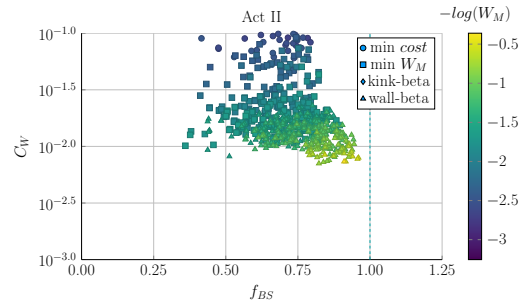
(a) Charybdis l_i Sampling



(b) Arc l_i Sampling



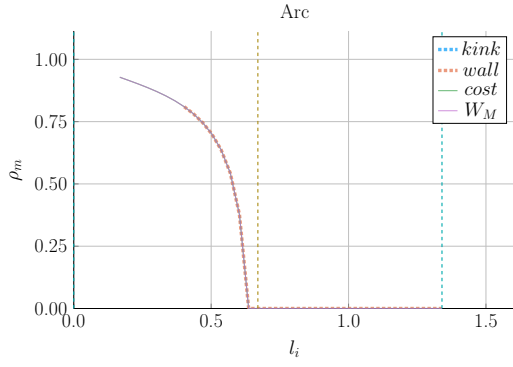
(c) Act I l_i Sampling



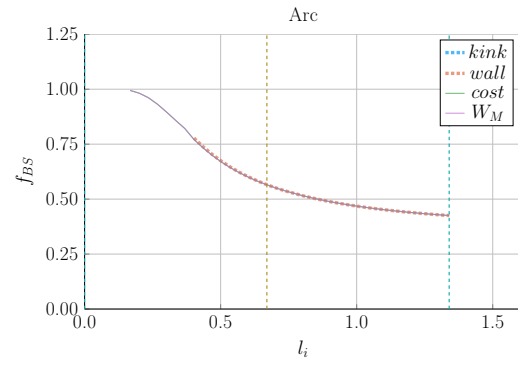
(d) Act II l_i Sampling

Figure 6-15: Bootstrap Current Monte Carlo Sampling

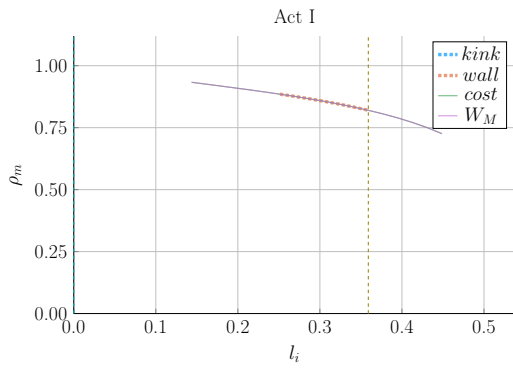
The purpose of these plots is to show that a high bootstrap current always reduces the cost of a steady state reactor – highly independent of actual input quantities (i.e. ϵ , l_i , etc.)



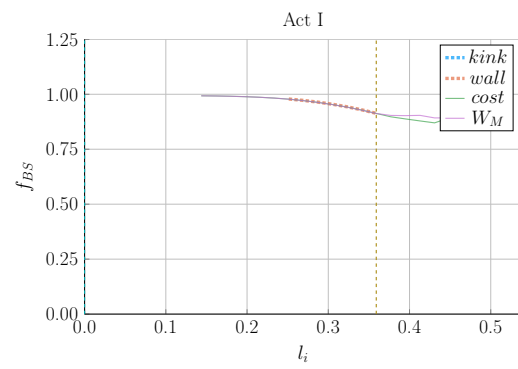
(a) Arc Peak Radius



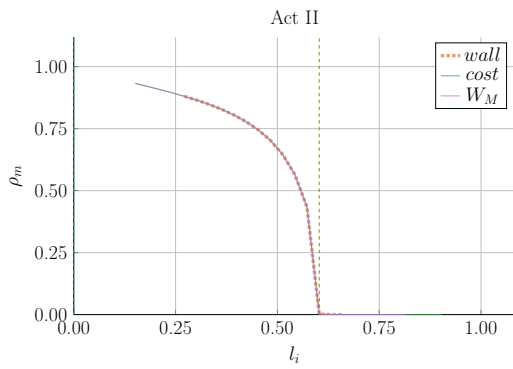
(b) Arc Bootstrap Fraction



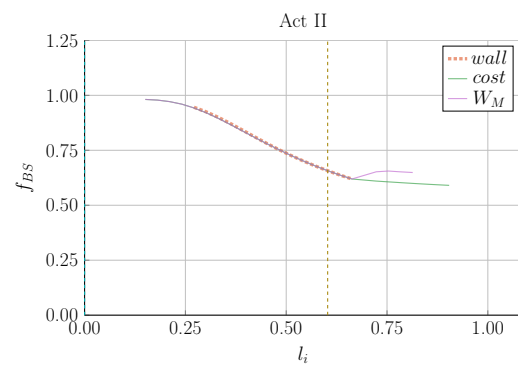
(c) Act I Peak Radius



(d) Act I Bootstrap Fraction



(e) Act II Peak Radius



(f) Act II Bootstrap Fraction

Figure 6-16: Internal Inductance Sensitivities

The internal inductance has a strong influence on the peaking radius (ρ_m) of the hollow profile and the bootstrap current fraction (f_{BS}). Lowering the internal inductance thus makes a profile more hollow, which in turn increases the bootstrap fraction.

2109 Contextualizing the H-Factor

2110 From before, increasing the H-factor always led to more cost effective steady-state
2111 reactors. This is because the enhanced confinement allows for smaller machines.
2112 This was already heavily explored in Fig. 6-1. These plots also show that steady
2113 state reactors would not be physically possible using a default H factor of one! In
2114 other words, steady-state tokamaks require some technical advancement before they
2115 can ever be used as fusion reactors. The same cannot be said for pulsed machines.

2116 For pulsed reactors, increasing H always reduces capital cost, but may actually in-
2117 crease the cost-per-watt. This is because the fusion power can decrease at a faster rate
2118 than the capital cost in a pulsed tokamak – both of which appear in Eq. (1.3) defining
2119 the cost-per-watt. ~~The reason for this is because fusion powers are much smaller in~~
2120 ~~pulsed machines.~~ This interesting result demonstrates the unusual behaviors of highly
2121 non-linear systems: masterclass intuition may not match model results.

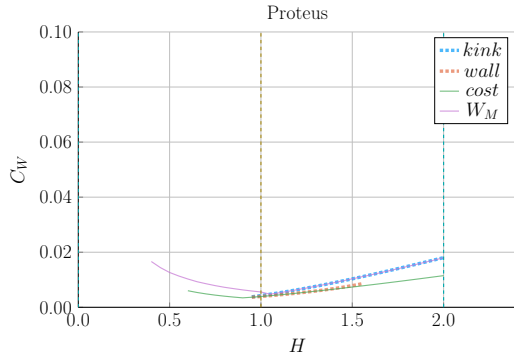
2122 Showcasing the Current Drive Efficiency

2123 The last exploration is less about building an ~~economicefficient~~ machine and more
2124 about understanding the self-consistent current drive efficiency in steady-state toka-
2125 maks. Using the Ehst-Karney model¹⁷ coupled with ~~standard analysis~~ ~~Jeff's textbook~~⁴
2126 leads to a remarkably simple and accurate solver. ~~As shown in Fig. 6-18, the~~ ~~The~~ model
2127 captures the physics almost ~~exactlyspot-on~~ for the different designs.*

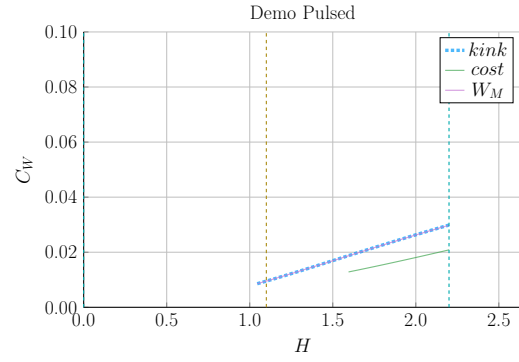
2128 In a similar fashion as the bootstrap fraction results, the variable that most captures
2129 how to directly maximize η_{CD} is the LHCD ~~wavelaser~~ launch angle, θ_{wave} . When
2130 below 90° it is considered outside launch, whereas up to 135° it is considered inside
2131 launch. Notably, these curves are not monotonic, there is an optimum launching
2132 angle – ~~as shown in Fig. 6-19.~~

2133 It should be noted that the launch angle was not found to have a major impact. This

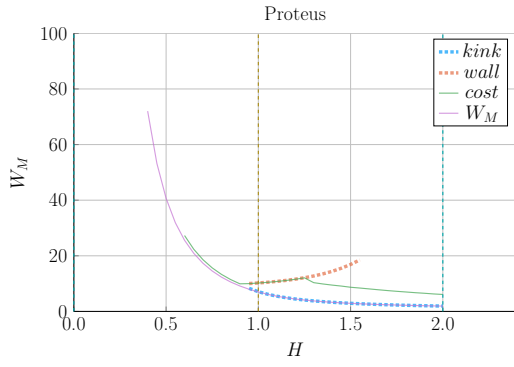
*It did, however, not converge for the DEMO steady reactor. This is probably due to lack of self-consistency for η_{CD} in their systems framework.



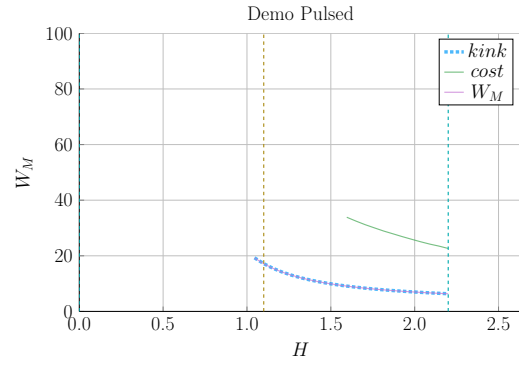
(a) Proteus Cost-per-Watt



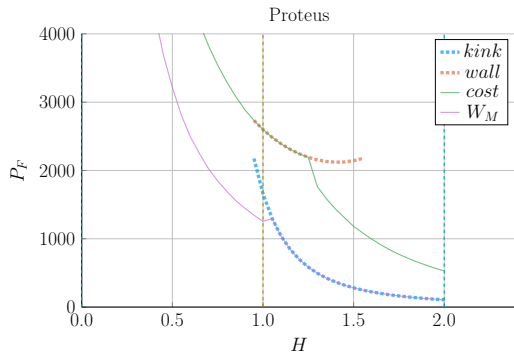
(b) Demo Pulsed Cost-per-Watt



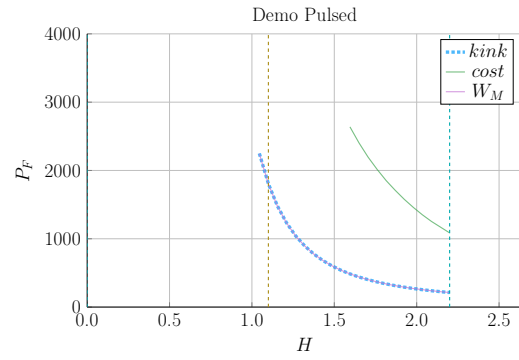
(c) Proteus Capital Cost



(d) Demo Pulsed Capital Cost

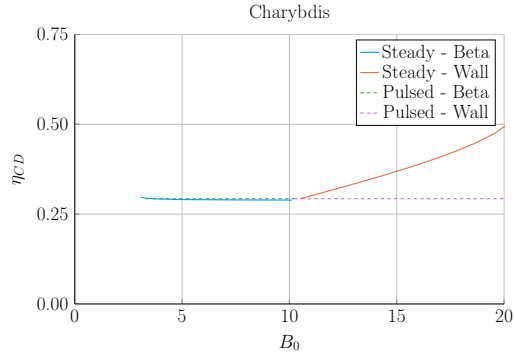


(e) Proteus Fusion Power

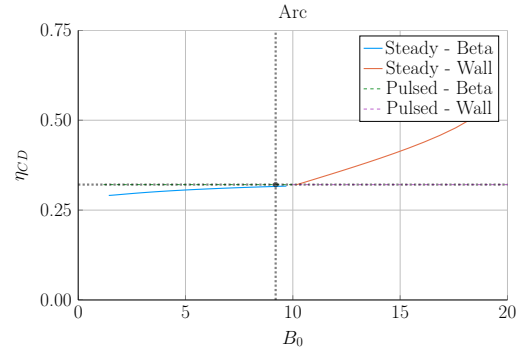


(f) Demo Pulsed Fusion Power

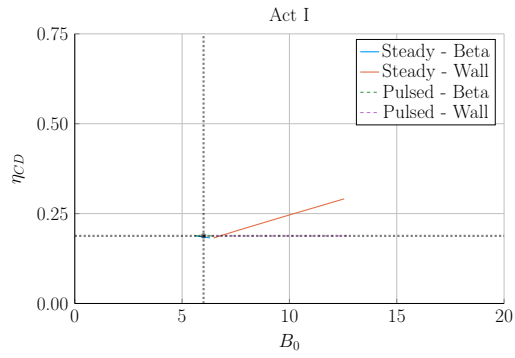
Figure 6-17: Pulsed H Sensitivities



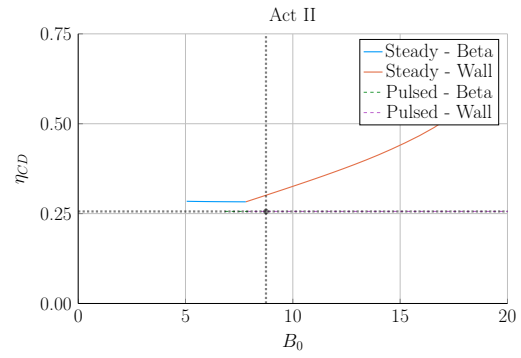
(a) Charybdis



(b) Arc



(c) Act I



(d) Act II

Figure 6-18: Steady State Current Drive Efficiency

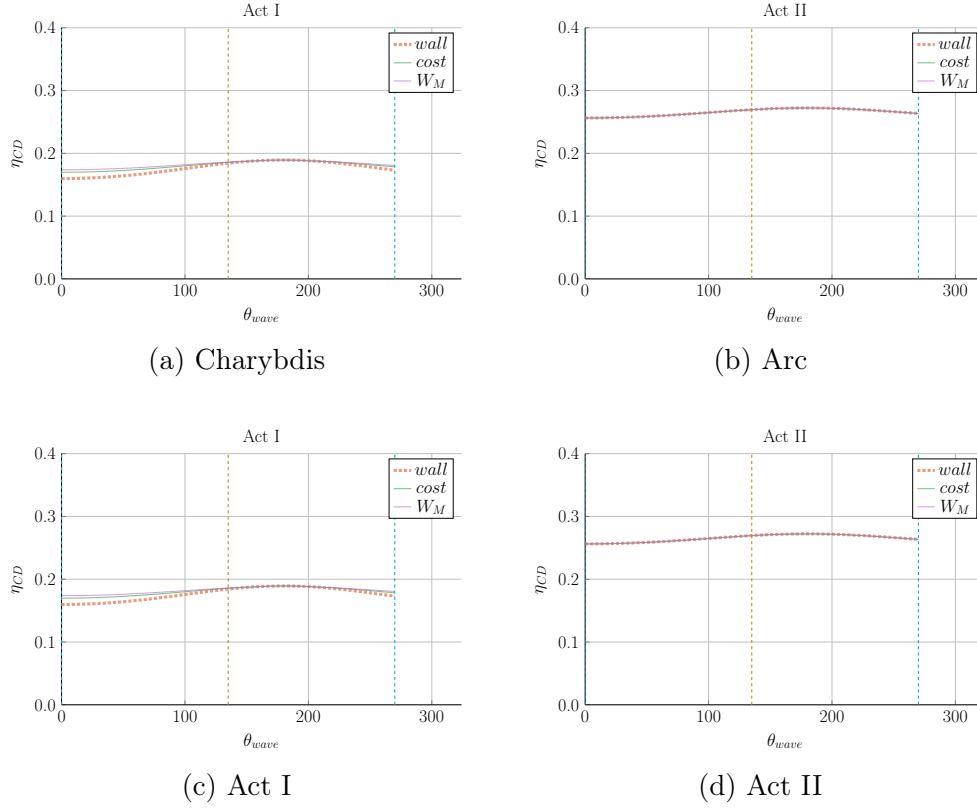


Figure 6-19: Current Drive Efficiency vs Launch Angle

2134 may be a due to an oversimplification of the model, as sources suggest inside launch
 2135 is preferable for multiple reasons./citeadxmodel.

2136 Chapter 7

2137 Planning Future Work for the Model

2138 This model may run and produce interesting results, but there is always more to be
2139 done. This chapter explores three potential fusion reactors that could help guide real
2140 world designs. These are: a stellarator (Ladon), a steady-state/pulsed composite hybrid
2141 (Janus), and a tokamak capable of reaching H, L, and I modes (Daedalus). The
2142 chapter then concludes by describing several possible model improvements, includ-
2143 ing: adding radiation sources, using pedestal profiles, and improving flux balance.

2144 ~~This model may run and produce interesting results, but there is always more to do.~~
2145 ~~This chapter explores three potential fusion reactors that could help guide real world~~
2146 ~~designs. It then goes into a laundry list of possible model improvements.~~

2147 ~~The three reactors covered are: a stellarator (Ladon), a steady-state/pulsed hybrid~~
2148 ~~(Janus), and a tokamak capable of reaching H, L, and I modes (Daedalus).~~

2149 7.1 Incorporating Stellarator Technology – Ladon

2150 A stellarator is, at a basic level, a tokamak helically twisted along the length of its
2151 major circle. For a long time they were dismissed because of their poor transport
2152 properties.~~the difficulty involved in building spiraled magnets.~~ Recent technological
2153 improvements, though, have eased this situation – as seen with the Wendelstein 7-

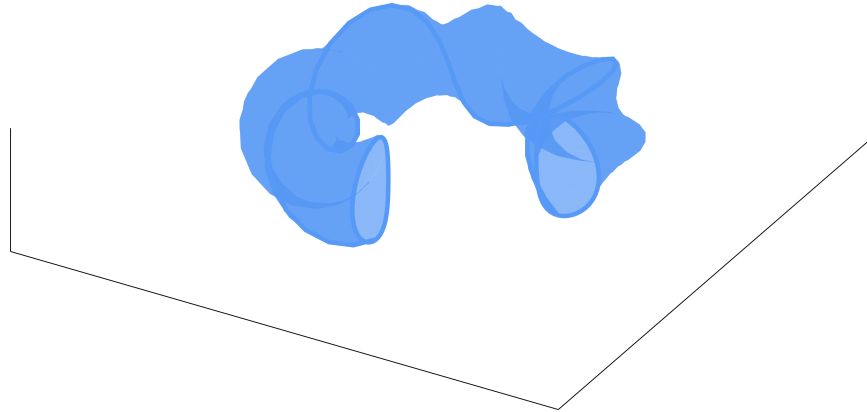
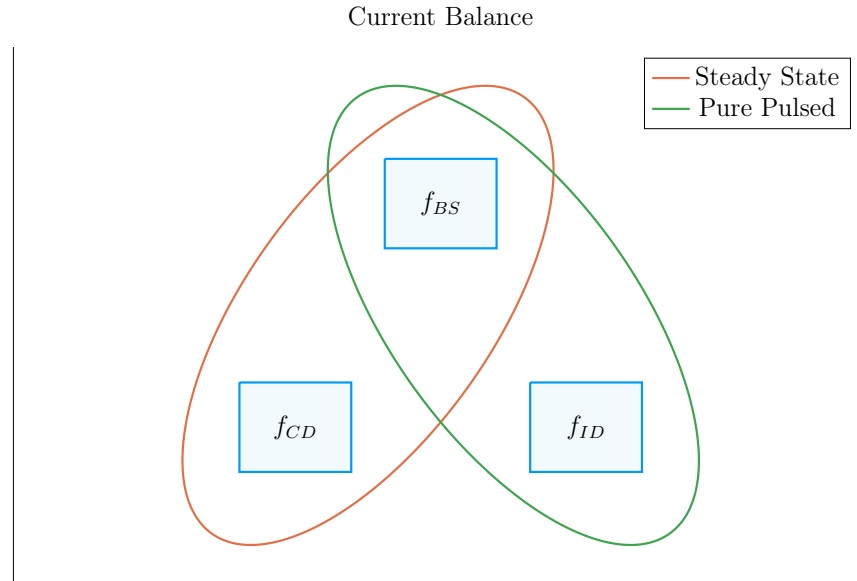


Figure 7-1: Cut-Away of Stellarator Reactor

2154 X device in Germany. The problem now is engrained in the ~~underdeveloped~~~~missing~~
 2155 scaling laws stemming from a lack of machines and, more fundamentally, data points.

2156 To model Ladon, this paper's proposed stellarator, one would need to replace at
 2157 least: the Greenwald density limit and the confinement time scaling law. In place of
 2158 the Greenwald density will likely be some other density or current limit, possibly the
 2159 Bremsstrahlung density limit.²⁸ This may require the density to be carried throughout
 2160 analysis – thus appearing explicitly in one column of Table 5.1.

2161 ~~Optimistically, expanding this model would just involve developing a new confinement~~
 2162 ~~time scaling law and replacing the Greenwald density limit. The reason the Greenwald~~
 2163 ~~density limit is no longer important is because stability is much easier to maintain in~~
 2164 ~~a stellarator. Most likely, the density limit will now be governed by Bremsstrahlung~~
 2165 ~~radiation. If this were the case, each equation would need to be redivided using it.~~
 2166 ~~Ladon would be the reactor built using this enhancement.~~



In a tokamak, there needs to be a certain amount of current – and that current has to come from somewhere. All good reactors have an adequate bootstrap current. What provides the remaining current is what distinguishes steady state from pulsed operation.

2167 7.2 Making a CompositeHybrid Reactor – Janus

2168 The next interesting reactor would be a ~~composite~~hybrid tokamak incorporating
 2169 pulsed and steady-state operation: Janus. Fundamentally, this would involve cur-
 2170 rent coming from both LHCD (steady-state), as well as inductive (pulsed) sources.
 2171 This was actually used in Demo Pulsed, but the current drive was not handled self-
 2172 consistently. Coupling these two current sources could reduce reliance on bootstrap
 2173 current and lead to much more compact machines.

2174 The arguments against this are mainly technical: why build two difficult auxiliary
 2175 systems when one is needed – especially when they probably work against each other.
 2176 Although rational, it may turn out that the larger current achievable with two sources
 2177 leads to a smaller, more economic machine.~~the argument implicitly assumes a current~~
 2178 ~~is achievable through only one source (i.e. either through LHCD or from a central~~
 2179 ~~solenoid). Using two may allow for stronger plasma currents.~~

2180 7.3 Bridging Confinement Scalings – Daedalus

2181 The final potential reactor – Daedalus – is designed ~~so that it can beto collect as~~
 2182 ~~many scaling laws as possible. As a baseline, it should be able to~~ run in H-Mode,
 2183 L-Mode, and I-Mode. Because L-Mode is available on any machine, the first step is
 2184 ~~actually~~ building under H-Mode. The goal then is to find reactors that can also reach
 2185 I-Mode – ~~simultaneouslythus~~ improving the scaling law’s fit and ~~possibly~~ making the
 2186 actual reactor more ~~economiceost effective~~.

2187 Presented below are the three confinement scaling laws, as well as the generalized
 2188 formula. As should be noted, the I-Mode scaling currently lacks a true radial de-
 2189 pendence – as it has only been found on two machines. This is one reason Daedalus
 2190 would be so valuable.

$$\tau_E^G = K_\tau H \frac{I_P^{\alpha_I} R_0^{\alpha_R} a^{\alpha_a} \kappa^{\alpha_\kappa} \bar{n}^{\alpha_n} B_0^{\alpha_B} A^{\alpha_A}}{P_{src}^{\alpha_P}} \quad (3.26)$$

$$\tau_E^H = 0.145 H \frac{I_P^{0.93} R_0^{1.39} a^{0.58} \kappa^{0.78} \bar{n}^{0.41} B_0^{0.15} A^{0.19}}{P_{src}^{0.69}} \quad (3.28)$$

2191

$$\tau_E^L = 0.048 H \frac{I_P^{0.85} R_0^{1.2} a^{0.3} \kappa^{0.5} \bar{n}^{0.1} B_0^{0.2} A^{0.5}}{P_{src}^{0.5}} \quad (7.1)$$

2192

$$\tau_E^I = \frac{0.014 H}{0.68^{\lambda_R} \cdot 0.22^{\lambda_a}} \cdot \frac{I_P^{0.69} R_0^{\lambda_R} a^{\lambda_a} \kappa^{0.0} \bar{n}^{0.17} B_0^{0.77} A^{0.0}}{P_{src}^{0.29}} \quad (7.2)$$

2193

$$\lambda_R + \lambda_a = 2.2 \quad (7.3)$$

2194 A final point to make is reemphasizing that the I-Mode scaling law is ~~significantly~~
 2195 ~~underdevelopednot battle-tested~~. It is the target of ongoing research at the MIT
 2196 PSFC.

2197 7.4 Addressing Model Shortcomings

2198 Before moving on to the final conclusions, we will give a quick recap of several of the
2199 more overly simplified phenomena in the more audacious simplifications used within
2200 this fusion systems framework. These include: approximating temperature profiles as
2201 simple parabolas, neglecting all radiation except Bremsstrahlung, and handling flux
2202 sources at too basic a level. This list is non-comprehensive, as more sophisticated
2203 analysis would also help: the divertor heat load, the neutron wall loading, etc.

2204 7.4.1 Integrating Pedestal Temperature Profiles

2205 One of the biggest shortcomings of this model is not handling plasma profiles self-
2206 consistently – instead replacing them with simple parabolas. The most dubious simplification
2207 in the code at this point is modeling temperature profiles as parabolas. Although these
2208 parabolas work for densities and L-Mode plasma temperatures, the same cannot be
2209 said about H-Mode temperatures. This is because they have a distinct pedestal region
2210 on the outer edge of the plasma.

2211 The usage of pedestal temperatures – discussed in the appendix – improves two as-
2212 pects of the model: the fusion power and the bootstrap current. These were shown in
2213 the results to be over-calculated and underestimated, respectively. Pedestals, having
2214 a lower core temperature, would decrease the total fusion power. As well, they would
2215 boost bootstrap current due to the quick drop near the plasma’s edge (i.e. they have
2216 a large derivative there).

2217 These improvements could easily be added to the code, because temperature was
2218 addressed as a difficult parameter to handle from the beginning.

2219 7.4.2 Expanding the Radiation Loss Term

2220 The next area that would be improved by more sophisticated theory would be the
2221 radiation loss term. From before, it was pointed out that the Bremsstrahlung ra-

2222 diation was the dominant term within the plasma core and, therefore, provided a
2223 first-order approximation. Drawing the radiation losses closer to real world values
2224 would involve adding line radiation and synchrotron radiation. The former of which
2225 would be needed as high-Z impurities become more important.

2226 7.4.3 Taking Flux Sources Seriously

2227 The final oversimplification in the model deals with the flux sources involved in a
2228 pulsed reactor – existing at almost every level. First, the derivation of flux balance
2229 started with a simple transformer between a solenoid primary and a plasma secondary.

2230 ~~Even this initial step is probably too simple.~~

2231 After we developed an equation for flux balance, we compared it to ones in the
2232 literature (i.e. PROCESS) to build confidence in the model. To draw this equation
2233 closer to theirs, we then added a PF coil contribution a posteriori. This implicitly
2234 ignored coupling between most of the components. Thus leading to another source
2235 of error for the model. Moreover, this formula for PF coil contribution was much
2236 simpler than ones found in other fusion systems codes.

2237 Even though this model may be extremely simple, it does remarkably well at matching
2238 more sophisticated codes – and does so at a much faster pace. These suggestions were
2239 ~~all just ways to account for more realistic physics. draw results closer to real world~~
2240 ~~values.~~

2241 Chapter 8

2242 Concluding Reactor Discussion

2243 The goal of this document was to fairly compare pulsed and steady-state tokamaks
2244 – using a single, comprehensive model. The main conclusion is that both modes of
2245 operation can produce economic reactors, assuming some technological advancement.
2246 The advancement most supported by the results was in magnet technology, as MIT
2247 is currently exploring with high-temperature superconducting (HTS) tape. The goal
2248 of this document was to develop a simple fusion systems model that can work for
2249 both pulsed and steady-state tokamaks. The main conclusion was that the best way
2250 to build a more efficient, compact reactor is to invest in strong magnets—as MIT
2251 is doing with high-temperature superconducting (HTS) tape. Further it was shown
2252 that to best utilize materials, the tape should be incorporated into the toroidal field
2253 coils for steady-state machines and in the central solenoid for pulsed ones.

2254 Although some skepticism should be allotted to these conclusions, it was shown that
2255 this simple algebraic solver was capable of matching more sophisticated frameworks
2256 with speed and ease. This model may not provide an engineer’s level of rigor for cost
2257 measurements, but does produce empirically-drawn trends applicable to a physics au-
2258 dience. Ultimately, it serves to complement higher dimension codes when researchers
2259 want to investigate new areas of reactor space. Although some skepticism should be
2260 allotted to these conclusions, it was shown that this simple algebraic solver matched
2261 sophisticated multiyear research studies with speed and ease. This model may not

2262 provide an engineer's rigor in measuring cost, but the same can be said for any code
2263 or theory. The fusion system is as nonlinear a problem as they come, but we still
2264 managed to build a framework that can hone even a well-trained physicist's intuition.
2265 The final point to make is that this model actually predicts that HTS technology can
2266 provide the optimum magnetic field strength for a reactor. Once HTS doubles the
2267 maximum achievable teslas, the law of diminishing returns heavily kicks in. This of
2268 course assumes H-Mode D-T plasmas at the Greenwald density limit.

2269 What the results truly show, though, is no economic reactor can be built using existing
2270 technology – regardless of whether it runs as pulsed or steady-state. This is why every
2271 design from the literature exceeds standard values for H and N_G . Some technological
2272 advancement is needed. These may then come from research and development into:

- 2273 • building stronger magnets using HTS tape
- 2274 • discovering reliable regimes of enhanced confinement
- 2275 • producing higher bootstrap fractions with tailored profiles
- 2276 • optimizing aspect ratio and elongation geometric parameters

2277 As mentioned, using HTS tape to nearly double achievable magnet strengths is one
2278 such advancement capable of making reactors economically viable. To best utilize
2279 this resource, though, HTS tape should only appear in the TF coils for steady-state
2280 machines and in the central solenoid for pulsed ones. This was because the opti-
2281 mum toroidal field strength for pulsed machines was found to be achievable with
2282 conventional low-temperature superconducting (LTS) magnets.

2283 Further, it was shown that past the regime of magnet strengths relevant to HTS, cost
2284 curves undergo considerably diminished returns. As such, HTS technology would be
2285 the final major magnet advancement in the current H-Mode, D-T plasma paradigm.

Appendix A

Cataloging ~~Static~~Fixed Variables

Table A.1: List of ~~Static~~Fixed Variables

Name	Value
is_pulsed	is reactor pulsed or steady-state
H	h factor for ELMy H-mode scaling
Q	Physics Gain (P_F/P_H)
ϵ	inverse aspect ratio
κ_{95}	elongation at 95 flux surface
δ_{95}	triangularity at 95 flux surface
ν_n	parabolic density peaking factor
ν_T	parabolic temperature peaking factor
Z_{eff}	effective charge
f_D	dilution factor
A	average mass number (in amus)
l_i	internal inductance (interchangeable with ρ_m)
ρ_m	normalized radius of current peak (interchangeable with l_i)
N_G	Greenwald density fraction
η_T	thermal efficiency of the reactor
η_{RF}	efficiency of the RF antenna
τ_{FT}	time of flattop of reactor pulse
B_{CS}	strength of magnetic field in central solenoid
$(\beta_N)_{max}$	max allowed normalized beta normal
$(q_{*95})_{max}$	min allowed safety factor
$(P_W)_{max}$	maximum allowed wall loading power per surface area

2288 Appendix B

2289 Simulating with Fussy.jl

2290 Fussy.jl is a 0-D fusion systems code written using the Julia language. The reason for
2291 choosing Julia over say Matlab and Python was due to metaprogramming concerns
2292 and its tight-knit computational community, respectively. Incorporating the model
2293 used throughout this paper, the code is quick to run and matches more sophisticated
2294 frameworks with high fidelity.

2295 This chapter will be broken down into three steps. The first is getting a user up
2296 and running with the code. Once the user gets to this point, hopefully they will
2297 wonder how the code is structured. This will be the second step. The final step
2298 will be explaining the various functions callable on reactor objects – the atomic data
2299 structure for Fussy.jl.

2300 B.1 Getting the Code to Work

2301 The hardest step of any codebase is getting it up and running. These instructions
2302 should get a user to a point where they are a few internet searches away from a
2303 working copy of Fussy.jl. As an aide, you can view an interactive collection of Fussy.jl
2304 Jupyter notebooks at the following website:

2305 www.fusion.codes

2306 Although `fusion.codes` is a nice tool for viewing this document's results, it is a little
2307 slow for producing new data – and it also lacks a method for storing it. Therefore,
2308 an advanced user should first download a copy of Julia from:

2309 julialang.org/downloads

2310 Currently the `Fussy.jl` codebase is written using `v0.6`, but should be `v1.0` compatible
2311 by 2019. Using Julia nomenclature, `Fussy.jl` is a Julia package. It can be cloned using
2312 Julia conventions from the following Github repository:

2313 <https://github.com/djseagal/Fussy.jl.git>

2314 Once the `Fussy.jl` package has been cloned into your Julia package library, you should
2315 be able to access it through the Julia REPL or a Jupyter notebook. You can now
2316 reproduce every plot in this text. A quick test to see if your code works is:

2317

```
2318     using Fussy
2319     cur_reactor = Reactor(15)
2320
2321     @assert cur_reactor.T_bar == 15
```

2322 B.2 Sorting out the Codebase

2323 Assuming the user got to this section, the code works and now you want to know
2324 what you can do with it. The place to start is in the `src` folder, again viewable online
2325 at:

2326 git.io/tokamak

2327 Within the `src` folder are several subfolders as well as a few files (e.g. `Fussy.jl` and
2328 `defaults.jl`). In an attempt to not bore the reader, we will be painting with thick
2329 brushstrokes. Further, the `methods` subfolder will be the topic of the next section –
2330 as most involve calls on a reactor object.

2331 **B.2.1 Typing out Structures**

2332 The place to start in any modeling framework is its data structures. These type
2333 definitions allow the building of nested hierarchies of constructed objects. The most
2334 atomic of these is the Reactor struct, but several other ones allow for solving broader
2335 scoped questions (i.e. Scans, Sensitivities, and Samplings.)

2336 **The Reactor Structure**

2337 Reactors are the most atomic data structure in this fusion systems model. They
2338 store all the fields needed to represent a reactor as it exists in reactor space. This
2339 obviously includes its temperature, current, and radius, but also includes derived
2340 quantities, such as the cost-per-watt and bootstrap fraction. They can be initialized,
2341 solved, updated, and honed. Most other data structures are just wrappers to hold
2342 these reactors – they are described next.

2343 **The Scan Structure**

2344 A Scan object is a collection of reactors made from scanning a list of temperatures.
2345 For example, a scan of five temperatures from 5 keV to 25 keV would result in several
2346 arrays of five reactors. Most often, one of these lists would correspond to beta reactors,
2347 one to kink reactors, and one to wall loading reactors. There may then be fewer than
2348 five reactors in a list if some of the reactors are invalid or fundamentally unsolvable.
2349 This is the data structure that produces the various comparison plots in the results.

2350 **The Sensitivity Structure**

2351 Sensitivity studies are how computationalists test the effect of changing a variable
2352 over multiple values – i.e. do a 20% sensitivity around the H factor. Like Scans,
2353 Sensitivities store various lists of reactors, each corresponding to an interesting data
2354 point. These include limit reactors where the beta limit and kink limit are just

2355 satisfied or when the beta limit and wall loading are just satisfied. Additionally, they
2356 include the minimum capital cost reactors and the minimum cost-per-watt ones.

2357 **The Sampling Structure**

2358 The Sampling struct was created to do simple Monte Carlo runs over a reactor's
2359 ~~static~~~~fixed~~ values. While sensitivities only allow one variable to change at a time,
2360 samplings randomly assign a list of variables to some neighborhood of possible values.
2361 These are how the scatter plots are made. Succinctly, where sensitivity studies show
2362 local changes to variables, Monte Carlo samplings show global trends in reactor design.

2363 **The Equation Structure**

2364 In order to store the various equations from Table 5.1 is the Equation Struct. It stores
2365 the γ exponents for: R_0 , B_0 , and I_P . – as well as the function representing $G(\bar{T})$.
2366 Repeated these are the unknowns in:

$$R_0^{\gamma_R} \cdot B_0^{\gamma_B} \cdot I_P^{\gamma_I} = G(\bar{T}) \quad (5.3)$$

2367 Concretely, there are 16 objects that use this struct – one for each equation (e.g. for
2368 fusion power, the beta limit, and temperature assignment).

2369 **The Equation Set Structure**

2370 The step up from the Equation struct are the Equation Sets. These collections of
2371 three equations allow R_0 , B_0 , and maybe I_P to be substituted out of the current
2372 balance root-solving equation. This is where Eqs. (5.4) to (5.10) come into play.

2373 B.2.2 Referencing Input Decks and Solutions

2374 With more than twenty ~~static~~~~fixed~~ variables in the model, the range of tokamak
2375 reactors is basically infinite. To help users build a net of designs to explore reactor
2376 space are seven input decks. These are the ones given in the results: Arc, Act I
2377 /II, Demo Steady/Pulsed, Proteus and Charybdis. Coupled with the non-prototype
2378 reactors are solution reactors that store various quantities from the original papers
2379 (e.g. P_F , f_{BS} , R_0). These are how the comparison tables were constructed.

2380 B.2.3 Acknowledging Utility Functions

2381 For the uninitiated, utility functions are grab bag functions that do not really belong
2382 in a codebase – but do anyway. This sentiment does not mean they are worthless,
2383 just not fusion related at all. In Fussy.jl, the most notable are a normalized integral
2384 calculator, a filter that includes numeric tolerances, and a robust root solver.

2385 Although since incorporated into the official Roots.jl package, `find_roots` allows
2386 finding an arbitrary number of roots within a bounded range. This was needed
2387 because many roots can be found at various levels of the reactor solving problem –
2388 i.e. for I_P , \bar{T} , η_{CD} , etc.

2389 B.2.4 Mentioning Base Level Files

2390 In addition to subdirectories within the `src` folder are three files: Fussy.jl, abstracts.jl,
2391 and defaults.jl. Fussy.jl is the package’s main file that actually stores the Fussy
2392 module. While, abstracts.jl stores various abstract structures that help clean up
2393 other files.

2394 Finally, defaults.jl stores various default values that are important to the codebase.
2395 For example, this is where the various scaling law exponents are stored. It is also
2396 where the bounding values for the different root solving problems live. These include
2397 minimum and maximum values for: I_P , \bar{T} , η_{CD} .

2398 Now that a majority of the files have been discussed, we can turn to the reactor
2399 methods. These constitute most of the interesting functionality within the codebase.

2400 B.3 Delving into Reactor Methods

2401 The reactor is the most atomic data structure in this model. It therefore makes
2402 sense that it has many instance methods. These include all the coefficients, fluxes,
2403 powers, etc. It also includes methods that solve a reactor, perform a match on some
2404 field's value, or converge η_{CD} to self-consistency. The various subdirectories within
2405 the `src/methods/reactors` folder will now be discussed.

2406 Calculations

2407 The calculation subdirectory of reactor methods are used to set various important
2408 values in the solver. For ~~dynamicfloating~~ variables, these include: \bar{n} , R_0 , B_0 , and
2409 I_P . This folder also includes the calculation of the Bosch-Hale reactivity and the
2410 Ehst-Karney current drive efficiency.

2411 Coefficients and Composites

2412 The coefficients and composites directories correspond to the model's ~~staticfixed~~ and
2413 ~~dynamicfloating~~ coefficients, respectively. For clarity, ~~staticfixed~~ coefficients, includ-
2414 ing K_n and K_{CD} , were labeled with a K. Whereas, ~~dynamicfloating~~ coefficients then
2415 started with G's – i.e. G_{PB} and G_V .

2416 Fluxes and Powers

2417 Within flux balance and power balance were around a dozen terms or sub-terms.
2418 Although not directly used in the conservation equations, sub-terms are used to com-
2419 pare the model to ones from the literature. For clarity, fluxes include: Φ_{CS} , Φ_{PF} ,
2420 Φ_{RU} , Φ_{FT} , Φ_{res} , and Φ_{ind} . The powers, then, include: P_F , P_{BR} , P_κ , P_{src} , P_W , etc.

2421 Profiles

2422 The next collection of reactor methods are the various profiles. Most obviously, these
2423 include radial plasma profiles for density, temperature, and current. However, this
2424 folder also includes the magnetic field strength as a function of radius – as was used
2425 within current drive efficiency calculations.

2426 Geometries

2427 Additionally, there are many geometric relations. These include the various tokamak
2428 thicknesses: a, b, c, d – as well as the radius and height of the central solenoid. This
2429 group also includes the volume, perimeter, surface area, and cross-sectional area.
2430 It also includes the many subscripted fields. For example, the elongation (i.e. κ_{95})
2431 includes the following alternative definitions: κ_X , κ_P , and κ_T

2432 Formulas

2433 The final set of reactor methods are formulas that do not really fit anywhere else.
2434 If a method is not related to geometry, power, calculations, etc, it ends up here.
2435 For example, this group includes: β_N , f_{BS} , C_W , and τ_E . Total, there are around 25
2436 formulas – as of the writing of this document.

2437 B.4 Demonstrating Code Usage

2438 Now that the Fussy.jl package has been described in detail, the final step is showing a
2439 simple example that can recreate a figure from the results chapter. This will closely
2440 match the Jupyter notebook available at:

2441 www.git.io/fussy_sensitivity

2442 Our goal will be to make a cost curve for the ARC reactor as a function of H – a so
2443 called sensitivity study plot.

2444 B.4.1 Initializing the Workspace

2445 The first step for any Fussy.jl Jupyter notebook is loading the required packages – i.e.
2446 the Fussy.jl and Plots.jl packages. This can be done using the following commands:

```
2447     addprocs(6)
2448
2449     @everywhere using Fussy
2450     using Plots
```

2451 The Plots.jl package may take a minute to load – similar to Matlab’s initial boot
2452 time. If the kernel raises an error about Plots.jl not being installed, use the following
2453 lines:

```
2454     import Pkg
2455     Pkg.add("Plots")
```

2456 B.4.2 Running a Study

2457 Now that the necessary packages have been loaded, we can move on to actually
2458 running the sensitivity study. We will split this command into two steps to make it
2459 more explicit.

2460 The first step will be making several variables that store: boolean flags, numbers, and
2461 symbols – which are like strings, but prefaced with a colon (:) instead of surrounded
2462 by double quotes (").

```
2463     cur_param = :H
2464     cur_deck = :arc
2465     is_pulsed = false
2466     is_consistent = true
2467     cur_sensitivity = 1.0
```

*The `addprocs` and `@everywhere` commands are to parallelize the code. This is because `addprocs(6)` activates 6 worker processes and `@everywhere Fussy.jl` adds Fussy.jl to the main kernel and worker processes.

```
2468     cur_num_points = 41
```

2469 These six variables almost completely describe a sensitivity study. The first two
2470 saw we are using the Arc reactor deck and running a sensitivity over the H-factor
2471 parameter. Next, the two boolean values refer to the reactor (1) being treated as
2472 pulsed or steady-state and (2) whether to handle η_{CD} self-consistently.* Ergo, what
2473 these two flags do is make sure ARC is being handled as a steady-state reactor with
2474 a self-consistent η_{CD} . The last two variables are then ways to change the sensitivity
2475 of the study (with 1.0 \rightarrow 100%) and the number of reactors it will produce (i.e. 41).
2476 Now all six of these variables can be piped into a call to the **Study** struct to start
2477 running the sensitivity study:

```
2478     cur_study = Study(  
2479         cur_param,  
2480         deck = cur_deck,  
2481         is_pulsed = is_pulsed,  
2482         is_consistent = is_consistent,  
2483         sensitivity = cur_sensitivity,  
2484         num_points = cur_num_points  
2485     )
```

2486 Note here that the equal signs inside the parentheses are called keyword arguments,
2487 which are common to most modern programming languages. After executing the
2488 command, the code will need to run for a few minutes.

2489 B.4.3 Extracting Results

2490 At this point, a user should have a completed sensitivity study they wish to plot.
2491 To make the plot useful, the study data structure first has to be unpacked and its
2492 contents cleaned. This is the goal of this subsection.

2493 First and foremost, a study has four families of reactors within it: beta-wall (i.e.

*Note that, currently, a pulsed reactor cannot be self-consistent in η_{CD} – it therefore causes an error.

2494 "wall"), beta-kink (i.e. "kink"), minimum capital cost (i.e. "W_M"), and minimum
2495 cost-per-watt (i.e. "cost"). Therefore, we will extract these reactor lists into a new
2496 dictionary data structure:

```
2497     cur_dict = Dict()  
2498  
2499     cur_dict["Beta-Wall"] = cur_study.wall_reactors  
2500     cur_dict["Beta-Kink"] = cur_study.kink_reactors  
2501  
2502     cur_dict["Min Cost per Watt"] = cur_study.cost_reactors  
2503     cur_dict["Min Capital Cost"] = cur_study.W_M_reactors
```

2504 Next, we will want to filter out all the invalid reactors that constitute non-physically
2505 realizable ones. These would likely be reactors that could fit in your hand or take up
2506 a whole city block.

```
2507     for (cur_key, cur_value) in cur_dict  
2508         cur_dict[cur_key] = filter(  
2509             cur_reactor -> cur_reactor.is_valid,  
2510             deepcopy(cur_value)  
2511         )  
2512     end
```

2513 B.4.4 Plotting Curves

2514 Our goal is now to turn our unpacked, clean reactor lists into plots – i.e. measuring
2515 costs-per-watt as a function of H. For simplicity, this will lack a lot of the features
2516 shown in the Jupyter notebook from the beginning of the section. Additionally, we
2517 will be doing it in an iterative process made possible by the Plots.jl framework.

2518 The first step is simply making a plot object

```
2519     cur_plot = plot()
```

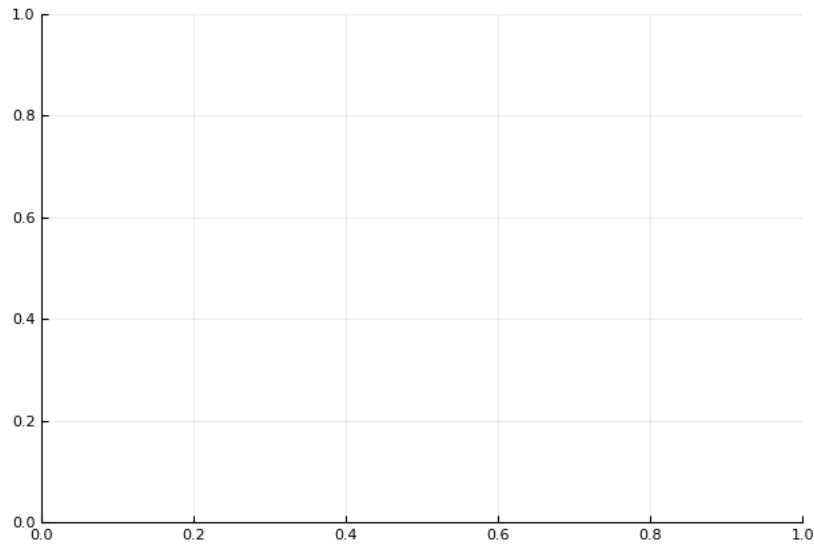



Figure B-1: A Blank Plot

A simple 2-D plot with no labels or data.

2520 After execution, this should produce the plank 2-D plot shown in Fig. B-1.

2521 Next we will add a simple title and labels for the axes:

```
2522     title!("Arc")
```

```
2523
```

```
2524     xlabel!("H")
```

```
2525     ylabel!("Cost")
```

2526 The exclamation marks ensure this title and the labels are added to the `cur_plot`.

2527 Upon execution, you should see a plot with this information (Fig. B-2).

2528 Now we will loop over the dictionary of reactors and add them one at a time.

```
2529     for (cur_key, cur_value) in cur_dict
```

```
2530         cur_x = map(cur_reactor -> cur_reactor.H, cur_value)
```

```
2531         cur_y = map(cur_reactor -> cur_reactor.cost, cur_value)
```

```
2532         plot!(cur_x, cur_y, label=cur_key)
```

```
2533     end
```

```
2534     plot!()
```

2535 This results in the not very useful plot shown in Fig. B-3. Note that each label is

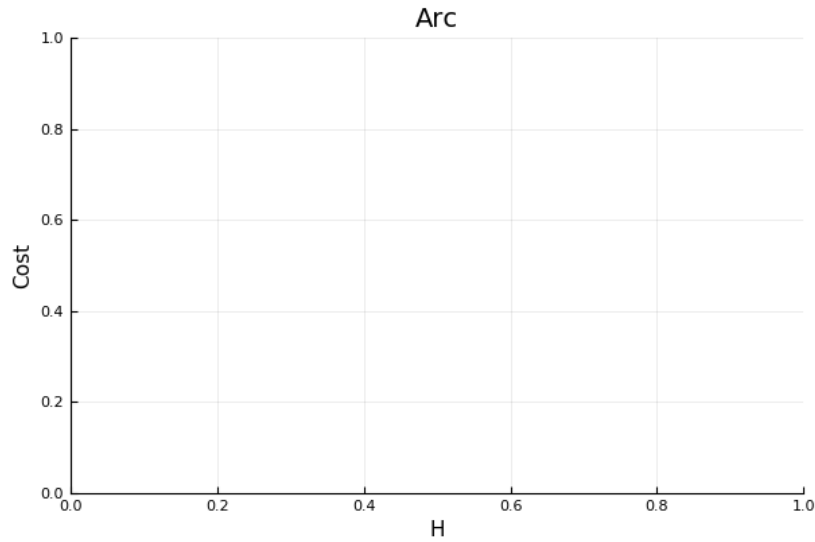


Figure B-2: An Empty Plot

A simple 2-D plot with labels, but no data.

2536 exactly the key assigned to it in `cur_dict`.

2537 The final step is adding proper limits to make what is going on obvious to the reader:

2538 `ylims!(0, 0.03)`

2539 The addition of which can be seen in Fig. B-4.

2540 This completes the example. At this point, you should now be able to use every

2541 feature of `Fussy.jl`. Good luck!

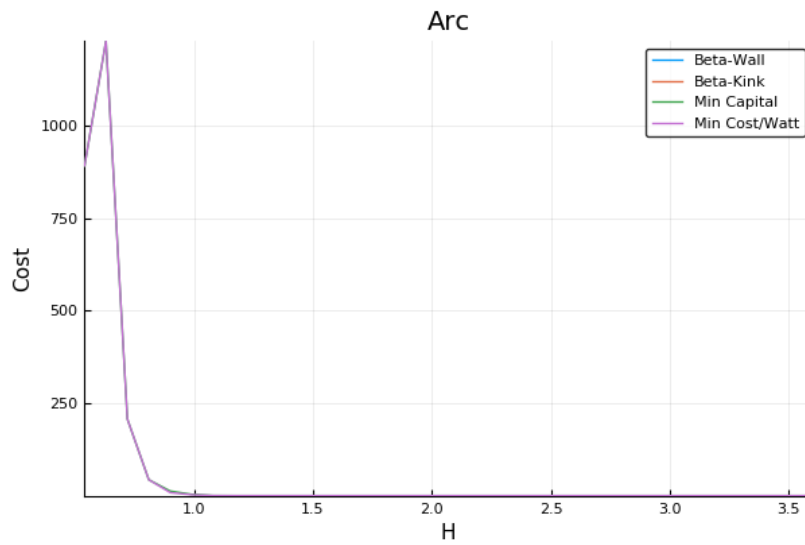


Figure B-3: An Unscaled Plot

A simple 2-D plot with Bad Limits.

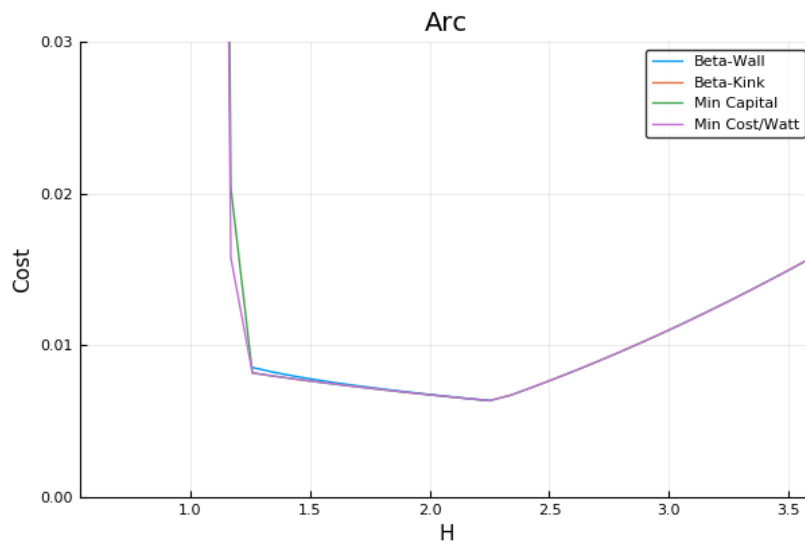


Figure B-4: A Scaled Plot

An example plot showing cost as a function of the H factor.

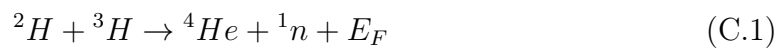
2542 Appendix C

2543 Discussing Fusion Power

2544 C.1 Fusion Power – P_F

2545 This requires a more first-principles approach than those used up until now. As such,
2546 a quick background is given to motivate the parameters it adds – i.e. the dilution
2547 factor (f_D) and the Bosch-Hale fusion reactivity (σv).

2548 The natural place to start when talking about fusion is the binding-energy per nucleon
2549 plot (see Fig. C-1). As can be seen, the function reaches a maximum value around
2550 the element Iron (A=56). What this means at a basic level is: elements lighter than
2551 iron can *fuse* into a heavier one (i.e. hydrogens into helium), whereas heavier elements
2552 can *fission* into lighter ones (e.g. uranium into krypton and barium). This is what
2553 differentiates fission (uranium-fueled) reactors from fusion (hydrogen-fueled) ones.
2554 For fusion reactors, the most common reaction in a first-generation tokamak will be:



2555

$$E_F = 17.6 \text{ MeV} \tag{C.2}$$

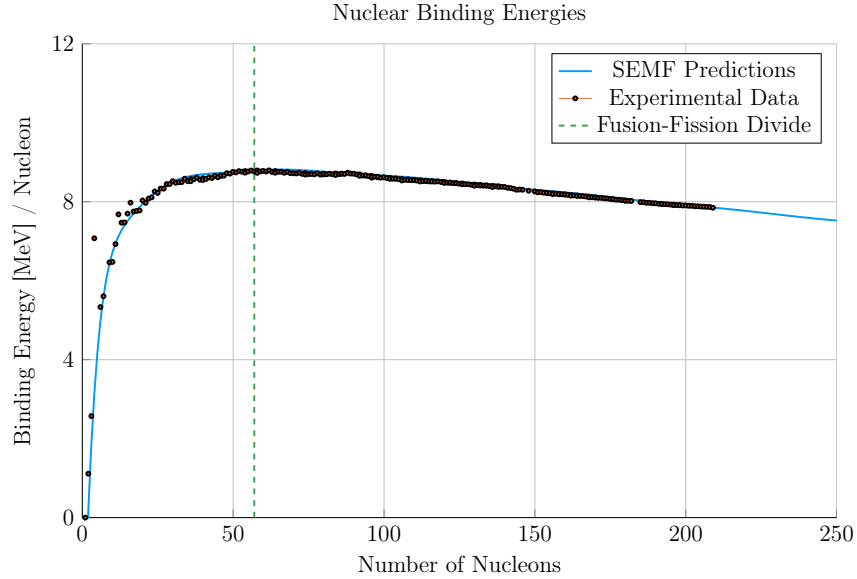


Figure C-1: Comparing Nuclear Fusion and Fission

The binding energy per nucleon is what differentiates nuclear fusion from fission. Nuclei heavier than Iron fission (e.g. Uranium), while light ones – such as Hydrogen – fuse.

2556 What this reaction describes is two isotopes of hydrogen – i.e. deuterium and tritium
 2557 – fusing into a heavier element, helium, while simultaneously ejecting a neutron. The
 2558 entire energy of the fusion reaction (E_F) is then divvied up 80-20 between the neutron
 2559 and helium, respectively. Quantitatively, the helium (hereafter referred to as an alpha
 2560 particle) receives 3.5 MeV.

2561 The final point to make before returning to the fusion power derivation is the main
 2562 difference between the two fusion products: helium (i.e. the alpha particle) and the
 2563 neutron. First, neutrons lack a charge – they are neutral. This means they cannot
 2564 be confined with magnetic fields. As such, they simply move in straight lines until
 2565 they collide with other particles. As the structure of a tokamak is mainly metal, the
 2566 neutron is much more likely to collide there than the gaseous plasma, which is orders
 2567 of magnitude less dense. Conversely, alpha particles are charged – when stripped of
 2568 their electrons – and can therefore be kept within the plasma using magnets. What
 2569 this means practically is that of the 17.6 MeV that comes from every fusion reaction,
 2570 only 3.5 MeV remains inside the plasma (within the helium particle species).

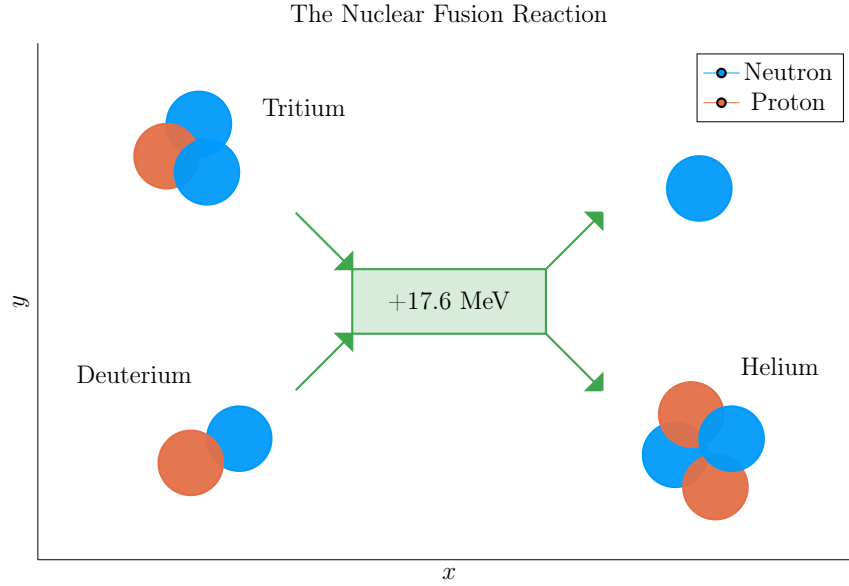


Figure C-2: The D-T Fusion Reaction

In a first generation tokamak reactor, the main source of energy will come from two hydrogen isotopes fusing into a helium particle – and ejecting a 14.1 MeV neutron.

As mentioned before, this fusion power is divided up 80-20 between the neutron and alpha particle. These relations will be used shortly. For now, they can be described mathematically as:

$$P_{\alpha} = 0.2 \cdot P_F \quad (\text{C.3})$$

$$P_n = 0.8 \cdot P_F \quad (\text{C.4})$$

C.2 Reactivity – $\langle \sigma v \rangle$

When discussing reactivity, the place to start is talking about fusion power,

$$P_F = \int E_F n_D n_T \langle \sigma v \rangle d\mathbf{r} \quad (\text{C.5})$$

For the tokamak geometry given, volume integrals can be reduced to 0-D forms.

2579 An arbitrary $F(\rho)$ has that:

$$F_V = 4 \pi^2 R_0 a^2 \kappa g \int_0^1 F(\rho) \rho d\rho \quad (\text{C.6})$$

2580 Given that $E_F = 17.6$ MeV and,

$$n_D = n_T = f_D \frac{n_e}{2} = \frac{f_D}{2} \cdot (\bar{n} (1 + \nu_n) (1 - \rho^2)^{\nu_n}) \quad (\text{C.7})$$

2581 Fusion power can be expressed as,

$$P_F = K_F \cdot (\bar{n}^2 R_0^3) \cdot (\sigma v) \quad [MW] \quad (\text{C.8})$$

2582

$$(\sigma v) = 10^{21} (1 + \nu_n)^2 \int_0^1 (1 - \rho^2)^{2\nu_n} \langle \sigma v \rangle \rho d\rho \quad (\text{C.9})$$

2583

$$K_F = 278.3 (f_D^2 \epsilon^2 \kappa g) \quad (\text{C.10})$$

2584 The Bosch-Hale parametrization of the volumetric reaction rates is then given by,^{29,30}

$$\langle \sigma v \rangle = C_1 \cdot \theta \cdot \exp(-3\xi) \cdot \sqrt{\frac{\xi}{m_\mu c^2 T^3}} \quad [\text{m}^3/\text{s}] \quad (\text{C.11})$$

2585

$$\theta = T \cdot \left(1 - \frac{T(C_2 + T(C_4 + TC_6))}{1 + T(C_3 + T(C_5 + TC_7))} \right)^{-1} \quad (\text{C.12})$$

2586

$$\xi = \left(\frac{B_G^2}{4\theta} \right)^{1/3} \quad (\text{C.13})$$

2587 Where approximate DT volumetric reaction rate ($10 \lesssim T [\text{keV}] \lesssim 20$)

$$\langle \sigma v \rangle_{\text{DT}} = 1.1 \times 10^{-24} \cdot T^2 \quad [\text{m}^3/\text{s}] \quad (\text{C.14})$$

2588 In our model, each appearance of T is set to the profile defined earlier.

Bosch-Hale parametrization coefficients for volumetric reaction rates

	${}^2\text{H}(\text{d,n}){}^3\text{He}$	${}^2\text{H}(\text{d,p}){}^3\text{H}$	${}^3\text{H}(\text{d,n}){}^4\text{He}$	${}^3\text{He}(\text{d,p}){}^4\text{He}$
B_G [keV $^{1/2}$]	31.3970	31.3970	34.3827	68.7508
$m_\mu c^2$ [keV]	937 814	937 814	1 124 656	1 124 572
C_1	5.43360×10^{-12}	5.65718×10^{-12}	1.17302×10^{-9}	5.51036×10^{-10}
C_2	5.85778×10^{-3}	3.41267×10^{-3}	1.51361×10^{-2}	6.41918×10^{-3}
C_3	7.68222×10^{-3}	1.99167×10^{-3}	7.51886×10^{-2}	-2.02896×10^{-3}
C_4	0.0	0.0	4.60643×10^{-3}	-1.91080×10^{-5}
C_5	-2.96400×10^{-6}	1.05060×10^{-5}	1.35000×10^{-2}	1.35776×10^{-4}
C_6	0.0	0.0	-1.06750×10^{-4}	0.0
C_7	0.0	0.0	1.36600×10^{-5}	0.0
Valid range (keV)	$0.2 < T_i < 100$	$0.2 < T_i < 100$	$0.2 < T_i < 100$	$0.5 < T_i < 190$

 Tabulated Bosch-Hale reaction rates [m 3 s $^{-1}$]

T (keV)	${}^2\text{H}(\text{d,n}){}^3\text{He}$	${}^2\text{H}(\text{d,p}){}^3\text{H}$	${}^3\text{H}(\text{d,n}){}^4\text{He}$	${}^3\text{He}(\text{d,p}){}^4\text{He}$
1.0	9.933×10^{-29}	1.017×10^{-28}	6.857×10^{-27}	3.057×10^{-32}
1.5	8.284×10^{-28}	8.431×10^{-28}	6.923×10^{-26}	1.317×10^{-30}
2.0	3.110×10^{-27}	3.150×10^{-27}	2.977×10^{-25}	1.399×10^{-29}
3.0	1.602×10^{-26}	1.608×10^{-26}	1.867×10^{-24}	2.676×10^{-28}
4.0	4.447×10^{-26}	4.428×10^{-26}	5.974×10^{-24}	1.710×10^{-27}
5.0	9.128×10^{-26}	9.024×10^{-26}	1.366×10^{-23}	6.377×10^{-27}
8.0	3.457×10^{-25}	3.354×10^{-25}	6.222×10^{-23}	7.504×10^{-26}
10.0	6.023×10^{-25}	5.781×10^{-25}	1.136×10^{-22}	2.126×10^{-25}
12.0	9.175×10^{-25}	8.723×10^{-25}	1.747×10^{-22}	4.715×10^{-25}
15.0	1.481×10^{-24}	1.390×10^{-24}	2.740×10^{-22}	1.175×10^{-24}
20.0	2.603×10^{-24}	2.399×10^{-24}	4.330×10^{-22}	3.482×10^{-24}

2589

Appendix D

2590

Selecting Plasma Profiles

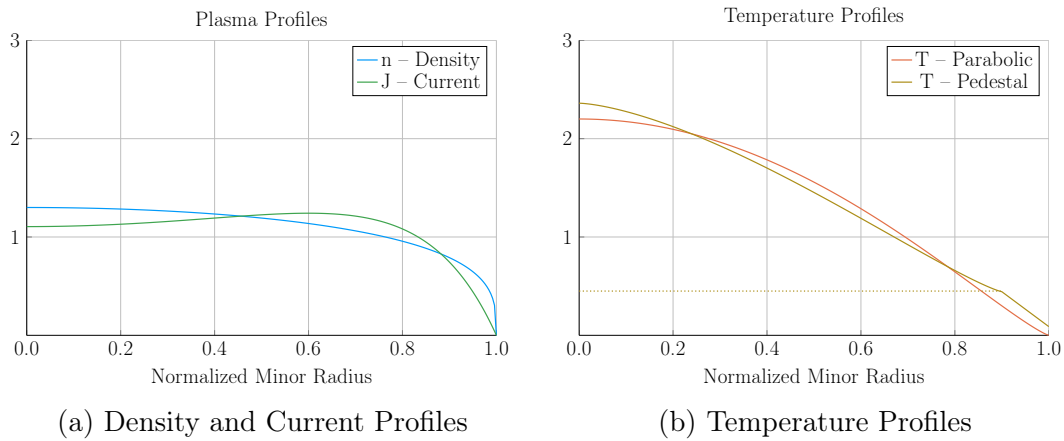


Figure D-1: Radial Plasma Profiles

The three most fundamental properties of a fusion plasma are its temperature, density, and current. These profiles allow the model to reduce from three dimensions to half of one.

2591

D.1 Density – n

2592

The Density is important to us. We use it in the Greenwald density limit, so it should

2593

be clean in both line-averaged and volume-averaged forms. Because of its flat profile,

2594

a parabola is a good approximation for H-mode pulses:

$$n(\rho) = \bar{n} \cdot (1 + \nu_n) \cdot (1 - \rho^2)^{\nu_n} \quad (\text{D.1})$$

2595 The line average density is related to \bar{n} through:

$$\hat{n} = \bar{n} \cdot \left(\frac{\pi^{1/2}}{2} \right) \cdot \frac{\Gamma(\nu_n + 2)}{\Gamma(\nu_n + 3/2)} \quad (\text{D.2})$$

2596 The convenience of this function comes from how the volumetric average comes out.

2597 To relate this to the volume integral, we use:

$$\bar{x} = \frac{1}{V} \int x(\rho) dV \quad (\text{D.3})$$

2598 For a normalized radial profile that does not depend on angle,

$$V = \int_0^1 \rho d\rho = 1/2 \quad (\text{D.4})$$

2599 Then, when $x = n$,

$$\bar{n} = 2 \int_0^1 n(\rho) \rho d\rho = \bar{n} \quad (\text{D.5})$$

2600 Additionally, the Greenwald Density limit that we will use throughout,

$$\hat{n} = N_G \cdot \left(\frac{I_M}{\pi a^2} \right) \quad (\text{D.6})$$

2601 can now be written in the following form:

$$\bar{n} = K_n \cdot \left(\frac{I_M}{R_0^2} \right) \quad (\text{D.7})$$

2602

$$K_n = \frac{2 N_G}{\epsilon^2 \pi^{3/2}} \cdot \left(\frac{\Gamma(\nu_n + 3/2)}{\Gamma(\nu_n + 2)} \right) \quad (\text{D.8})$$

2603 D.2 Temperature – T

2604 The Temperature is the swept variable in our model framework. Therefore, it's the
 2605 one we can allow people to be the most cavalier with. Additionally, as temperature
 2606 profiles are highly peaked, their pedestal region is sometimes wrongfully neglected
 2607 with a parabola.

$$T(\rho) = \bar{T} \cdot (1 + \nu_T) \cdot (1 - \rho^2)^{\nu_T} \quad (\text{D.9})$$

2608 Therefore, our model sometimes treats the system as if it had a pedestal region. This
 2609 is mainly for the bootstrap current and fusion power, which were previously known
 2610 to misalign and overshoot, respectively.

$$T(\rho) = \begin{cases} T_{para} , & x \in [0, \rho_{ped}] \\ T_{line} , & x \in (\rho_{ped}, 1] \end{cases} \quad (\text{D.10})$$

2611 Where the piecewise functions are given by,

$$T_{para} = T_{ped} + (T_0 - T_{ped}) \cdot \left(1 - \left(\frac{\rho}{\rho_{ped}} \right)^{\lambda_T} \right)^{\nu_T} \quad (\text{D.11})$$

2612

$$T_{line} = T_{sep} + (T_{ped} - T_{sep}) \cdot \left(\frac{1 - \rho}{1 - \rho_{ped}} \right) \quad (\text{D.12})$$

2613 This temperature profile is related to the volume-averaged temperature through,

$$\bar{T} \cdot V = \int_0^{\rho_{ped}} T_{para}(\rho) \rho d\rho + \int_{\rho_{ped}}^1 T_{line}(\rho) \rho d\rho \quad (\text{D.13})$$

2614 Starting with the second integral,

$$\int_{\rho_{ped}}^1 T_{line}(\rho) \rho d\rho = \frac{1}{3} \cdot (1 - \rho_{ped}) \cdot ((T_{sep} + T_{ped}/2) + \rho_{ped} \cdot (T_{ped} + T_{sep}/2)) \quad (D.14)$$

The first integral can be handled by breaking it into to,

$$\begin{aligned} \int_0^{\rho_{ped}} T_{para}(\rho) \rho d\rho &= T_{ped} \cdot \int_0^{\rho_{ped}} \rho d\rho + \\ &(T_0 - T_{ped}) \cdot \int_0^{\rho_{ped}} \left(1 - \left(\frac{\rho}{\rho_{ped}}\right)^{\lambda_T}\right)^{\nu_T} \cdot \rho d\rho \end{aligned} \quad (D.15)$$

2615 The first sub-integral is then,

$$T_{ped} \cdot \int_0^{\rho_{ped}} \rho d\rho = \frac{T_{ped} \rho_{ped}^2}{2} \quad (D.16)$$

2616 Utilizing the following transformation,

$$u = \frac{\rho}{\rho_{ped}} \quad (D.17)$$

$$2617 \quad d\rho = \rho_{ped} du \quad (D.18)$$

$$2618 \quad u(\rho = \rho_{ped}) = 1 \quad (D.19)$$

2619 The second sub-integral becomes (assuming independence from T_0 and T_{ped}),

$$(T_0 - T_{ped}) \cdot \rho_{ped}^2 \cdot \int_0^1 (1 - u^{\lambda_T})^{\nu_T} \cdot u du \quad (D.20)$$

2620 Where:

$$\int_0^1 (1 - u^{\lambda_T})^{\nu_T} \cdot u du = \frac{\Gamma(1 + \nu_T) \Gamma\left(\frac{2}{\lambda_T}\right)}{\lambda_T \cdot \Gamma\left(1 + \nu_T + \frac{2}{\lambda_T}\right)} \quad (D.21)$$

2621 We are now in a position to solve for T_0 in terms of \bar{T} :

$$T_0 = T_{ped} + \frac{\bar{T} - K_{TU}}{K_{TD}} \quad (D.22)$$

$$K_{TU} = T_{ped} \rho_{ped}^2 + \frac{(1 - \rho_{ped})}{3} \cdot ((2T_{sep} + T_{ped}) + \rho_{ped} \cdot (2T_{ped} + T_{sep})) \quad (D.23)$$

$$K_{TD} = \rho_{ped}^2 \cdot \left(\frac{2}{\lambda_T} \right) \cdot \frac{\Gamma(1 + \nu_T) \Gamma\left(\frac{2}{\lambda_T}\right)}{\Gamma\left(1 + \nu_T + \frac{2}{\lambda_T}\right)} \quad (D.24)$$

2624 Which although not pretty, can be plugged into the original equation.

2625 D.3 Pressure – p

2626 The first point to make is that we are not using the same temperature profile for
2627 the pressure as for the temperature. This is because it would lead to hypergeometric
2628 functions that are not worth the headache.

2629 As most of the pressure is at the center, we use simple parabolic profile. This leads
2630 to:

$$\bar{p} = 0.1581 (1 + f_D) \frac{(1 + \nu_n)(1 + \nu_T)}{1 + \nu_n + \nu_T} \bar{n} \bar{T} \quad [atm] \quad (D.25)$$

2631 D.4 Bootstrap Current – f_{BS}

2632 We start with,

$$f_{BS} = \frac{I_{BS}}{I_P} = \frac{2\pi a^2 \kappa}{I_P} \int_0^1 J_B \rho d\rho \quad (D.26)$$

2633 Expanding the previous equation using the following relations,

$$J_B = -4.85 \cdot R_0 \epsilon^{1/2} \cdot \left(\frac{\rho^{1/2} n T}{d\psi/d\rho} \right) \cdot \left(\frac{dn/d\rho}{n} + 0.54 \cdot \frac{dT/d\rho}{T} \right) \quad (D.27)$$

2634

$$\frac{d\psi}{d\rho} = \frac{\mu_0 R_0 I_P}{\pi} \cdot \left(\frac{\kappa}{1 + \kappa^2} \right) \cdot b_p(\rho) \quad (D.28)$$

2635 Yields:

$$f_{BS} = -K_{BS} \int_0^1 (1 - \rho^2)^{\nu_n} \cdot \left(\frac{\rho^{3/2}}{b_p(\rho)} \right) \cdot \left(\frac{T}{n} \cdot \frac{dn}{d\rho} + 0.54 \cdot \frac{dT}{d\rho} \right) d\rho \quad (D.29)$$

2636

$$K_{BS} = K_n \cdot \left(\frac{2\pi^2 \cdot 4.85 \cdot \epsilon^{5/2}}{\mu_0} \right) \cdot (1 + \nu_n) \cdot (1 + \kappa^2) \quad (D.30)$$

2637 Here, b_p comes from:

$$b_p(\rho) = \frac{-e^{\gamma\rho^2}(\gamma\rho^2 - 1 - \gamma) - 1 - \gamma}{\rho(e^\gamma - 1 - \gamma)} \quad (D.31)$$

2638 And the value of γ comes from the the normalized internal inductance:

$$l_i = \frac{4\kappa}{1 + \kappa^2} \int_0^1 b_p^2 \frac{d\rho}{\rho} \quad (D.32)$$

2639 With our profiles,

$$-\left(\frac{T}{n} \cdot \frac{dn}{d\rho} \right) = 2\nu_n \cdot \left(\frac{T \cdot \rho}{1 - \rho^2} \right) \quad (D.33)$$

2640 While treating temperature differently results in,

$$-\left(\frac{dT}{d\rho} \right)_{para} = \left(\frac{T_0 - T_{ped}}{\rho_{ped}^{\lambda_T}} \right) \cdot (\nu_T \lambda_T) \cdot \rho^{\lambda_T - 1} \cdot \left(1 - \left(\frac{\rho}{\rho_{ped}} \right)^{\lambda_T} \right)^{\nu_T - 1} \quad (D.34)$$

2641

$$-\left(\frac{dT}{d\rho} \right)_{line} = \left(\frac{T_{ped} - T_{sep}}{1 - \rho_{ped}} \right) \quad (D.35)$$

2642 Where we will be using the new symbol definition,

$$\partial T = - \left(\frac{dT}{d\rho} \right) \quad (\text{D.36})$$

Which ultimately allows us to write,

$$f_{BS} = K_{BS} \int_0^1 H_{BS} d\rho \quad (\text{D.37})$$

$$H_{BS} = (1 - \rho^2)^{\nu_n - 1} \cdot \left(\frac{\rho^{3/2}}{b_p(\rho)} \right) \cdot \left(2\nu_n \cdot \rho \cdot T + 0.54 \cdot (1 - \rho^2) \cdot \partial T \right) \quad (\text{D.38})$$

2643 Where the values of T are determined through,

$$T_{para} = T_{ped} + (T_0 - T_{ped}) \cdot \left(1 - \left(\frac{\rho}{\rho_{ped}} \right)^{\lambda_T} \right)^{\nu_T} \quad (\text{D.39})$$

2644

$$T_{line} = T_{sep} + (T_{ped} - T_{sep}) \cdot \left(\frac{1 - \rho}{1 - \rho_{ped}} \right) \quad (\text{D.40})$$

2645 And the values of ∂T are:

$$\partial T_{para} = \left(\frac{T_0 - T_{ped}}{\rho_{ped}^{\lambda_T}} \right) \cdot (\nu_T \lambda_T) \cdot \rho^{\lambda_T - 1} \cdot \left(1 - \left(\frac{\rho}{\rho_{ped}} \right)^{\lambda_T} \right)^{\nu_T - 1} \quad (\text{D.41})$$

2646

$$\partial T_{line} = \left(\frac{T_{ped} - T_{sep}}{1 - \rho_{ped}} \right) \quad (\text{D.42})$$

2647 D.5 Volume Averaged Powers

2648 The first thing to consider in a fusion reactor is power balance. It is what separates

2649 a net power producing reactor from a power-consuming research device.

2650 ~~It is what separates a profitable device from a toaster. It's given by:~~

$$P_\alpha + P_H = P_\kappa + P_B \quad (D.43)$$

$$P_\alpha = \frac{P_F}{5} \quad (D.44)$$

$$P_H = \frac{P_F}{Q} \quad (D.45)$$

$$P_\kappa = \frac{3}{2\tau_E} \int p \, d\mathbf{r} \quad [3D] \quad (D.46)$$

$$P_B = 5.35e3 Z_{eff} \int n_n^2 \sqrt{T} \, d\mathbf{r} \quad [3D] \quad (D.47)$$

As mentioned before, P_F is handled by (σv) and therefore the lefthand-side uses the pedestal temperature profiles. However, for the same reasons as discussed earlier, the righthand-side (P_κ and P_B) need to use the parabolic temperature profiles.

Using the parabolic profiles (for n and T) gives for the Bremsstrahlung radiation,

$$P_B = K_B \cdot \left(R_0^3 \bar{n}^2 \sqrt{\bar{T}} \right) \quad [MW] \quad (D.48)$$

$$K_B = 0.1056 \cdot Z_{eff} \cdot (\epsilon^2 \kappa g) \cdot \frac{(1 + \nu_n)^2 (1 + \nu_T)^{1/2}}{1 + 2\nu_n + 0.5\nu_T} \quad (D.49)$$

And a similar exercise for the thermal conduction losses results in:

$$P_\kappa = K_\kappa \cdot \left(\frac{R_0^3 \bar{n} \bar{T}}{\tau_E} \right) \quad [MW] \quad (D.50)$$

$$K_\kappa = 0.4744 \cdot (1 + f_D) \cdot (\epsilon^2 \kappa g) \cdot \frac{(1 + \nu_n)(1 + \nu_T)}{1 + \nu_n + \nu_T} \quad (D.51)$$

Appendix E

Determining Plasma Flux Surfaces

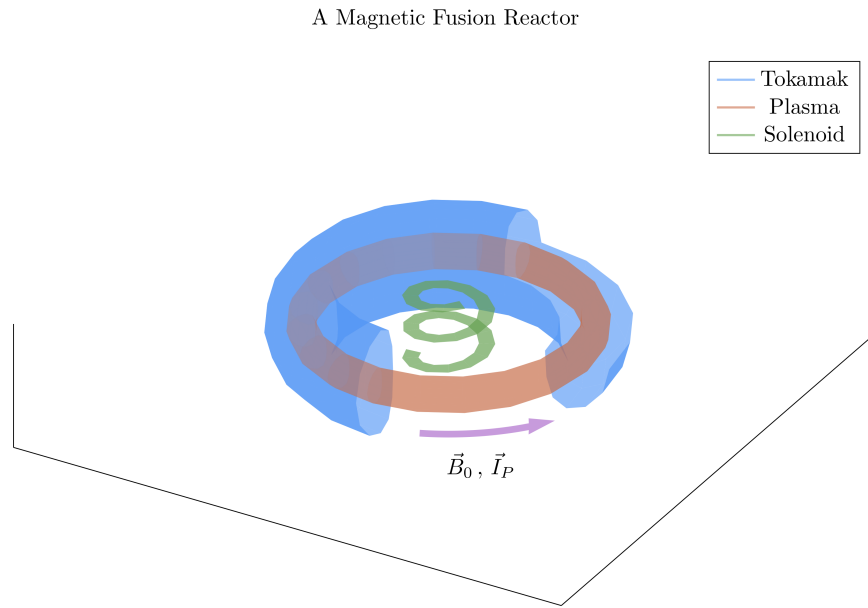


Figure E-1: Cut-Away of Tokamak Reactor

The three main components of a magnetic fusion reactor are: the tokamak structure, the plasma fuel, and the spring-like solenoid at the center.

E.1 Flux Surface Coordinates

We begin with the shape of the outer plasma surface (i.e. the 95% flux surface) written in terms of normalized coordinates x and y as follows – with α being an angle-like

2667 coordinate:

$$R = R_0 + ax(\alpha) \quad (\text{E.1})$$

2668

$$Z = ay(\alpha) \quad (\text{E.2})$$

2669

$$0 \leq \alpha \leq 2\pi \quad (\text{E.3})$$

2670 The surface representation can now be written as:

$$x(\alpha) = c_0 + c_1 \cos(\alpha) + c_2 \cos(2\alpha) + c_3 \cos(3\alpha) \quad (\text{E.4})$$

2671

$$y(\alpha) = \kappa \sin(\alpha) \quad (\text{E.5})$$

2672 The constraints determining c_j – for $j = 1, 2, 3$ – are chosen as:

$$x(0) = 1 \quad (\text{E.6})$$

2673

$$x(\pi) = -1 \quad (\text{E.7})$$

2674

$$x\left(\frac{\pi}{2}\right) = -\delta \quad (\text{E.8})$$

2675

$$x_{\alpha\alpha}(\pi) = 0.3 \cdot (1 - \delta^2) \quad (\text{E.9})$$

2676 The last constraint, which is related to the surface curvature at $\alpha = \pi$, is chosen to
 2677 make sure that the surface is always convex. A trial and error empirical fit resulted
 2678 in the choice $x_{\alpha\alpha}(\pi) = 0.3 \cdot (1 - \delta^2)$. The constraint relations are easily evaluated and
 2679 then solved, leading to values for the c_j ,

$$c_0 = -\frac{\delta}{2} \quad (\text{E.10})$$

2680

$$c_1 = g \quad (\text{E.11})$$

2681

$$c_2 = \frac{\delta}{2} \quad (\text{E.12})$$

2682

$$c_3 = 1 - g \quad (\text{E.13})$$

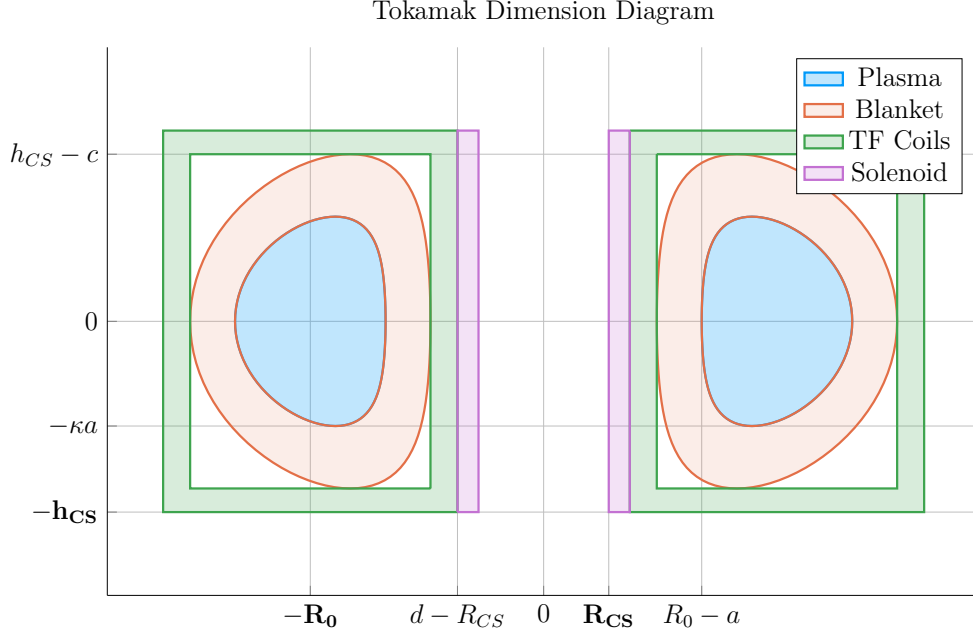


Figure E-2: Dimensions of Tokamak Cross-Section

Here, g is a shaping parameter approximately equal to one:

$$g = \frac{9 - 2\delta - 0.3 \cdot (1 - \delta^2)}{8} \quad (\text{E.14})$$

E.2 Cross-sectional Area and Volume

The plasma cross-sectional area and volume can be evaluated by straightforward calculations,

$$\begin{aligned} A &= \int \int dR dZ = a^2 \int \int dx dy = a^2 \int_0^{2\pi} x \frac{dy}{d\alpha} d\alpha \\ &= \pi a^2 \kappa g \end{aligned} \quad (\text{E.15})$$

$$\begin{aligned} V &= \int \int \int R dR dZ d\Phi = 2\pi a^2 \int \int R dx dy \\ &= 2\pi a^2 R_0 \int_0^{2\pi} \left(x + \epsilon \frac{x^2}{2} \right) \frac{dy}{d\alpha} d\alpha \approx 2\pi a^2 R_0 \int_0^{2\pi} x \frac{dy}{d\alpha} d\alpha \\ &= 2\pi^2 R_0 a^2 \kappa g \end{aligned} \quad (\text{E.16})$$

2688 The second form of the volume integral makes use of the small inverse aspect ratio
 2689 expansion, $\epsilon \ll 1$, which is a good approximation and used throughout the analysis.

2690 E.3 Surface and Volume Integrals

2691 Eqs. (E.4) and (E.5) are simple formulas describing the shape of the outer plasma
 2692 surface. We next modify the model so that it gives a plausible description of the
 2693 interior flux surfaces as well. The idea is to introduce a normalized flux label, which
 2694 is radial-like in behavior. This label is denoted by ρ and $\rho \in [0, 1]$ with $\rho = 1$ being
 2695 the outer plasma surface (i.e. the 95% surface) and $\rho = 0$ being the magnetic axis.
 2696 Additional trial and error results in the following representation for the flux surfaces,

$$x(\rho, \alpha) = \sigma(1 - \rho^2) + c_0\rho^4 + c_1\rho \cos(\alpha) + c_2\rho^2 \cos(2\alpha) + c_3\rho^3 \cos(3\alpha) \quad (\text{E.17})$$

2697

$$y(\rho, \alpha) = \kappa\rho \sin(\alpha) \quad (\text{E.18})$$

2698 with σ being the shift of the magnetic axis. Usually, $\sigma \sim 0.1$ for a high field tokamak.
 2699 Lastly, we note that in the course of the work it will be necessary to integrate functions
 2700 of ρ over the volume and cross-sectional area of the plasma. Specifically we will need
 2701 to evaluate:

$$Q_V = \int \int \int Q(\rho) R dR dZ d\Phi \approx 2\pi R_0 a^2 \int \int Q(\rho) dx dy \quad (\text{E.19})$$

2702

$$Q_A = \int \int Q(\rho) dR dZ = a^2 \int \int Q(\rho) dx dy \quad (\text{E.20})$$

2703 Here, $Q(\rho)$ is an arbitrary function of ρ such as pressure or temperature. In the large
 2704 aspect ratio limit, both integrals require the evaluation of the same quantity:

$$K = \int \int Q(\rho) dx dy \quad (\text{E.21})$$

2705 To evaluate this integral, we need to convert from x, y coordinates to ρ, α coordinates.

2706 Using the Jacobian of the transformation leads to

$$K = \int \int Q(\rho)(x_\rho y_\alpha - x_\alpha y_\rho) d\rho d\alpha \quad (\text{E.22})$$

2707 Here,

$$\begin{aligned} x_\rho y_\alpha - x_\alpha y_\rho = & \kappa \sin(\alpha) \cdot (c_1 \rho \sin(\alpha) + 2c_2 \rho^2 \sin(2\alpha) + 3c_3 \rho^3 \sin(3\alpha)) \\ & + \kappa \rho \cos(\alpha) \cdot \left[\right. \\ & \quad - 2\rho\sigma + 4\rho^3 c_0 + c_1 \cos(\alpha) \\ & \quad + 2c_2 \rho \cos(2\alpha) + 3c_3 \rho^2 \cos(3\alpha) \\ & \left. \right] \end{aligned} \quad (\text{E.23})$$

2708 Since Q is only a function of ρ , the α integral can be carried out analytically. The
2709 only term that survives the averaging are the ones containing c_1 . A simple integration
2710 over α then yields the desired results:

$$Q_V = 4\pi^2 R_0 a^2 \kappa g \int_0^1 Q(\rho) \rho d\rho \quad (\text{E.24})$$

2711

$$Q_S = 2\pi a^2 \kappa g \int_0^1 Q(\rho) \rho d\rho \quad (\text{E.25})$$

2712

2713 Appendix F

2714 Expanding on the Bootstrap Current

2715 The bootstrap current fraction – f_{BS} – is an important parameter that enters in
2716 the design of tokamak reactors. It must be calculated with reasonable accuracy to
2717 determine how much external current drive is required. The value of f_{BS} thus has
2718 a strong impact on the overall fusion energy gain. Obtaining reasonable accuracy
2719 requires a moderate amount of analysis, which is presented in a following section.
2720 The results are summarized below.

2721 F.1 Summarized Results

2722 The analysis is based on an expression for the bootstrap current valid for arbitrary
2723 cross section assuming (1) equal temperature electrons and ions $T_e = T_i = T$, (2) large
2724 aspect ratio $\epsilon \ll 1$, and (3) negligible collisionality $\nu_* \rightarrow 0$. Under these assumptions
2725 the bootstrap current $\mathbf{J}_{BS} \approx J_{BS} \mathbf{e}_\phi$ has the form

$$J_{BS} = -3.32 f_T R_0 n T \left(\frac{1}{n} \frac{dn}{d\psi} + 0.054 \frac{1}{T} \frac{dT}{d\psi} \right) \quad (\text{F.1})$$

2726 Here, $f_T \approx 1.46(r/R_0)^{1/2}$ is an approximate expression for the trapped particle frac-
2727 tion and ψ is the poloidal flux.

2728 The analysis next section shows that Eq. (F.1) leads to an expression for the bootstrap
 2729 fraction, assuming for simplicity elliptical flux surfaces, that can be written as:

$$f_{BS} = \frac{I_{BS}}{I} = \frac{2\pi a^2 \kappa}{I} \int_0^1 J_{BS} \rho d\rho = \frac{K_{BS}}{K_n} \frac{\bar{n} \bar{T} R_0^2}{I_P^2} \quad (\text{F.2})$$

2730

$$K_{BS} = 4.879 \cdot K_n \cdot \left(\frac{1 + \kappa^2}{2} \right) \cdot \epsilon^{5/2} \cdot H_{BS} \quad (\text{F.3})$$

2731

$$H_{BS} = (1 + \nu_n)(1 + \nu_T)(\nu_n + 0.054\nu_T) \int_0^1 \frac{\rho^{5/2} (1 - \rho^2)^{\nu_n + \nu_T - 1}}{b_p} d\rho \quad (\text{F.4})$$

2732

$$b_p(\rho) = \frac{-e^{\gamma\rho^2}(\gamma\rho^2 - 1 - \gamma) - 1 - \gamma}{\rho(e^\gamma - 1 - \gamma)} \quad (\text{F.5})$$

2733

$$\bar{J}_\phi(\rho) = -\frac{I}{\pi a^2 \kappa} \left[\frac{\gamma^2(1 - \rho^2)e^{\gamma\rho^2}}{e^\gamma - 1 - \gamma} \right] \quad (\text{F.6})$$

2734 In this expression b_p is a normalized form of the poloidal magnetic field derived from
 2735 a prescribed model for the *total* flux surface averaged current density profile $\bar{J}_\phi(\rho)$.
 2736 The $\bar{J}_\phi(\rho)$ profile, in analogy with the density and temperature profiles, is not self-
 2737 consistent but is chosen to have a plausible experimental shape characterized by the
 2738 parameter γ . The profile can have either an on-axis ($\gamma < 1$) or off-axis peak ($\gamma > 1$).
 2739 The normalized internal inductance l_i and radial location of the current peak ρ_m are
 2740 related to the value of γ by:

$$l_i = \frac{4\kappa}{1 + \kappa^2} \int_0^1 b_p^2 \rho d\rho \quad (\text{F.7})$$

2741

$$\rho_m = \begin{cases} \left(\frac{\gamma}{\gamma-1} \right)^{1/2}, & \gamma > 1 \\ 0, & \gamma < 1 \end{cases} \quad (\text{F.8})$$

2742 F.2 Detailed Analysis

2743 The starting point for the analysis is the general expression for the bootstrap current
 2744 in a tokamak with arbitrary cross section.³¹ This expression can be simplified by

2745 assuming (1) equal temperature electrons and ions $T_e = T_i = T$, (2) large aspect ratio
 2746 $\epsilon \ll 1$, and (3) negligible collisionality $\nu_* \rightarrow 0$. The bootstrap current $\mathbf{J}_{BS} \approx J_{BS} \mathbf{e}_\phi$
 2747 reduces to

$$J_{BS} = -3.32 f_T R_0 n T \left(\frac{1}{n} \frac{dn}{d\psi} + 0.054 \frac{1}{T} \frac{dT}{d\psi} \right) \quad (\text{F.9})$$

2748 Several values of the trapped particle fraction f_T have been given in the literature.³²
 2749 For simplicity we use a form valid for large aspect ratio. This is a slightly optimistic
 2750 value but saves a large amount of detailed calculation. It can be written as,

$$f_T \approx 1.46 (r/R_0)^{1/2} = 1.46 \epsilon^{1/2} \rho^{1/2} \quad (\text{F.10})$$

2751 Here, as in the main text, ρ is a radial-like flux surface label that varies between
 2752 $0 \leq \rho \leq 1$. In other words $\psi = \psi(\rho)$. Under these assumptions the bootstrap current
 2753 reduces to:

$$J_{BS} = -4.85 R_0 \epsilon^{1/2} \left(\frac{\rho^{1/2} n T}{d\psi/d\rho} \right) \left(\frac{1}{n} \frac{dn}{d\rho} + 0.054 \frac{1}{T} \frac{dT}{d\rho} \right) \quad (\text{F.11})$$

2754 Since we have specified profiles for $n(\rho)$ and $T(\rho)$ all that remains in order to be able
 2755 to evaluate $J_{BS}(\rho)$ is to determine $\psi' = d\psi/d\rho$. Keep in mind that at this point, in
 2756 spite of the approximations that have been made, the expression for $J_{BS}(\rho)$ is still
 2757 valid for arbitrary cross section.

2758 The analysis that follows shows how to calculate ψ' for an arbitrary cross section
 2759 including finite aspect ratio. As an example an explicit expression for large aspect
 2760 ratio, finite elongation ellipse is obtained. Consider the Grad-Shafranov equation for
 2761 the flux: $\Delta^* \psi = -\mu_0 R J_\psi$. We integrate this equation over the volume of an arbitrary
 2762 flux surface making use of Gauss' theorem, which leads to:

$$\int_S \frac{\mathbf{n} \cdot \nabla \psi}{R^2} dS = -\mu_0 \int_V \frac{J_\phi}{R} d\mathbf{r} \quad (\text{F.12})$$

2763 Next, assume that the coordinates of the flux surface can be expressed in terms of ρ
 2764 and an angular-like parameter α with $0 \leq \alpha \leq 2\pi$. In other words, the flux surface

coordinates can be written as $R = R(\rho, \alpha) = R_0 + ax(\rho, \alpha)$ and $Z = Z(\rho, \alpha) = ay(\rho, \alpha)$. The functions $R(\rho, \alpha)$ and $Z(\rho, \alpha)$ are assumed to be known. The term on the left hand side can be evaluated by noting that

$$dl = dlt \quad (\text{F.13})$$

$$dl = (R_\alpha^2 + Z_\alpha^2)^{1/2} d\alpha \quad (\text{F.14})$$

$$\mathbf{t} = \frac{R_\alpha \mathbf{e}_R + Z_\alpha \mathbf{e}_Z}{(R_\alpha^2 + Z_\alpha^2)^{1/2}} \quad (\text{F.15})$$

$$\mathbf{n} = \mathbf{e}_\phi \times \mathbf{t} = \frac{Z_\alpha \mathbf{e}_R - R_\alpha \mathbf{e}_Z}{(R_\alpha^2 + Z_\alpha^2)^{1/2}} \quad (\text{F.16})$$

$$dS = R d\phi dl = 2\pi R (R_\alpha^2 + Z_\alpha^2)^{1/2} d\alpha \quad (\text{F.17})$$

It then follows that

$$\mathbf{n} \cdot \nabla \psi = \frac{1}{(R_\alpha^2 + Z_\alpha^2)^{1/2}} \left(Z_\alpha \frac{\partial \psi}{\partial R} - R_\alpha \frac{\partial \psi}{\partial Z} \right) = \frac{1}{(R_\alpha^2 + Z_\alpha^2)^{1/2}} \frac{d\psi}{d\rho} Z_\alpha \rho_R - R_\alpha \rho_Z \quad (\text{F.18})$$

We can rewrite the last term by noting that

$$\begin{aligned} dR = R_\rho d\rho + R_\alpha d\alpha &\rightarrow d\rho = (Z_\alpha dR - R_\alpha dZ) / (R_\rho Z_\alpha - R_\alpha Z_\rho) \\ dZ = Z_\rho d\rho + Z_\alpha d\alpha &\rightarrow d\alpha = (-Z_\rho dR + R_\rho dZ) / (R_\rho Z_\alpha - R_\alpha Z_\rho) \end{aligned} \quad (\text{F.19})$$

from which follows

$$\begin{aligned} \rho_R &= \frac{Z_\alpha}{(R_\rho Z_\alpha - R_\alpha Z_\rho)} \\ \rho_Z &= -\frac{R_\alpha}{(R_\rho Z_\alpha - R_\alpha Z_\rho)} \end{aligned} \quad (\text{F.20})$$

the normal gradient reduces to

$$\mathbf{n} \cdot \nabla \psi = \frac{R_\alpha^2 + Z_\alpha^2}{(R_\rho Z_\alpha - R_\alpha Z_\rho)} \frac{d\psi}{d\rho} \quad (\text{F.21})$$

2776 Using this relation we see that the left hand side of Eq. (F.12) can now be written as:

$$\int_S \frac{\mathbf{n} \cdot \nabla \psi}{R^2} dS = 2\pi \frac{d\psi}{d\rho} \int_0^{2\pi} \frac{R_\alpha^2 + Z_\alpha^2}{(R_\rho Z_\alpha - R_\alpha Z_\rho)} \frac{d\alpha}{R} \quad (\text{F.22})$$

2777 Consider now the right hand side of Eq. (F.12). The critical assumption is that the
 2778 current density is approximated by its flux surface averaged value, $J_\phi(\rho, \alpha) \approx \bar{J}_\phi(\rho)$.
 2779 This is obviously not self-consistent with the Grad-Shafranov equation. Even so, it
 2780 should suffice for present purposes where we only need to evaluate global volume
 2781 integrals. Also, in the same spirit as prescribing $n(\rho)$ and $T(\rho)$ we assume that $\bar{J}_\phi(\rho)$
 2782 is also prescribed. Under these assumptions the right hand side of Eq. (F.12) simplifies
 2783 to:

$$\begin{aligned} -\mu_0 \int_V \frac{J_\phi}{R} d\mathbf{r} &= -2\pi\mu_0 \int_A J_\phi dA \\ &= -2\pi\mu_0 \int_0^\rho d\rho \int_0^{2\pi} J_\phi (R_\rho Z_\alpha - R_\alpha Z_\rho) d\alpha \\ &\approx -2\pi\mu_0 \int_0^\rho d\rho \left[\bar{J}_\phi \int_0^{2\pi} (R_\rho Z_\alpha - R_\alpha Z_\rho) d\alpha \right] \end{aligned} \quad (\text{F.23})$$

2784 Combining the results in Eqs. (F.22) and (F.23) leads to the required general expres-
 2785 sion for $d\psi/d\rho$,

$$\frac{d\psi}{d\rho} \int_0^{2\pi} \frac{R_\alpha^2 + Z_\alpha^2}{(R_\rho Z_\alpha - R_\alpha Z_\rho)} \frac{d\alpha}{R} = -\mu_0 \int_0^\rho d\rho \left[\bar{J}_\phi \int_0^{2\pi} (R_\rho Z_\alpha - R_\alpha Z_\rho) d\alpha \right] \quad (\text{F.24})$$

2786 Next, to help specify a plausible choice for \bar{J}_ϕ it is useful to define the kink safety
 2787 factor and the actual local safety factor. The kink safety factor is defined by

$$q_* = \frac{2\pi a^2 B_0}{\mu_0 R_0 I} \left(\frac{1 + \kappa^2}{2} \right) \quad (\text{F.25})$$

2788 where

$$I = \int J_o dA = \int_0^1 d\rho \left[\bar{J}_o \int_0^{2\pi} (R_\rho Z_\alpha - R_\alpha Z_\rho) d\alpha \right] \quad (\text{F.26})$$

2789 This leads to

$$\frac{1}{q_*} = \frac{\mu_0 R_0}{2\pi a^2 B_0} \left(\frac{2}{1 + \kappa^2} \right) \int_0^1 d\rho \left[\bar{J}_\phi \int_0^{2\pi} (R_\rho Z_\alpha - R_\alpha Z_\rho) d\alpha \right] \quad (\text{F.27})$$

2790 Similarly, the local safety factor can be expressed as

$$q(\rho) = \frac{F(\rho)}{2\pi} \int \frac{dl}{RB_p} \quad (\text{F.28})$$

2791 Here, $F(\rho) = RB_o$. Substituting $RB_p = \mathbf{n} \cdot \nabla \psi$ then yields

$$q(\rho) = \frac{F(\rho)}{2\pi\psi'} \int_0^{2\pi} \frac{1}{R} (R_\rho Z_\alpha - R_\alpha Z_\rho) d\alpha \quad (\text{F.29})$$

2792 with $\psi' = d\psi/d\rho$.

2793 For present purposes we can obtain relatively simple analytic expressions for all the
 2794 quantities of interest by assuming the flux surfaces are concentric ellipses, character-
 2795 ized by $R = R_0 + a\rho \cos \alpha$ and $Z = \kappa a\rho \sin \alpha$. We assume low β so that $F(\rho) \approx R_0 B_0$.
 2796 This model accounts for elongation but neglects the effects of triangularity and finite
 2797 aspect ratio. The derivatives in Eqs. (F.24), (F.27) and (F.29) can now be easily
 2798 evaluated. Also, after some trial and error we chose $\bar{J}_\phi(\rho)$ to be a plausible profile
 2799 which is peaked off-axis at $\rho = \rho_m$.

$$\bar{J}_\phi(\rho) = -\frac{I}{\pi a^2 \kappa} \left[\frac{\gamma^2 (1 - \rho^2) e^{\gamma \rho^2}}{e^\gamma - 1 - \gamma} \right] \quad (\text{F.30})$$

2800 Here, $\gamma = 1/(1 - \rho_m^2)$.

2801 These profiles are substituted into Eq. (F.24) after which each of the integrals can be
 2802 evaluated analytically. A straightforward calculation yields:

$$\begin{aligned}
\rho \frac{d\psi}{d\rho} &= -2\mu_0 R_0 a^2 \left(\frac{\kappa^2}{1+\kappa^2} \right) \int_0^\rho \bar{J}_\phi \rho d\rho \\
&= \frac{\mu_0 R_0 I}{\pi} \left(\frac{\kappa}{1+\kappa^2} \right) \frac{(1+\gamma-\gamma\rho^2) e^{\gamma\rho^2} - 1 - \gamma}{e^\gamma - 1 - \gamma}
\end{aligned} \tag{F.31}$$

2803 The safety factors are given by

$$\begin{aligned}
\frac{1}{q_*} &= \frac{\psi'(1)}{\kappa a^2 B_0} \\
\frac{q(\rho)}{q_*} &= \frac{\rho\psi'(1)}{\psi'(\rho)}
\end{aligned} \tag{F.32}$$

2804 Eq. (F.31) is now substituted into the expression for the bootstrap current given by
2805 Eq. (F.11). The resulting expression can then be integrated over the plasma cross
2806 section to yield the bootstrap fraction. A straightforward calculation leads to:

$$f_{BS} = \frac{I_{BS}}{I} = \frac{2\pi a^2 \kappa}{I} \int_0^1 J_{BS} \rho d\rho = \frac{K_{BS}}{K_n} \frac{\bar{n} \bar{T} R_0^2}{I_P^2} \tag{F.33}$$

2807

$$K_{BS} = 4.879 \cdot K_n \cdot \left(\frac{1+\kappa^2}{2} \right) \cdot \epsilon^{5/2} \cdot H_{BS} \tag{F.34}$$

2808

$$H_{BS} = (1+\nu_n)(1+\nu_T)(\nu_n+0.054\nu_T) \int_0^1 \frac{\rho^{5/2} (1-\rho^2)^{\nu_n+\nu_T-1}}{b_p} d\rho \tag{F.35}$$

2809

$$b_p(\rho) = \frac{-e^{\gamma\rho^2}(\gamma\rho^2-1-\gamma)-1-\gamma}{\rho(e^\gamma-1-\gamma)} \tag{F.36}$$

2810 This is the desired result.

Bibliography

- [1] W Biel, M Beckers, R Kemp, R Wenninger, and H Zohm. Systems code studies on the optimization of design parameters for a pulsed DEMO tokamak reactor, 2016.
- [2] C E Kessel, M S Tillack, F Najmabadi, F M Poli, K Ghanous, N Gorelenkov, X R Wang, D Navaei, H H Toudeshki, C Koehly, L El-Guebaly, J P Blanchard, C J Martin, L Mynsburge, P Humrickhouse, M E Rensink, T D Rognlien, M Yoda, S I Abdel-Khalik, M D Hageman, B H Mills, J D Rader, D L Sadowski, P B Snyder, H. St. John, A D Turnbull, L M Waganer, S Malang, and A F Rowcliffe. The ARIES advanced and conservative tokamak power plant study. *Fusion Science and Technology*, 67(1):1–21, 2015.
- [3] GS Lee, J Kim, SM Hwang, Choong-Seock Chang, Hong-Young Chang, MH Cho, BH Choi, K Kim, KW Cho, S Cho, et al. The kstar project: An advanced steady state superconducting tokamak experiment. *Nuclear Fusion*, 40(3Y):575, 2000.
- [4] Jeffrey P Freidberg. *Plasma Physics and Fusion Energy*, volume 1. 2007.
- [5] B. N. Sorbom, J. Ball, T. R. Palmer, F. J. Mangiarotti, J. M. Sierchio, P. Bonoli, C. Kasten, D. A. Sutherland, H. S. Barnard, C. B. Haakonsen, J. Goh, C. Sung, and D. G. Whyte. ARC: A compact, high-field, fusion nuclear science facility and demonstration power plant with demountable magnets. *Fusion Engineering and Design*, 100:378–405, nov 2015.
- [6] M Kovari, R Kemp, H Lux, P Knight, J Morris, and D J Ward. " PROCESS " : A systems code for fusion power plants—Part 1: Physics. *Fusion Engineering and Design*, 89(12):3054–3069, 2014.
- [7] Meszaros et al. Demo I Input File.
- [8] H. Fountain. A dream of clean energy at a very high price. <https://www.nytimes.com/2017/03/27/science/fusion-power-plant-iter-france.html>, 2017. Accessed: 2018-12-6.
- [9] J. Tirone. World’s biggest science experiment seeks more time and money. <https://www.bloomberg.com/news/articles/2016-06-15/world-s-biggest-science-experiment-seeks-more-time-and-money>, 2016. Accessed: 2018-12-6.

- [10] David J. Griffiths. *Introduction to electrodynamics*.
- [11] P J Knight and M D Kovari. A User Guide to the PROCESS Fusion Reactor Systems Code, 2016.
- [12] D C Mcdonald, J G Cordey, K Thomsen, C Angioni, H Weisen, O J W F Kardaun, M Maslov, A Zabolotsky, C Fuchs, L Garzotti, C Giroud, B Kurzan, P Mantica, A G Peeters, and J Stober. Scaling of density peaking in H-mode plasmas based on a combined database of AUG and JET observations. *Nucl. Fusion*, 47:1326–1335, 2018.
- [13] T Onjun, G Bateman, A H Kritz, and G Hammett. Models for the pedestal temperature at the edge of H-mode tokamak plasmas. *Physics of Plasmas*, 9(10), 2002.
- [14] G Saibene, L D Horton, R Sartori, and A E Hubbard. Physics and scaling of the H-mode pedestal The influence of isotope mass, edge magnetic shear and input power on high density ELMy H modes in JET Physics and scaling of the H-mode pedestal. *Control. Fusion*, 42:15–35, 2000.
- [15] Martin Greenwald. Density limits in toroidal plasmas, 2002.
- [16] J Jacquinet,) Jet, S Putvinski,) Jct, G Bosia, Jct), A Fukuyama, U) Okayama, R Hemsworth, Cea Cadarache), S Konovalov, Rrc Kurchatov), W M Nevins, Llnl), F Perkins, K A Rasumova, Rrc-) Kurchatov, F Romanelli, Enea-) Frascati, K Tobita, Jaeri), K Ushigusa, J W Van, U Dam, V Texas), Rrc Vdovin, S Kurchatov), R Zweben, Erm Koch, Kms-) Brussels, J.-G Wégrowe, Cea-) Cadarache, V V Alikaev, B Beaumont, A Bécoulet, S Bern-Abei, Pppl), V P Bhatnagar, Ec Brussels), S Brémond, and M D Carter. Chapter 6: Plasma auxiliary heating and current drive. *ITER Physics Basis Editors Nucl. Fusion*, 39, 1999.
- [17] D A Ehst and C F F Karney. Approximate formula for radiofrequency current drive efficiency with magnetic trapping, 1991.
- [18] Ian H Hutchinson. Principles of plasma diagnostics. *Plasma Physics and Controlled Fusion*, 44(12):2603, 2002.
- [19] Tobias Hartmann, Thomas Hamacher, Hon-Prof rer nat Hartmut Zohm, and Hon-Prof rer nat Sibylle Günter. Development of a Modular Systems Code to Analyse the Implications of Physics Assumptions on the Design of a Demonstration Fusion Power Plant.
- [20] N A Ukan. ITER Physics Design Guidelines at High Aspect Ratio. pages 1–4, 2009.
- [21] J P Freidberg, F J Mangiarotti, and J Minervini. Designing a tokamak fusion reactor - How does plasma physics fit in? *Physics of Plasmas*, 22(7):070901, 2015.

- [22] B Labombard, E Marmor, J Irby, T Rognlien, and M Umansky. ADX: a high field, high power density, advanced divertor and RF tokamak Nuclear Fusion. Technical report, 2017.
- [23] S P Hirshman and G H Neilson. External inductance of an axisymmetric plasma. *Physics of Fluids*, 29(3):790–793, 1986.
- [24] P Libeyre, N Mitchell, D Bessette, Y Gribov, C Jong, and C Lyraud. Detailed design of the ITER central solenoid. *Fusion Engineering and Design*, 84:1188–1191, 2009.
- [25] Jeff P Freidberg, Antoin Cerfon, and Jungpyo Lee. Tokamak elongation: how much is too much? I Theory. *arXiv.org*, pages 1–34, 2015.
- [26] E. J. Doyle, W. A. Houlberg, Y. Kamada, V. Mukhovatov, T. H. Osborne, A. Polevoi, G Bateman, J. W. Connor, J. G. Cordey, T Fujita, X Garbet, T. S. Hahm, L. D. Horton, A. E. Hubbard, F Imbeaux, F Jenko, J. E. Kinsey, Y Kishimoto, J Li, T. C. Luce, Y Martin, M Ossipenko, V Parail, A Peeters, T. L. Rhodes, J. E. Rice, C. M. Roach, V Rozhansky, F Ryter, G Saibene, R Sartori, A. C.C. Sips, J. A. Snipes, M Sugihara, E. J. Synakowski, H Takenaga, T Takizuka, K Thomsen, M. R. Wade, and H. R. Wilson. Chapter 2: Plasma confinement and transport. *Nuclear Fusion*, 47(6):S18–S127, jun 2007.
- [27] H Lux, R Kemp, E Fable, and R Wenninger. Radiation and confinement in 0-D fusion systems codes. Technical report.
- [28] Louis Giannone, J Baldzuhn, R Burhenn, P Grigull, U Stroth, F Wagner, R Brakel, C Fuchs, HJ Hartfuss, K McCormick, et al. Physics of the density limit in the w7-as stellarator. *Plasma physics and controlled fusion*, 42(6):603, 2000.
- [29] H Bosch and G M Hale. Improved formulas for fusion cross-sections and thermal reactivities. 611.
- [30] Zachary S Hartwig and Yuri A Podpaly. Magnetic Fusion Energy Formulary. Technical report, 2014.
- [31] John Wesson and David J Campbell. *Tokamaks*, volume 149. Oxford University Press, 2011.
- [32] C. E. Kessel. Bootstrap current in a tokamak. *Nuclear Fusion*, 34(9):1221–1238, 1994.